

POLITECNICO DI TORINO

Dipartimento di Ingegneria Meccanica e Aerospaziale

Corso di Laurea in Ingegneria Aerospaziale

Tesi di Laurea

**Three dimensional model of a sail  
thrust by Solar and Planetary  
Radiation Pressure**

Investigation of the effect of PRP for a capturing manoeuvre of Venus



**Relatori**

Prof. Lorenzo Casalino

Dr. Matteo Ceriotti

Elia SINDONI  
matricola S245974

APRILE 2020

# Contents

List of Figures	III
List of Tables	VII
Abbreviation	2
Abstract	3
1 Introduction	4
<b>I Three dimensional analysis of sailing with Solar and Planetary Radiation Pressure</b>	<b>7</b>
<b>2 Solar sailing physics</b>	<b>9</b>
2.1 Quantum description . . . . .	9
2.2 Electromagnetic description . . . . .	10
2.3 Radiative transfer methods . . . . .	11
<b>3 Three-dimensional model</b>	<b>15</b>
3.1 Acceleration in a optical force model . . . . .	15
3.1.1 Two-dimensional introduction . . . . .	15
3.1.2 Three-dimensional extension . . . . .	17
3.2 Radiation Pressure contribution . . . . .	20
3.2.1 Evaluation of the SRP contribution . . . . .	21
3.3 Evaluation of the PRP contribution . . . . .	21
3.3.1 Albedo Radiation Pressure . . . . .	22
3.3.2 Black Body Radiation Pressure . . . . .	24
<b>4 Evaluation of attainable values of acceleration</b>	<b>27</b>
4.1 Radial Acceleration . . . . .	28
4.1.1 Solar Radiation Pressure . . . . .	29
4.1.2 Albedo Radiation Pressure . . . . .	32
4.1.3 Black Body Radiation Pressure . . . . .	35
4.1.4 Solar Radiation Pressure + Planetary Radiation Pressure . . . . .	37
4.2 Transverse Acceleration . . . . .	40

4.2.1	Solar Radiation Pressure . . . . .	41
4.2.2	Albedo Radiation Pressure . . . . .	42
4.2.3	Black Body Radiation Pressure . . . . .	43
4.2.4	Solar Radiation Pressure + Planetary Radiation Pressure . . . . .	44
4.3	3D example for Venus . . . . .	48
<b>II Dynamic of the sail</b>		<b>51</b>
<b>5</b>	<b>Orbital Dynamic</b>	<b>53</b>
5.1	Introduction to the Gauss' variational equations . . . . .	53
5.2	Gao's control laws . . . . .	55
5.3	Capturing manoeuvre . . . . .	58
<b>6</b>	<b>Results</b>	<b>61</b>
6.1	Results of orbital manoeuvre with Gao's control law . . . . .	61
6.1.1	Quasi-circular orbit - decrease of $a, e, i$ . . . . .	61
6.1.2	Quasi-circular orbit - increase of $a, e$ and decrease of $i$ . . . . .	65
6.1.3	Highly-elliptical orbit - decrease of $a, e, i$ . . . . .	66
6.1.4	Inclined orbit - increase of $a, e, i$ . . . . .	69
6.1.5	Inclined orbit with RAAN - increase of $a, e$ and decrease of $i$ . . . . .	71
6.1.6	Inclined orbit with RAAN - increase of $a, e$ and $i$ . . . . .	74
6.1.7	Quasi-circular orbit out of PRP dominating region - increase of $a, e$ and decrease of $i$ . . . . .	75
6.2	Results of capturing manoeuvre . . . . .	78
6.2.1	Parametric study - $a_o, r_p$ and $i_h$ . . . . .	78
6.2.2	Parametric study - Comparison with and without PRP . . . . .	80
<b>7</b>	<b>Conclusion</b>	<b>87</b>
	<b>Conclusion</b>	<b>88</b>
	<b>Bibliography</b>	<b>91</b>
	<b>Aknowledges</b>	<b>93</b>

# List of Figures

1.1	LightSail 2 during sail deployment sequence, image from the Planetary Society	6
2.1	Electromagnetic description of radiation pressure [1]	10
2.2	Radiation field specific intensity [1]	12
2.3	Planetary radiation pressure with a finite angular sized disc	14
3.1	Offset angle between $\hat{n}$ and $\hat{m}$ [23]	17
3.2	Reference system $a$ or $xyz$	18
3.3	Acceleration unit vector $m$ in a generic reference system [23]	19
3.4	Cylindrical eclipse model	21
3.5	Reflection angle	22
3.6	Surface heated by the photons flux	23
3.7	Area where the Albedo Radiation Pressure exists	24
3.8	Sail surface struck by the photons	25
4.1	Points chosen for the validation of the model	29
4.2	Maximisation of the radial acceleration for a double-coating sail around Earth subject to SRP	29
4.3	Maximisation of the radial acceleration for a single-coating sail around Earth subject to SRP	30
4.4	Maximisation of the radial acceleration for a double-side coating sail around Venus subject to SRP	31
4.5	Maximisation of the radial acceleration for a single-side coating sail around Venus subject to SRP	32
4.6	Maximisation of the radial acceleration for a double-side coating sail around Earth subject to ARP	33
4.7	Maximisation of the radial acceleration for a single-side coating sail around Earth subject to ARP	33
4.8	Maximisation of the radial acceleration for a double-side coating sail around Venus subject to ARP	34
4.9	Maximisation of the radial acceleration for a single-side coating sail around Venus subject to ARP	34
4.10	Maximisation of the radial acceleration for a double-side coating sail around Earth subject to BBRP	35

4.11	Maximisation of the radial acceleration for a single-side coating sail around Earth subject to BBRP . . . . .	36
4.12	Maximisation of the radial acceleration for a double-side coating sail around Venus subject to BBRP . . . . .	36
4.13	Maximisation of the radial acceleration for a single-side coating sail around Venus subject to BBRP . . . . .	37
4.14	Maximisation of the radial acceleration for a double-side coating sail around Earth subject to SRP and PRP . . . . .	37
4.15	Maximisation of the radial acceleration for a single-side coating sail around Earth subject to SRP and PRP . . . . .	38
4.16	Maximisation of the radial acceleration for a double-side coating sail around Venus subject to SRP and PRP . . . . .	39
4.17	Maximisation of the radial acceleration for a single-side coating sail around Venus subject to SRP+PRP . . . . .	39
4.18	Maximisation of the transverse acceleration for a double-side coating sail around Earth subject to SRP . . . . .	41
4.19	Maximisation of the transverse acceleration for a double-side coating sail around Venus subject to SRP . . . . .	42
4.20	Maximisation of the transverse acceleration for a double-side coating sail around Earth subject to ARP . . . . .	42
4.21	Maximisation of the transverse acceleration for a double-coating sail around Venus subject to ARP . . . . .	43
4.22	Maximisation of the transverse acceleration for a double-side coating sail around Earth subject to BBRP . . . . .	44
4.23	Maximisation of the transverse acceleration for a double-side coating sail around Venus subject to BBRP . . . . .	44
4.24	Maximisation of the transverse acceleration for a double-side coating sail around Earth subject to SRP and PRP . . . . .	45
4.25	Maximisation of the transverse acceleration for a double-coating sail around Venus subject to SRP and PRP . . . . .	46
4.26	Maximisation of the transverse acceleration for a single-side coating sail around Venus subject to SRP and PRP . . . . .	47
4.27	Maximisation of the out-of-plane acceleration for a double-side coating sail around Venus subject to SRP and PRP in an inclined plane . . . . .	48
4.28	Maximisation of the out-of-plane acceleration for a double-side coating sail around Venus subject to SRP in an inclined plane . . . . .	49
5.1	Illustration of orbit plane unit direction vectors [26] . . . . .	54
5.2	Example of the division of the orbit in arches proposed by Gao . . . . .	55
5.3	Example of $\frac{d\mathbf{i}}{dt}(\nu)$ trend and threshold value . . . . .	57
5.4	Example of the direction of acceleration vector requested to increase orbital elements with Gao's guidance scheme . . . . .	58
5.5	Example of hyperbolic orbit and capturing control law . . . . .	60
6.1	Initial and final orbit with and without PRP, quasi-circular orbit with low inclination around Venus . . . . .	63

6.2	Trend of the orbital elements with and without PRP during three revolutions, quasi-circular orbit with low inclination around Venus . . . . .	63
6.3	Trend of the acceleration with and without PRP during three revolutions, quasi-circular orbit with low inclination around Venus . . . . .	64
6.4	Trend of the orbital elements with and without PRP during ten revolutions, quasi-circular orbit with low inclination around Venus . . . . .	64
6.5	Initial and final orbit with and without PRP, quasi-circular orbit with low inclination around Venus . . . . .	65
6.6	Trend of the orbital elements with and without PRP during three revolutions, quasi-circular orbit with low inclination around Venus . . . . .	65
6.7	Trend of the acceleration with and without PRP during three revolutions, quasi-circular orbit with low inclination around Venus . . . . .	66
6.8	Initial and final orbit with and without PRP, highly-elliptical orbit with low inclination around Venus . . . . .	67
6.9	Trend of the orbital elements with and without PRP during three revolutions, highly-elliptical orbit with low inclination around Venus . . . . .	68
6.10	Trend of the acceleration with and without PRP during three revolutions, highly-elliptical orbit with low inclination around Venus . . . . .	68
6.11	Trend of the orbital elements with and without PRP during ten revolutions, highly-elliptical orbit with low inclination around Venus . . . . .	69
6.12	Initial and final orbit with and without PRP, quasi-circular orbit with high inclination around Venus . . . . .	70
6.13	Trend of the orbital elements with and without PRP during three revolutions, quasi-circular orbit with high inclination around Venus . . . . .	70
6.14	Trend of the acceleration with and without PRP during three revolutions, quasi-circular orbit with high inclination around Venus . . . . .	71
6.15	Initial and final orbit with and without PRP, elliptical orbit with medium inclination and rotated RAAN around Venus . . . . .	72
6.16	Trend of the orbital elements with and without PRP during three revolutions, elliptical orbit with medium inclination and rotated RAAN around Venus . . . . .	73
6.17	Trend of the acceleration with and without PRP during three revolutions, elliptical orbit with medium inclination and rotated RAAN around Venus . . . . .	73
6.18	Trend of the orbital elements with and without PRP during ten revolutions, elliptical orbit with medium inclination and rotated RAAN around Venus . . . . .	74
6.19	Trend of the orbital elements with and without PRP during three revolutions, elliptical orbit with a medium inclination and rotated RAAN around Venus . . . . .	75
6.20	Initial and final orbit with and without PRP, quasi-circular orbit with low inclination around Venus . . . . .	76
6.21	Trend of the orbital elements with and without PRP during three revolutions, quasi-circular orbit with low inclination around Venus . . . . .	77
6.22	Trend of the acceleration with and without PRP during three revolutions, quasi-circular orbit with low inclination around Venus . . . . .	77
6.23	Trend of the orbital elements with and without PRP during ten revolutions, quasi-circular orbit with low inclination around Venus . . . . .	78

6.24	Example of the four study-case orbits . . . . .	79
6.25	Curve of the parameters that allow the capturing manoeuvre - $i$ 5 deg, $\omega$ 0 deg . . . . .	79
6.26	Initial conditions that allow the capturing manoeuvre for an orbit with inclination- $i$ 5 deg . . . . .	81
6.27	Initial conditions that allow the capturing manoeuvre for an orbit with inclination- $i$ 85 deg . . . . .	82
6.28	Trend of semimajor axis and eccentricity (a), and direction of the acceleration vectors - $i$ 5 deg, $\omega$ 0 deg . . . . .	83
6.29	Magnitude and components of the acceleration vector - $i$ 5 deg, $\omega$ 0 deg . . . . .	83
6.30	Trend of semimajor axis and eccentricity (a), and direction of the acceleration vectors - $i$ 5 deg, $\omega$ 180 deg . . . . .	84
6.31	Magnitude and components of the acceleration vector - $i$ 5 deg, $\omega$ 180 deg . . . . .	84
6.32	Trend of semimajor axis and eccentricity (a), and direction of the acceleration vectors - $i$ 85 deg, $\omega$ 0 deg . . . . .	85
6.33	Magnitude and components of the acceleration vector - $i$ 85 deg, $\omega$ 0 deg . . . . .	85
6.34	Trend of semimajor axis and eccentricity (a), and direction of the acceleration vectors - $i$ 85 deg, $\omega$ 180 deg . . . . .	86
6.35	Magnitude and components of the acceleration vector - $i$ 85 deg, $\omega$ 0 deg . . . . .	86

# List of Tables

4.1	Data of the planets [Nasa planetary data sheet] . . . . .	28
4.2	Comparison of the cone angle $\alpha_p$ for single-side and double-side coating in Earth area with only SRP [rad] . . . . .	31
4.3	Comparison of the cone angle $\alpha_p$ for single-side and double-side coating in Venus area with only SRP [rad] . . . . .	32
4.4	Comparison of the cone angle $\alpha_p$ for single-side and double-side coating in Earth area with only ARP [rad] . . . . .	33
4.5	Comparison of the cone angle $\alpha_p$ for single-side and double-side coating in Venus area with only ARP [rad] . . . . .	35
4.6	Comparison of the cone angle $\alpha_p$ for single-side and double-side coating in Earth area with only SRP+PRP [rad] . . . . .	38
4.7	Comparison of the cone angle $\alpha_p$ for single-side and double-side coating in Venus area with only SRP+PRP [rad] . . . . .	40
4.8	Comparison of the cone angle $\alpha_p$ and of the radial acceleration for double-side coating in Venus area with and without PRP [rad] . . . . .	40
4.9	Comparison of the cone angle $\alpha_p$ and of the transverse acceleration for double-side coating in Earth area with and without PRP [rad] . . . . .	45
4.10	Comparison of the cone angle $\alpha_p$ and of the transverse acceleration for double-side coating in Venus area with and without PRP [rad] . . . . .	46
4.11	Comparison of the cone angle $\alpha_p$ and of the transverse acceleration for single-side coating in Venus area with and without PRP [rad] . . . . .	47
4.12	Comparison of cone angle $\alpha_p$ and clock angle $\delta_p$ for a double-side coating in Venus area with and without PRP [rad] . . . . .	49
4.13	Comparison of the out-of-plane acceleration for double-side coating in Venus area with and without PRP [rad] . . . . .	50
6.1	Orbital elements quasi-circular orbit . . . . .	62
6.2	Semimajor axis, eccentricity and inclination after three revolutions . . . . .	62
6.3	Semimajor axis, eccentricity and inclination after three revolutions . . . . .	66
6.4	Orbital elements highly-elliptical orbit . . . . .	67
6.5	Semimajor axis, eccentricity and inclination after three revolutions . . . . .	67
6.6	Orbital elements highly-elliptical orbit . . . . .	69
6.7	Semimajor axis, eccentricity and inclination after three revolutions . . . . .	71
6.8	Orbital elements elliptical orbit with medium inclination . . . . .	72
6.9	Semimajor axis, eccentricity and inclination after three revolutions . . . . .	74

6.10 Semimajor axis, eccentricity and inclination after three revolutions . . . . .	75
6.11 Orbital elements elliptical orbit with medium inclination . . . . .	76
6.12 Semimajor axis, eccentricity and inclination after three revolutions . . . . .	76

*We know what we are,  
but not what we may be*

*[Hamlet, William Shakespeare]*

# Abbreviation

<b>ARP</b>	Albedo Radiation Pressure
<b>BBRP</b>	Black Body Radiation Pressure
<b>JAXA</b>	Japanese Aerospace Exploration Agency
<b>LEO</b>	Low Earth Orbit
<b>PRP</b>	Planetary Radiation Pressure
<b>RAAN</b>	Right Ascension of Ascending Node
<b>SRP</b>	Solar Radiation pressure

# Abstract

Solar sailing is by far one of the most intriguing and promising concepts for the space exploration, since it is free from the need of carrying a propellant on board of the spacecraft. In literature, many studies have demonstrated the suitability of solar sailing for a wide range of different applications; however, up until now almost all of them have taken into account only the solar radiation pressure (SRP) to calculate the sail force. This assumption is acceptable for most of the missions but, since the planet emits radiation or reflects part of the one coming from the Sun, for planetary missions, a new contribution should be factored in the calculation of the total radiation pressure. Therefore, this work analysed the combined effect of both planetary radiation pressure (PRP) and SRP with a three-dimensional approach, extending a previous work developed for the two-dimensional case. The study has been focused, in particular, on the Earth and Venus; the first one for the remarkable amount of possible applications, the second one for the promising results obtained in the two-dimensional study. In the case of Venus, the PRP is the dominating contribution within a distance of about two planetary radii, while for the Earth this region is smaller and closer to the planet. Both for Venus and Earth, results show a potential increase in net acceleration and a change in optimal attitude to maximise the acceleration in a given direction; moreover, the PRP provides a force even in the eclipse area, where the planet blocks solar photons. Last part of the work analysed some manoeuvres with and without PRP, to compare the results on the change of semimajor axis, eccentricity and inclination of the orbit; furthermore, the effect of PRP on the capturing manoeuvre of Venus was studied. The results show that PRP has a positive influence on the performance of the sail, in particular for the changing of the orbital elements. The effect of PRP on the capturing manoeuvre becomes relevant especially when the manoeuvre is done near the eclipse area and within a certain distance from the planet.

# Chapter 1

## Introduction

Although the concept of the solar sail appears innovative and futuristic, the idea of using light for propulsive purposes was born with the development itself of the space propulsion. However, for a long time, the use of sails has remained theoretical and only in the last decades some designs come to life thanks to the new manufacturing techniques, the many progressions in material science and the miniaturisation of satellites. In the 90s', moreover, some experiments have been crucial to test in-flight and validate key technologies that now are the basics for a lot of the modern concepts of solar sailing. In particular, reference is made to the studies about deployment mechanics, inflatable structures and reflective materials[1].

Since its beginning, the propulsion has been based on Newton's law of action-reaction, in other words, the thrust is generated by an exchange of momentum, typically between some device on the aircraft/spacecraft and a fluid. In the aeronautical world, the fluid is the air and the aircraft is immersed in it, unlike a spacecraft which operates in an ambient almost empty. Since the spacecraft have to carry on board a reaction mass (the propellant), space exploration has been deeply influenced due to the weight limitation and the corresponding high costs.

However, even though the approximation of the space as a vacuum is understandable when the comparison is with Earth's atmosphere, it is not entirely right. The light propagates in the space and its photons, even if they do not have a mass, carry a momentum that can be gain by a structure to generate thrust; this idea is at the base of the solar sails concept and allows a unique form of space propulsion, free from the need of bringing from Earth a reaction mass. In addition to the benefits in terms of weight, using an ambient source has no time limits so that a solar sail can generate continuous acceleration and the mission can be fully operative as long as the sail film lasts in the space environment; therefore the only limitation is the lifetime of the materials. The price for all these intriguing advantages is that acceleration from a solar sail is very small since each photon carry a minimal momentum; considering, for example, a sail located in an Earth orbit, at best it will experience a force of  $9 \cdot 10^{-6} N$  per square metre [1]. If not carefully studied, the banal solution of a sail with a large surface that intersects more photons can drastically increase the structural weight, reducing the payload mass and even not having a beneficial effect on the acceleration.

As it will see in the next paragraphs, the resultant force depends on the reflective properties

of the coating film, but in first approximation, it can be said that it is directed as the normal to the sail surface. For this reason, the acceleration can be reduced or increased changing the orientation of the sail in relation to the photons source and even the attitude can be controlled modifying the reflective properties or the orientation of some parts of the sail. Thanks to this flexibility, a huge range of different missions is possible, and more of these have been already studied and analysed in scientific literature [2]. In their works, Eguchi [3] and Fekete [4] proposed fly-bys and rendezvous to the Moon, while inner [5] [6] and outer [7] [8] solar system rendezvous missions have been analysed by Garner, Leipold, Mengali and Quarta. Pelsoni and Ceriotti studied trajectories for near-Earth asteroids [9] and Leipold [10] and Casalino and Colasurdo [11] considered solar sail for escaping from the Solar System. The continuous acceleration that a sail can potentially provide makes it suitable for station keeping, e.g. in Halo orbit [12]. Furthermore, many interesting concepts have been done for planet-centred orbits such as the demonstration mission GeoSail [13] in Earth magnetotail or MESSAGE (MErcury Solar Sail Advanced Geoscience Exploration) [6] in a sun-synchronous orbit around Mercury. Other relevant application can be in escaping manoeuvres from Earth: studies have been already conducted by Macdonald and McInnes [14] using near-optimal trajectories and by Coverstone and Prussing [15] for escaping from GTO. Moreover, free from the need of propellant, the use of the solar sail allows non-Keplerian orbit [1] such as the pole sitter concept proposed by Ceriotti [16] for Earth and extended by Heiligers and Ceriotti [17] for other planets, where solar sailing is used with a SEP to maintain the spacecraft over the North or the South pole.

However, for now, most of these ideas are just theoretical, and only a few of them have been already launched and tested in space. The actual demonstration of the feasibility of solar sailing came thanks to the Japanese Aerospace Exploration Agency. In 2010 JAXA launched and deployed in space IKAROS, the spacecraft that tested solar sailing in an interplanetary mission to Venus. In the following years, other companies and association have developed solar sailing missions, e.g. NanoSail-D by NASA in 2010 and recently LightSail 2 by Planetary Society that has demonstrated the possibility of rising the apogee of an orbit by using only solar sail propulsion.

All the studies mentioned above consider only the Solar Radiation Pressure, and so the Sun as unique photons source. This consideration is acceptable mostly when the spacecraft is in outer space; however, when the sail comes near a celestial body such as a planet, another contribution should be considered. A planet, in fact, emits radiations and reflects partially the ones coming from the Sun. The first contribution is called black body radiation and is due to the thermodynamic equilibrium of the body with its environment. Its value is strictly linked to the Stefan-Boltzmann law. The contribution due to the reflection of solar radiation is called albedo and depends on the features of the reflecting surface, in other words, different soils have different albedo [18]; moreover even the seasons can influence it [19]. Unlike black-body radiation, the albedo contribution was already studied by Grøtte and Holzinger in a three-body problem, showing how its contribution allows new equilibrium points that can become stable using solar sail attitude control [20]. Despite the high interest and the numerous amount of concepts in body-centred trajectories, the studies on the planetary radiation pressure PRP are still few and only in De Iuliis's work [21] it has been fully considered in both its contributions. De Iuliis, in particular, analysed the benefit of the PRP in the net acceleration and made a comparison of the results with and without PRP in a real case scenario where the semimajor axis



Figure 1.1. LightSail 2 during sail deployment sequence, image from the Planetary Society

is increased. The study achieved its aim, but it was focused only in a 2D analysis, so the purpose of this work is to extend that analysis in a 3D case and to demonstrate the possibility of a capturing manoeuvre around Venus. Hence, the thesis is divided in two different parts, in the first one the general physics of solar sailing will be introduced in the chapter 2 and the three-dimensional model of solar and planetary radiation pressure will be presented in the chapter 3. As it will see, the attitude of the sail will be written as a function of two different angles that allow knowing the position of the sail-surface normal vector in a three-dimensional space. Some results of the model will be shown in chapter 4. In the second part of the thesis, the model will be used to perform orbital manoeuvres in order to change semimajor axis, eccentricity and inclination in section 5.2 and to investigate the effect of planetary radiation pressure in a capturing manoeuvre in section 5.3. The results of these simulations will be shown in chapter 6.

## Part I

# Three dimensional analysis of sailing with Solar and Planetary Radiation Pressure



# Chapter 2

## Solar sailing physics

As previously mentioned, a solar sail gains the momentum of the photons and uses that momentum to propel the spacecraft; the bigger its surface is, the more will be the photons which will hit the sail and, theoretically, the higher will be the acceleration, so, for this reason, a solar sail appears as a structure of rather big dimensions. Despite this fact, its weight must be extremely small in order to maximise the benefit, hence typically the surface is some microns thick and is made of lightweight materials such as Mylar; most of the weight is concentrated in the structure which keeps the sail unfolded.

From a physical point of view, there are two different approaches to explain how the sail works. The first one uses the quantum description of photons, while the second one uses the electromagnetic description of radiation. Both the ways have been extensively analysed in the literature, for this reason, they will be touched upon just for a better understanding of the following chapters. For the writing of the next sections, reference is made to McInnes' work [1].

### 2.1 Quantum description

As is known, photons are packets of quantized energy, whose value depends on their frequency  $\nu$  and can be obtained through Planck's law.

$$E = h\nu \tag{2.1}$$

where  $h$  is the Planck's constant. The same energy  $E$  can also be obtained with the mass-energy equivalence of special relativity for a moving body

$$E^2 = m_o^2 c^4 + p^2 c^2 \tag{2.2}$$

where  $c$  is the speed of light,  $m_o$  is the invariant mass of the body and  $p$  its momentum. The two terms represent respectively the rest energy and the kinetic energy of the body but, since a photon has zero mass, the equation can be simplified.

$$E = pc \tag{2.3}$$

Comparing the equation 2.1 and 2.3, the momentum of a single photon can be found

$$p = \frac{E}{c} = \frac{h\nu}{c} \tag{2.4}$$

The analysis can be extended for more photons considering an energy flux  $W$ ; by its definition, the flux of a physical dimension represents its value crossing a unit surface in unit time; hence the energy may be written as

$$\Delta E = WA\Delta t \quad (2.5)$$

and in the momentum relation

$$\Delta p = \frac{\Delta E}{c} = \frac{WA\Delta t}{c} \quad (2.6)$$

where  $A$  is the area normal to the incident radiation. The pressure is a force per unit area so, from Newton's law, it is the momentum transported per unit time, per unit area

$$P = \frac{1}{A} \frac{\Delta p}{\Delta t} = \frac{W}{c} \quad (2.7)$$

The relation links the pressure to the energy flux  $W$ , so the last step is to define its value. In the classic study of Solar Radiation Pressure, it depends on the solar luminosity  $L_s$  and on the distance  $r$  from the Sun; however, for practical purposes, it is commonly used the flux measured at the Earth's mean distance from the Sun, opportunely scaled.

$$W = \frac{L_s}{4\pi r^2} = \frac{L_s}{4\pi R_E^2} \left(\frac{R_E}{r}\right)^2 = W_E \left(\frac{R_E}{r}\right)^2 \quad (2.8)$$

where  $W_E$  is  $1361 \text{ W/m}^2$  [22].

## 2.2 Electromagnetic description

An equivalent result is obtained considering the momentum transported by the electromagnetic waves. These have two different components: the electric one  $\vec{E}$  that induces in the sail a current  $\vec{j}$ , and the magnetic one  $\vec{B}$  that interacts with the current and generates a Lorentz force. In fig 2.1 a representation of the vectors is shown.

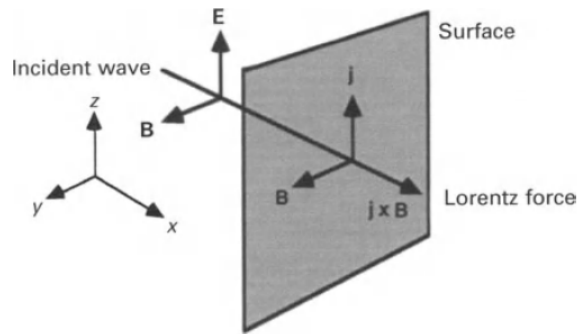


Figure 2.1. Electromagnetic description of radiation pressure [1]

The equation of Lorentz force is

$$\vec{F}_L = \vec{j} \times \vec{B} \quad (2.9)$$

and, considering for example that the waves propagate along x, it is possible to write the magnitude of the force on an infinitesimal element as

$$df = j_z B_y dx dy dz \quad (2.10)$$

with  $j_z$  the current volumetric density. From the equation of the infinitesimal force can be written the pressure

$$dP = j_z B_y dx \quad (2.11)$$

Substituting  $j_z$  through Maxwell's equations, the last relation can be rehashed and it can be demonstrated that the pressure exerted on the surface is equal to the total energy density of the electromagnetic wave.

$$\langle P \rangle = \langle U \rangle \quad (2.12)$$

where

$$U = \frac{1}{2} \epsilon_o E^2 + \frac{1}{2\mu_o} B^2 \quad (2.13)$$

The definition of energy density, namely an energy per unit volume, is used to link the two descriptions of the radiation pressure. For this analysis, in particular, the volume is given by the incident area  $A$  of the surface and by the distance between two waves; since this is the distance that the light travels in a period of time  $\Delta t$ , the energy density become

$$U = \frac{\Delta E}{A c \Delta t} \quad (2.14)$$

and again the energy flux appears in the relation

$$W = \frac{1}{A} \left( \frac{\Delta E}{\Delta t} \right) \quad (2.15)$$

Hence, it is obtained

$$P = U = \frac{W}{c} \quad (2.16)$$

Both the description arrives at the same conclusion but, since the reflection generated a contribution too, this result must be doubled or at least multiplied for an appropriate factor which considers the reflectivity properties of the materials.

## 2.3 Radiative transfer methods

The found relations offer a good approximation for solar radiation pressure; however, they do not consider that the radiation depends on both position and time, and that may have a distribution and a frequency. Furthermore, it has been assumed that its variation follows an inverse square law with the photons source distance but, although this assumption can be accepted when the source is far from the sail, it is not valid when the sail is close

to it, and it is necessary to take into account the finite angular size of its disc. When the sail orbits around a planet, considering its finite angular size is particularly relevant for the study of the planetary contribution. The radiative transfer methods provide a rigorous means of calculating the effect of radiation pressure and allow to overcome all the limitation previously mentioned. All the properties of the radiation field may be described by the specific intensity  $I_\nu(\vec{r}, \vec{u}; t)$  at position  $\vec{r}$  and time  $t$  propagating with frequency  $\nu$  in direction  $\vec{u}$ . The specific intensity is defined to be the energy  $dE$  transported across a directed surface element  $d\vec{A}$  in time  $dt$  into a solid angle  $d\Omega$  about direction  $\vec{u}$ .

$$dE = I_\nu(\vec{r}, \vec{u}; t)(\vec{u} \cdot d\vec{A}) d\Omega dt d\nu \quad (2.17)$$

where  $\vec{u} \cdot d\vec{A}$  is the projected surface area normal to the direction of propagation, as shown in fig.2.2. A relation for the energy can be obtained also from a microscopic perspective, in

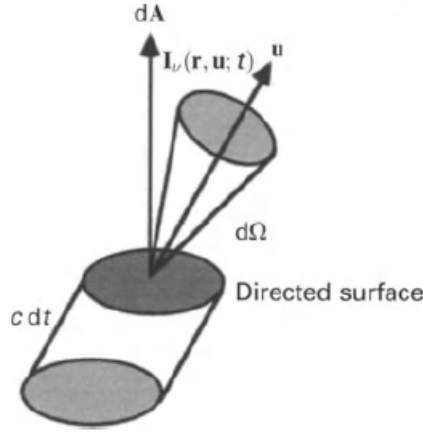


Figure 2.2. Radiation field specific intensity [1]

order to find an equation for the specific intensity. Through the photons number density function  $\psi_\nu(\vec{r}, \vec{u}; t)$  is possible to calculate the number of photons per unit volume at position  $\vec{r}$  at time  $t$  in a frequency range  $(\nu, \nu + d\nu)$  propagating with speed  $c$  into a solid angle  $d\Omega$  about direction  $d\vec{u}$ , and then the number of photons  $dN$  crossing a surface element  $d\vec{A}$  in time  $dt$

$$dN = \psi_\nu(\vec{r}, \vec{u}; t)(\vec{u} \cdot d\vec{A})(c dt) d\Omega d\nu \quad (2.18)$$

where  $(\vec{u} \cdot d\vec{A})(c dt)$  is the volume element containing photons emerging through  $d\vec{A}$  in time  $dt$  in direction  $\vec{u}$ . According to Planck's law, the energy of each photons is  $h\nu$ , so the energy transported by a certain number of photons is

$$dE = ch\nu \psi_\nu(\vec{r}, \vec{u}; t)(\vec{u} \cdot d\vec{A}) d\Omega d\nu dt \quad (2.19)$$

and from the comparison of the equations 2.17 and 2.19 it is found a relation between the specific intensity and the photon number density function.

$$I_\nu(\vec{r}, \vec{u}; t) = ch\nu \psi_\nu(\vec{r}, \vec{u}; t) \quad (2.20)$$

In a general case the radiation pressure  $\vec{P}(\vec{r}; t)$  is a tensor defined such that the element  $P^{ij}$  is the net rate of transport of the  $i$ th component of momentum through area  $dA$  oriented normal to  $j$ th co-ordinate axis. In other words, the radiation pressure tensor due to photons in the frequency range  $(\nu, \nu + d\nu)$  may be expressed as the momentum transported  $(h\nu/c)u^i$  by each photons in the  $i$ th direction and the number of photons  $c\psi_\nu(\vec{r}, \vec{u}; t)u^j$  with frequency  $\nu$  propagating in solid angle  $d\Omega$  about the direction  $u^j$  and crossing surface area  $dA$  in time  $dt$  integrated over all solid angles.

$$P^{ij}(\vec{r}; t) = \oint_{4\pi} c\psi_\nu(\vec{r}, \vec{u}; t) \left( \frac{h\nu}{c} u^i \right) u^j d\Omega = \frac{1}{c} \oint_{4\pi} I_\nu(\vec{r}, \vec{u}; t) u^i u^j d\Omega \quad (2.21)$$

The radiation pressure over the entire frequency range is obtained by integrating

$$\vec{P}(\vec{r}; t) = \frac{1}{c} \int_0^\infty \oint_{4\pi} I_\nu(\vec{r}, \vec{u}; t) u \vec{u} d\Omega \quad (2.22)$$

where  $u\vec{u}$  is the tensor quantity  $[u^i u^j]$ . The last equation is a powerful means to obtain the radiation pressure at any point and in any direction within the field of any source, moreover the radiation pressure on a body placed within the radiation field may be obtained by knowing its surface geometry and its optical properties.

For the purpose of this work, the equation 2.7 is accurate enough for the solar contribution, while the equation 2.22 will be used for the planetary contribution. In particular, it will be assumed that the planetary disc has uniform brightness, so any point of the disc will appear equally bright from any view angle; moreover the specific intensity will be considered time independent and isotropic across the disc. Hence, the PRP exerted on a radially oriented, perfectly reflecting sail at a planet-centred distance  $r$  is

$$P(r) = \frac{2}{c} \int_0^\infty \int_0^{2\pi} \int_0^{\theta_0} I_\nu \cos^2 \theta d\Omega d\nu \quad d\Omega = \sin \theta d\theta d\phi \quad (2.23)$$

where  $\theta_0$  is the angular radius of the disc and is given by  $\arcsin(R_p/r)$ , as shown in fig.2.3. The equation may be simplified noting the azimuthal symmetry and that the specific intensity is independent of the distance.

$$P(r) = \frac{4\pi}{c} I_0 \int_{\xi_0}^1 \xi^2 d\xi \quad \xi = \cos \theta \quad \xi_0 = \cos \theta_0 \quad (2.24)$$

where  $I_0$  is the specific intensity integrated over all the frequency. Solving the integration and substituting for  $\xi_0$  it is found that

$$P(r) = \frac{4\pi}{3c} I_0 \left\{ 1 - \left[ 1 - \left( \frac{R_p}{r} \right)^2 \right]^{3/2} \right\} \quad (2.25)$$

The equation can be simplify expanding in power of  $(R_p/r)^2$  for  $r \gg R_p$ . This assumption is against the idea of using the model close to the planet, but it is useful to find a relation for  $I_0$ .

$$P(r) = \frac{2\pi}{c} I_0 \left( \frac{R_p}{r} \right)^2 + \mathcal{O} \left( \frac{R_p}{r} \right)^4 \quad (2.26)$$

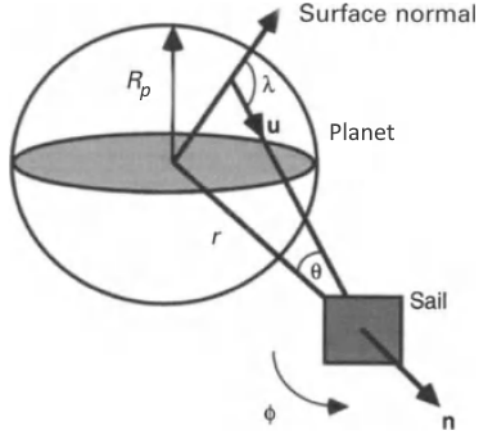


Figure 2.3. Planetary radiation pressure with a finite angular sized disc

At large values of  $r$  this expansion must match asymptotically with the expression for the radiation pressure from a distant point source.

$$P^*(r) = \frac{2}{c} \left( \frac{L}{4\pi R_p^2} \right) \left( \frac{R_p}{r} \right)^2 \quad (2.27)$$

By comparing the two equation, the frequency integrated specific intensity is identified as

$$I = \frac{L_p}{4\pi^2 R_p^2} \quad (2.28)$$

and relation for planetary radiation pressure exerted on a radially oriented solar sail from a uniformly bright, finite angular sized planetary disc is obtained as

$$P(r) = \frac{L_p}{3\pi c R_p^2} \left\{ 1 - \left[ 1 - \left( \frac{R_p}{r} \right)^2 \right]^{3/2} \right\} \quad (2.29)$$

The reason why this last equation is not used to calculate the solar radiation pressure is that after about 10 radii of the source, the deviation from the equation 2.7 tends to zero. The luminosity  $L_p$  of the planet will be analysed in chapter 3.

## Chapter 3

# Three-dimensional model

This chapter aims to create a three-dimensional model that allows calculating the acceleration given by the sail, known its characteristic acceleration and its position and attitude in the three-dimensional space. The characteristic acceleration  $a_o$  is a common way in the literature to compare different designs of the sails and it is defined as the acceleration experienced by a solar sail facing the Sun at a distance of one astronomical unit due to Solar Radiation Pressure. Knowing the characteristic acceleration, the ratio between the mass of the spacecraft and the surface of the sail, called sail loading  $\sigma^*$ , is set; in other words, the dimension of the sail is defined.

As it will be seen in the next sections, the attitude has been determined by two angles, the cone angle  $\alpha$  and the clock angle  $\delta$ , and the model to calculate the acceleration has been implemented in an algorithm to find the two angles that maximise the acceleration in a chosen direction.

In this work, a non-ideal sail is considered; for this reason, the optical properties of the materials have been taken into account.

### 3.1 Acceleration in a optical force model

#### 3.1.1 Two-dimensional introduction

When the optical properties of the material are considered for the calculation of the force, it is possible to develop a more exact model of the radiation pressure. The total force exerted on the sail then may be written as the sum of three different contributions

$$\vec{f} = \vec{f}_r + \vec{f}_a + \vec{f}_e \quad (3.1)$$

where the first term is due to reflection, the second one due to absorption and the third one due to emission of the sail by re-radiation. The contribution of each of them depends on the main optical properties of the sail film and in particular on the reflection coefficient  $\tilde{r}$ , the absorption coefficient  $\tilde{a}$  and the transmission coefficient  $\tilde{\tau}$ . These are linked through the relation

$$\tilde{r} + \tilde{a} + \tilde{\tau} = 1 \quad (3.2)$$

However, for a solar sail the transmission can be considered negligible so the previous equation becomes

$$\tilde{a} = 1 - \tilde{r} \quad (3.3)$$

It is convenient to define two different unit vectors in terms of normal and transverse components.

$$\hat{r} = \cos \alpha \hat{n} + \sin \alpha \hat{t} \quad (3.4)$$

$$\hat{s} = -\cos \alpha \hat{n} + \sin \alpha \hat{t} \quad (3.5)$$

where  $\hat{r}$  is the direction of the incident photons and  $\hat{s}$  is the direction of the reflected ones. The angle  $\alpha$  is generally called pitch angle in the two-dimensional model or cone angle in the three-dimensional one and is the angle between the incident photons and the normal of the surface. If all incident photons are absorbed, the force exerted on the sail will be in the direction  $\hat{r}$  and may be written as

$$\vec{f}_a = PA (\hat{r} \cdot \hat{n}) \hat{r} = PA \left( \cos^2 \alpha \hat{n} + \cos \alpha \sin \alpha \hat{t} \right) \quad (3.6)$$

However, a fraction  $\tilde{r}$  of the photons is reflected and, assuming that the reflection is only specular to the incident photons, it provides a force in the direction  $-\hat{s}$

$$\vec{f}_r = -\tilde{r} PA (\hat{r} \cdot \hat{n}) \hat{s} = \tilde{r} PA \left( \cos^2 \alpha \hat{n} - \cos \alpha \sin \alpha \hat{t} \right) \quad (3.7)$$

The last force component is that due to photons absorbed and then re-emitted as thermal radiation, however this contribution is typically an order of magnitude lower than the other two, so for this analysis it has been neglected. Substituting 3.3 in the previous relations, it is found

$$\hat{f}_n = PA(1 + \tilde{r}) \cos^2 \alpha \hat{n} \quad (3.8)$$

$$\hat{f}_t = PA(1 - \tilde{r}) \cos \alpha \sin \alpha \hat{t} \quad (3.9)$$

It is evident that if the sail is a perfect reflector, the coefficient  $\tilde{r}$  will be 1 and the force will have only a normal component. Dividing by the mass, the acceleration can be found

$$\hat{a}_n = \frac{P}{\sigma^*} (1 + \tilde{r}) \cos^2 \alpha \hat{n} \quad (3.10)$$

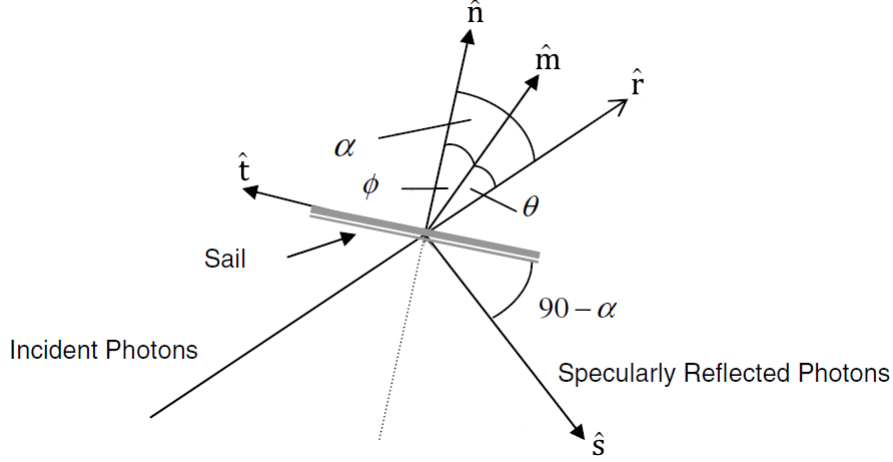
$$\hat{a}_t = \frac{P}{\sigma^*} (1 - \tilde{r}) \cos \alpha \sin \alpha \hat{t} \quad (3.11)$$

where again  $\sigma^*$  is the sail loading. The magnitude of the acceleration can be easily calculated through the norm of the two relations above. As regards its direction, as previously mentioned, a transverse component exists due to the optical properties of a non-ideal sail. In particular, there is an offset angle  $\phi$  between the normal to the surface and the acceleration vector  $\hat{m}$ , as shown in fig. 3.1. According to [23] this offset angle can be calculated using the optical coefficients and in particular

$$\tan \phi = \frac{h}{g} \tan \alpha \quad (3.12)$$

where in the simplified case in exam

$$g = 1 + \tilde{r} \quad (3.13)$$


 Figure 3.1. Offset angle between  $\hat{n}$  and  $\hat{m}$  [23]

$$h = 1 - \tilde{r} \quad (3.14)$$

The angle  $\phi$  is related to  $\alpha$ , but it could be easier to use a new angle,  $\theta$ , defined as the one between  $\hat{m}$  and  $\hat{r}$ .

$$\theta = \alpha - \phi \quad (3.15)$$

$$\tan \theta = \frac{(g - h) \tan \alpha}{g + h \tan^2 \alpha} \quad (3.16)$$

### 3.1.2 Three-dimensional extension

According to the optical laws, the reflection takes place always in the plane of the incident ray and the normal of the surface, for this reason the magnitude of acceleration in the two-dimensional and three-dimensional cases has to be the same. The relation of the magnitude has been developed from the normal and transverse components previously presented.

$$a = \sqrt{a_n^2 + a_t^2}$$

$$a = \frac{P}{\sigma^*} \sqrt{(1 + \tilde{r})^2 \cos^4 \alpha + (1 - \tilde{r})^2 \cos^2 \alpha \sin^2 \alpha}$$

$$a = \frac{P \cos \alpha}{\sigma^*} \sqrt{(1 + \tilde{r})^2 \cos^2 \alpha + (1 - \tilde{r})^2 \sin^2 \alpha}$$

$$a = \frac{P}{\sigma^*} \sqrt{\cos^2 \alpha + 2\tilde{r} \cos^2 \alpha + \tilde{r}^2 \cos^2 \alpha + \sin^2 \alpha + \tilde{r}^2 \sin^2 \alpha - 2\tilde{r} \sin^2 \alpha \cos \alpha}$$

$$a = \frac{P \cos \alpha}{\sigma^*} \sqrt{1 + \tilde{r}^2 + 2\tilde{r} (\cos^2 \alpha - \sin^2 \alpha)}$$

$$a = \frac{P \cos \alpha}{\sigma^*} \sqrt{1 + \tilde{r}^2 + 2\tilde{r} (2 \cos^2 \alpha - 1)} \quad (3.17)$$

The obtained equation agrees with the three dimensional model presented by Prof. McInnes [1] for an ideal sail and can be used both for Solar and Planetary Radiation Pressure, paying attention to the different pressure and cone angle  $\alpha$ . Known the magnitude, the direction is necessary to determine completely the acceleration vector.

Substituting  $0^\circ$  as cone angle, it is found the relation of the characteristic acceleration

$$a_o = (1 + \tilde{r}) \frac{P}{\sigma^*} \quad (3.18)$$

It is now useful to define three different reference systems. The first one (from now on  $a$

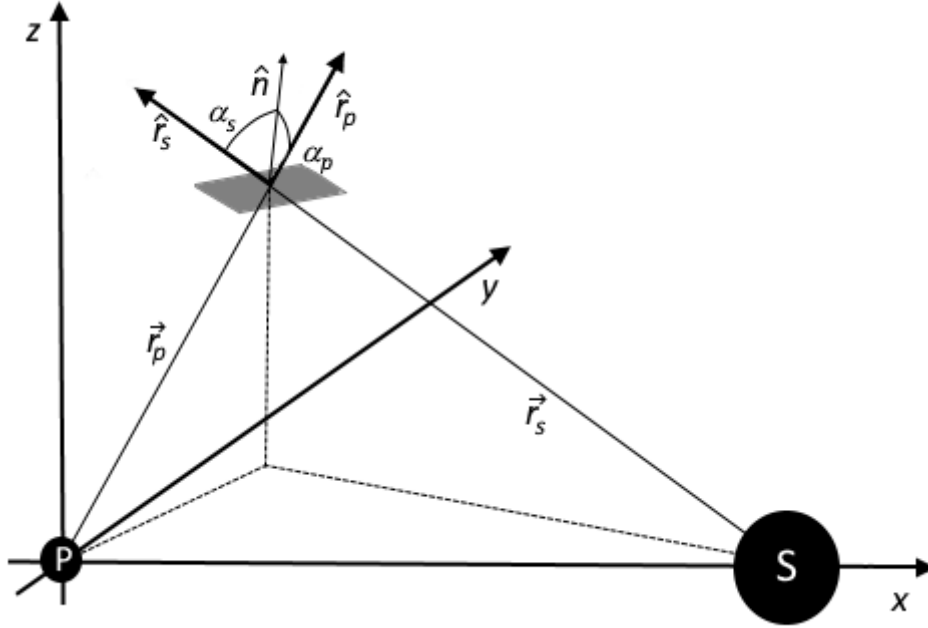


Figure 3.2. Reference system  $a$  or  $xyz$

or  $xyz$ ) has its origin in the centre of the planet, the  $x$  axis with the direction and verse of the line from the centre of the planet to the centre of the Sun, the  $z$  axis parallel to the angular velocity of the Earth about the Sun and the  $y$  axis orthogonal to the other two. A representation is shown in fig.3.2. The second and the third reference systems are called  $b$  and  $c$ , and are strictly related to the source whence the photons are emitted or reflected. In the case of the reference system  $b$ , the origin is in the centre of the sail, and its first axis coincides with the direction of the photons coming from the planet due to black body or albedo radiation; in other words, the first axis is the normalised vector that goes from the centre of the planet to the centre of the sail, the other two axes are calculated by the cross product with  $\vec{\omega}$ , where  $\vec{\omega}$  is the angular velocity of the Earth about the Sun and so corresponds to  $z$  direction.

$$\left[ \frac{\vec{r}_p}{|\vec{r}_p|}, \frac{\vec{\omega} \times \vec{r}_p}{|\vec{\omega} \times \vec{r}_p|}, \frac{\vec{r}_p \times (\vec{\omega} \times \vec{r}_p)}{|\vec{r}_p \times (\vec{\omega} \times \vec{r}_p)|} \right] \quad (3.19)$$

The vector  $\vec{r}_p$  is known in reference system  $a$  and is  $\vec{r}_p = [x_p, y_p, z_p]$ , so it is easy to translate vectors from a reference system to the other.

The transformation from  $a$  to  $b$  can be done with the rotation matrix

$$C_{a/b} = \left[ \frac{\vec{r}_p}{|\vec{r}_p|}, \frac{\vec{\omega} \times \vec{r}_p}{|\vec{\omega} \times \vec{r}_p|}, \frac{\vec{r}_p \times (\vec{\omega} \times \vec{r}_p)}{|\vec{r}_p \times (\vec{\omega} \times \vec{r}_p)|} \right]^T \quad (3.20)$$

The inverse matrix of  $C_{a/b}$  is required to do the opposite operation, but it can be demonstrated that  $C_{a/b}$  is an orthogonal matrix, so its inverse is equal to its transpose.

$$C_{b/a} = [C_{a/b}]^{-1} = [C_{a/b}]^T \quad (3.21)$$

Following [1], the attitude of the sail can be defined by the normal of the surface thanks to two angles, the cone angle  $\alpha_p$ , already introduced in the two-dimensional model and defined as the angle between  $\hat{n}$  and  $\hat{r}_p$ , and the clock angle  $\delta_p$ , defined as the angle between the projection of the sail normal and a reference direction onto a plane normal to the incident photons, in this case  $\frac{\vec{r}_p \times (\vec{\omega} \times \vec{r}_p)}{|\vec{r}_p \times (\vec{\omega} \times \vec{r}_p)|}$ . A representation is shown in fig.3.3.

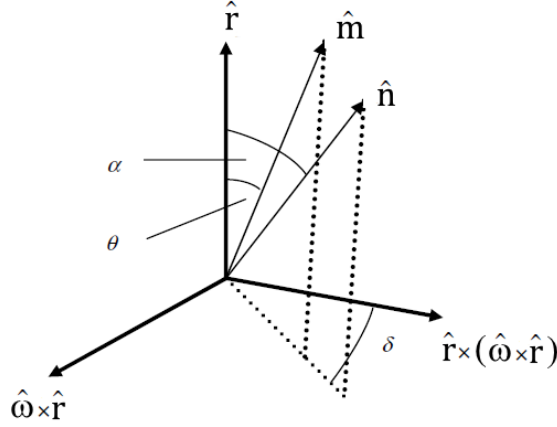


Figure 3.3. Acceleration unit vector  $m$  in a generic reference system [23]

The normal vector may be written in the reference system  $b$  and can be transported in  $a$  with the rotation matrix previously defined.

$$\hat{n}^b = [\cos \alpha_p, \sin \alpha_p \sin \delta_p, \sin \alpha_p \cos \delta_p] \quad (3.22)$$

$$\hat{n}^a = C_{b/a} \hat{n}^b = [C_{a/b}]^T \hat{n}^b \quad (3.23)$$

The defined normal vector takes as reference the front surface, for the back surface it is exactly the opposite

$$\hat{n}_b^a = -\hat{n}_f^a \quad (3.24)$$

Known the angle  $\alpha_p$ , it is possible to calculate  $\theta_p$  according to 3.16; the acceleration unit vector may be written as

$$\hat{m} = [\cos \theta, \sin \theta \sin \delta, \sin \theta \cos \delta] \quad (3.25)$$

The third reference system  $c$  is defined in the same way of  $b$ , but in this case, its first axis coincides with the direction of the photons coming from the Sun. Again the other two axes are calculated by the cross product with  $\vec{\omega}$ .

$$\left[ \frac{\vec{r}_s}{|\vec{r}_s|}, \frac{\vec{\omega} \times \vec{r}_s}{|\vec{\omega} \times \vec{r}_s|}, \frac{\vec{r}_s \times (\vec{\omega} \times \vec{r}_s)}{|\vec{r}_s \times (\vec{\omega} \times \vec{r}_s)|} \right] \quad (3.26)$$

with

$$\vec{r}_s = [R_{P/S_x} - x, R_{P/S_y} - y, R_{P/S_z} - z] \quad (3.27)$$

As for the  $b$  reference system, it is possible to define a normal vector to the surface.

$$\hat{n}^c = [\cos \alpha_s, \sin \alpha_s \sin \delta_s, \sin \alpha_s \cos \delta_s] \quad (3.28)$$

From a practical point of view, defining two other angles, it is not the best solution for the analysis. The normal vector is already defined in the reference system  $b$ , so the attitude of the sail is set in three-dimensional space. The only angle that must be known to calculate the magnitude of the acceleration due to the Solar Radiation Pressure is  $\alpha_s$ , and from its definition, it is the angle between the normal and solar rays unit vectors. Since both are known in the  $xyz$  reference system, it can be found

$$\alpha_s = \arccos(\hat{n}^a \cdot \hat{r}_s^a) \quad (3.29)$$

Seeing as  $\delta_s$  is not easy to be calculated as  $\alpha_s$ , another strategy has been taken into account to compute the acceleration unit vector. Since it lies on the  $\hat{n}_s - \hat{r}_s$  plane, it may be calculated rotating  $\hat{r}_s$  of the angle  $\theta$ . Both for the front and the back surfaces the angle  $\theta_s$  is calculated thanks to the formula proposed by [23]. The rotation is about the orthogonal axis of  $\hat{n} - \hat{r}_s$

$$p_f = \frac{\hat{n} \times \vec{r}_s}{|\hat{n} \times \vec{r}_s|} \quad (3.30)$$

$$p_b = \frac{(-\hat{n}) \times \vec{r}_s}{|(-\hat{n}) \times \vec{r}_s|} \quad (3.31)$$

The rotation matrix was taken from [24]

$$M_{p_t} = \begin{bmatrix} p_x^2 + (p_y^2 + p_z^2) \cos \theta & p_x p_y (1 - \cos \theta) - p_z \sin \theta & p_x p_z (1 - \cos \theta) + p_y \sin \theta \\ p_x p_y (1 - \cos \theta) + p_z \sin \theta & p_y^2 + (p_x^2 + p_z^2) \cos \theta & p_y p_z (1 - \cos \theta) - p_x \sin \theta \\ p_x p_z (1 - \cos \theta) - p_y \sin \theta & p_y p_z (1 - \cos \theta) + p_x \sin \theta & p_z^2 + (p_x^2 + p_y^2) \cos \theta \end{bmatrix} \quad (3.32)$$

Using this matrix, the acceleration unit vector can be found and multiplied to the magnitude

$$\hat{m}_{s_f}^a = (M_{p/t_f} \hat{r}_s^T)^T \quad (3.33)$$

$$\hat{m}_{s_b}^a = (M_{p/t_b} \hat{r}_s^T)^T \quad (3.34)$$

## 3.2 Radiation Pressure contribution

The previous section focused on the acceleration unit vector and the generic formulation of the magnitude of the sail in a non-ideal optical model force. In this section, the radiation pressure of the single contributions has been examined in depth.

### 3.2.1 Evaluation of the SRP contribution

All the ingredients to calculate the acceleration due to Solar Radiation Pressure have been already presented. As previously mentioned, since the distance from the Sun is further than ten solar radii, it is possible to use the inverse square law 2.7 and 2.8

$$P(r_s) = \frac{W}{c} = \frac{W_p}{c} \left( \frac{R_{sp}}{r_s} \right)^2 \quad (3.35)$$

where  $W_p$  is the solar energy flux at the planet distance,  $c$  is the speed of light,  $R_{sp}$  the average distance of the planet from the Sun, and  $r_s$  the distance of the sail from the Sun. The relation of the SRP is then substituted in the general equation of the acceleration magnitude 3.17.

$$\vec{a}_{SRP} = \frac{W_p \cos \alpha_s}{c\sigma^*} \left( \frac{R_{sp}}{r_s} \right)^2 \sqrt{1 + \tilde{r}^2 + 2\tilde{r} (2 \cos^2 \alpha_s - 1)} \hat{m}_s \quad (3.36)$$

where the cone angle  $\alpha_s$  and the acceleration unit vector  $\hat{m}$  have been previously defined. The acceleration due to SRP is zero in the umbra region since the sail is in eclipse. For this study, the eclipse area has been modelled as a cylindrical shadow with a radius equal to the one of the planet; in fact, seeing as the sail is far from the Sun, the divergence of solar rays is small, and they can be assumed as parallel. This simple model does not consider the penumbra but gives a good approximation.

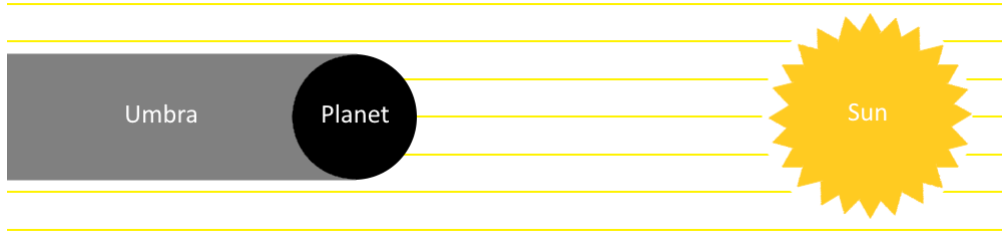


Figure 3.4. Cylindrical eclipse model

### 3.3 Evaluation of the PRP contribution

According to [1] and [21], and as found with radiative transfer methods for a planet modelled as a uniformly bright finite angular size disc, the planetary radiation pressure is

$$P(r_p) = \frac{L_{PRP}}{3\pi c R_p^2} \left\{ 1 - \left[ 1 - \left( \frac{R_p}{r_p} \right)^2 \right]^{\frac{3}{2}} \right\} \quad (3.37)$$

that substituted in the generic acceleration relation

$$\vec{a}_{PRP} = \frac{L_{PRP} \cos \alpha_p}{3\pi c R_p^2 \sigma^*} \left\{ 1 - \left[ 1 - \left( \frac{R_p}{r_p} \right)^2 \right]^{\frac{3}{2}} \right\} \sqrt{1 + \tilde{r}^2 + 2\tilde{r} (2 \cos^2 \alpha_p - 1)} \hat{m}_p \quad (3.38)$$

where  $L_{PRP}$  is the planetary luminosity and has a component caused by Black Body Radiation  $L_{BBRP}$  and one caused by Albedo Radiation  $L_{ARP}$ .

$$L_{PRP} = L_{ARP} + L_{BBRP} \quad (3.39)$$

### 3.3.1 Albedo Radiation Pressure

The albedo represents the fraction of the solar radiation that strikes the planet and is reflected. It can be defined in different ways, in the NASA planetary fact sheet two are presented:

- the geometric albedo, as «The ratio of the body's brightness at a phase angle of zero to the brightness of a perfectly diffusing disk with the same position and apparent size, dimensionless. V-band ( $0.549\mu m$ ). Earth is highly variable» (Dr. David R. Williams, NASA)
- the bond albedo, as «The fraction of incident solar radiation reflected back into space without absorption, dimensionless. Also called planetary albedo» (Dr. David R. Williams, NASA)

Apparently, in this study, the bond albedo should be the most suitable. The calculation of albedo contribution is based on [19].

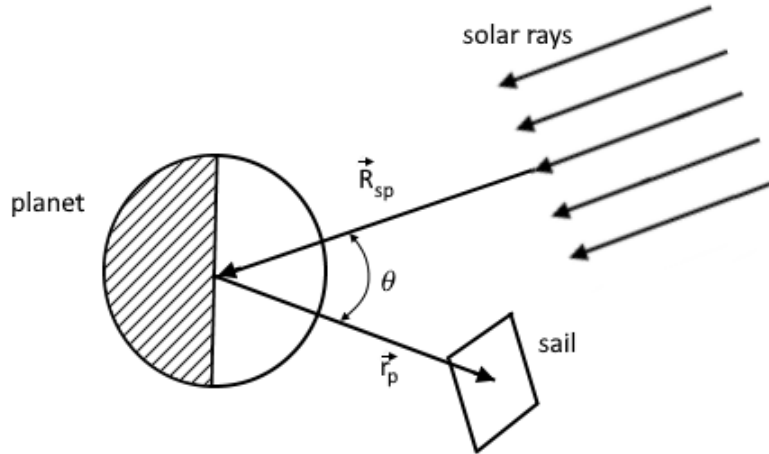


Figure 3.5. Reflection angle

The albedo flux can be written as

$$q_a = W_p \zeta F \cos \theta \quad (3.40)$$

where  $W_p$  is the solar flux at the planet orbit,  $\zeta$  is the bond albedo,  $F$  is a view factor (also called shape factor or configuration factor) and represents the fraction of the total radiant

energy that leaves the planet and strikes the sail surface,  $\theta$ , in this case, is the reflection angle. As shown in fig. 3.5, the reflection angle is the angle between the vector  $\vec{R}_{sp}$  that represents the distance of the planet from the Sun and the position vector of the sail relative to the planet  $\vec{r}_p$ . The value of  $\zeta$  should change both seasonally and geographically, but in this study, a mean value (according to NASA fact sheet) is used. The eq. 3.40 results in a value per square meter [ $W/m^2$ ], but in the equation of the force the luminosity  $L$  represents the power that goes from the source to the sail. Considering the planet as disk uniformly bright, the luminosity due to ARP becomes

$$L_{ARP} = q_a \pi R_p^2 \quad (3.41)$$

In [25], it is shown that a surface orbiting a planet can be oriented such that either one side or both sides are heated.

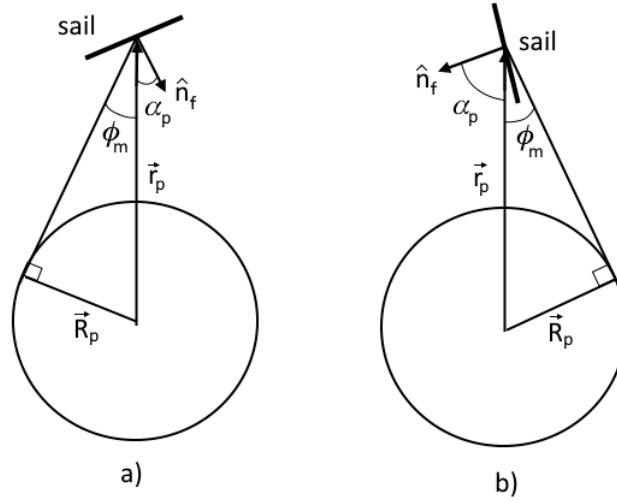


Figure 3.6. Surface heated by the photons flux

If only one side is heated,

$$\lambda + \phi_m \leq \frac{\pi}{2} \quad (3.42)$$

and the view factor is given by

$$F = \frac{\cos \lambda}{H^2} \quad (3.43)$$

where  $\lambda$  is the angle between the surface normal and the heat flux, and  $H = \frac{r_p}{R_p}$ . Seeing as it has been assumed that the heat flux arrives radially from the planet, in this work,  $\lambda$  corresponds to  $\alpha_p$ . The radius of the planet is  $R_p$ , and the distance from the centre of the planet to the heated surface is  $r_p$ . The angle  $\phi_m$  is defined in fig. 3.6 and it is equal to the  $\phi_m = \arcsin\left(\frac{1}{H}\right)$ . If both sides of the surface are heated,

$$\frac{\pi}{2} - \phi_m < \lambda \leq \frac{\pi}{2} + \phi_m \quad (3.44)$$

and a separate view factor must be calculated for each side. The total view factor for the surface is then the sum of the two. For each side the view factor is given by

$$F = \frac{2}{\pi} \left( \frac{\pi}{4} - \frac{1}{2} \arcsin \left( \frac{\sqrt{H^2 - 1}}{H \sin \lambda} \right) + \frac{2}{H^2} \left\{ \cos \lambda \arccos \left[ -\sqrt{H^2 - 1} \cot \lambda \right] + \right. \\ \left. -\sqrt{H^2 - 1} \sqrt{1 - H^2 \cos^2} \right\} \right) \quad (3.45)$$

So, in the analysis of the albedo contribution there are three different possibilities:

- the back surface is the one hit by the photons;
- the front surface is the one hit by the photons;
- both the surfaces are hit by the photons.

For the first two cases  $\lambda + \phi_m \leq \frac{\pi}{2}$ , so it is calculated the relative view factor for the back or the front surface with eq. 3.43 and then photons flux, luminosity and acceleration. For the third case, all values are calculated for both the surfaces and then they are summed up for the acceleration. Since the albedo is related to the reflection of light from the planet, its contribution is equal to zero in the area where the surface of the planet is not hit by the sun rays and so cannot reflect photons, in other words when  $x < 0$ .



Figure 3.7. Area where the Albedo Radiation Pressure exists

### 3.3.2 Black Body Radiation Pressure

If the planet is considered as a black body in equilibrium with its environment, it will emit photons according to the Stefan-Boltzmann Law, with luminosity

$$L_{BBRP} = 4\pi R_p^2 F \bar{\sigma} T_p^4 \quad (3.46)$$

where  $R_p$  is the radius of the planet,  $T_p$  is its mean temperature,  $F$  is the same view factor used for ARP and  $\bar{\sigma} = 5.670370.10^{-8} W/(m^2 K^4)$  is the Stefan-Boltzmann constant. The contribution of Black Body Radiation is uniform around the planet and goes in the radial direction. As for the ARP, there are three different possible cases; when the scalar product  $\hat{r}_p \cdot \hat{n}$  is positive, the normal is concordant with the direction of the planetary photons, so these will strike the back surface of the sail; instead, when the scalar product

is negative, the normal is pointing towards the source so that the photons will strike the front surface. In this case, since  $\frac{\pi}{2} < \alpha_p < \frac{3\pi}{2}$ , a minus is required in front of the equation. The components of the acceleration are calculated by the product of the magnitude with the unit vectors  $\hat{m}_f^a$  or  $\hat{m}_b^a$ .

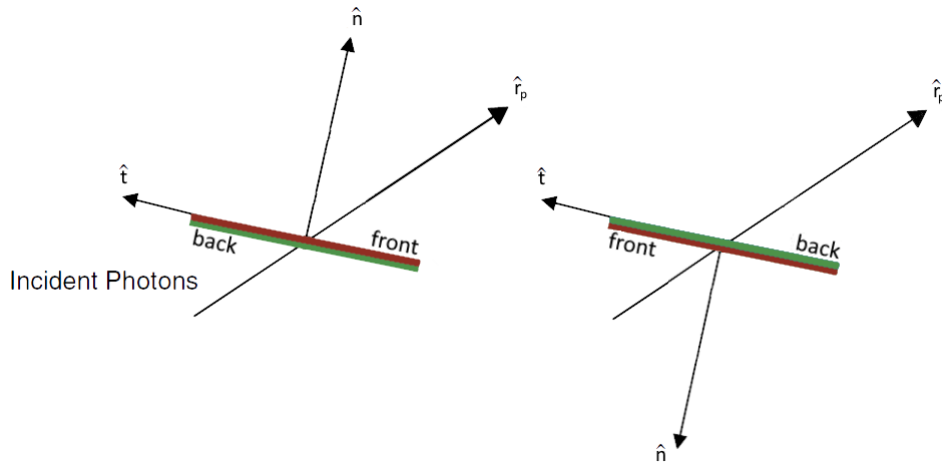


Figure 3.8. Sail surface struck by the photons



## Chapter 4

# Evaluation of attainable values of acceleration

The model presented in the previous chapters has been used to analyse the possible acceleration around some planets and in particular the Earth and Venus. The first one has been chosen for the many possible applications studied in the literature, while the second one for the promising results obtained in the two-dimensional analysis by De Iuliis [21]. Known the position in three dimensional space and the features of the sail, the MATLAB script scans all the combinations of cone angle  $\alpha_p$  and clock angle  $\delta_p$  and calculates for each set the corresponding acceleration. Then, the results have been compared with the required acceleration vector, the one closer is picked, and its attitude has been chosen as the optimal attitude for the sail in that point. This process has been conducted in a grid of points ( $50 \times 50$ ) around the planet, for 60 angles between 0 and  $2\pi$ . The reason why a two-dimensional grid has been chosen is to simplify the visualisation of the results, however, as it will be seen in the following chapters, every point of the three-dimensional space can be analysed, allowing to study orbits with different inclination. Since the aerodynamic forces have not been considered, in order to avoid the atmosphere only points at least 400 km above the planet surface have been taken into account. The sail surface has typically a reflective coating that changes its optical properties and usually maximises the reflection coefficient  $\tilde{r}$ . The coating can be used for both the sides of the surface or only the front one. In this part of the work, the two different cases have been analysed and in particular:

- single side coating, where the front surface has  $\tilde{r} = 0.9$  and  $\tilde{a} = 0.1$ , while the back surface has  $\tilde{r} = 0.1$  and  $\tilde{a} = 0.9$ ;
- double sides coating, where both the front and the back surfaces have  $\tilde{r} = 0.9$  and  $\tilde{a} = 0.1$ ;

The sail loading has been set equal to  $0.1 \text{ kg/m}^2$ , and consequently the characteristic acceleration is  $8.5559 \cdot 10^{-5} \text{ m/s}^2$  for the front surface. The data for the two planet are shown in table 4.1

The analysis has been conducted searching for the best acceleration in the radial and transverse direction that the sail can provide in the region around the planet. Moreover,

	$R_p$	$R_{sp}$	$T_m$	$\zeta$	$W$
Venus	6070 km	$57.91 \cdot 10^6 km$	737 K	0.76	2601 W
Earth	6378 km	$146.6 \cdot 10^6 km$	288 K	0.306	1350 W

Table 4.1. Data of the planets [Nasa planetary data sheet]

some specific points have been examined in depth to make a comparison with the two dimensional results [21] and to validate the model.

## 4.1 Radial Acceleration

The first analysis has been done for the radial case in the  $x - z$  plane. The results have been normalised with the characteristic acceleration so that they do not depend on the sail geometry and are valid for every flat sail regardless mass of the spacecraft or surface of the sail. For each study-case, the different contributions of SRP, BBRP and ARP have been studied first separately and then together. In particular, the following section shows the cases with:

- SRP only;
- ARP only;
- BBRP only;
- SRP+PRP;

The region of study is  $-3R_p \leq x \leq 3R_p$  and  $-3R_p \leq z \leq 3R_p$ . The points chosen for the comparison of the two coating cases are:

- $A=(2R_p, 0, -2R_p)$ ;
- $B=(3R_p, 0, 0)$ ;
- $C=(R_p, 0, 3R_p)$ ;
- $D=(-3R_p, 0, R_p)$ ;
- $E=(-2R_p, 0, 0)$ ;
- $F=(-R_p, 0, -3R_p)$ ;

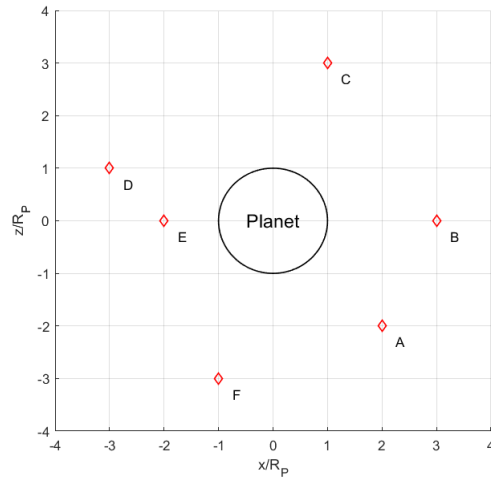


Figure 4.1. Points chosen for the validation of the model

### 4.1.1 Solar Radiation Pressure

This section focuses on the SRP contribution.

#### Earth

The first plots shown refers to the Earth.

The two cases, with single-side coating 4.3 and double-side coating 4.2, do not present

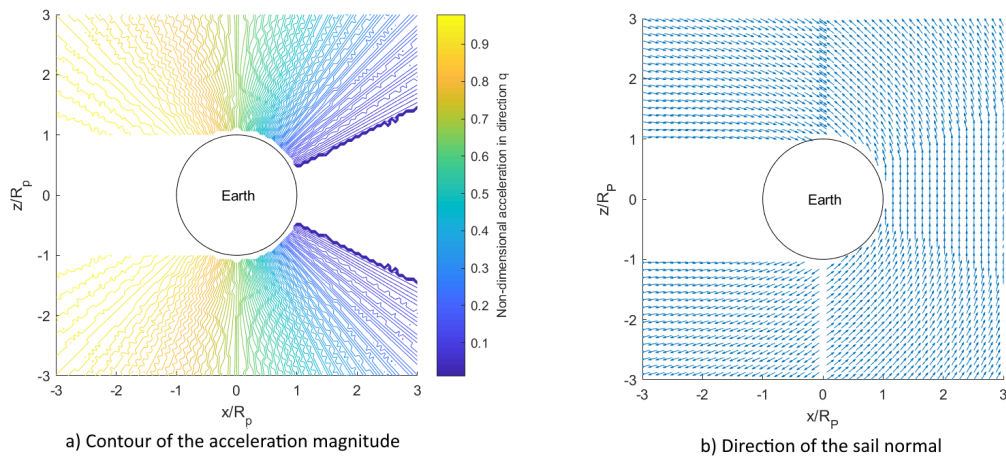


Figure 4.2. Maximisation of the radial acceleration for a double-coating sail around Earth subject to SRP

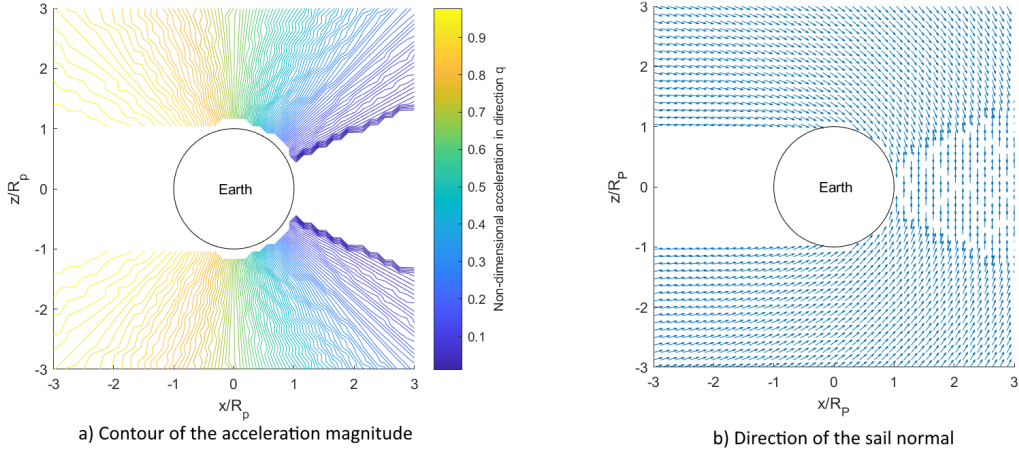


Figure 4.3. Maximisation of the radial acceleration for a single-coating sail around Earth subject to SRP

many differences and in both of them it is evident the umbra area where the SRP is zero. In 4.3 b) and 4.2 b), in the area between the Earth and the Sun, since the photons arrive in the opposite direction of the required acceleration, they cannot provide a positive radial contribution, so the sail gets in a perpendicular position to the solar rays to have a null acceleration instead of a negative one. Seeing as the direction of the solar rays has a small component radial to the planet, the non-dimensional magnitude is mostly less than one, and it only increases when the two vectors tend to align.

In the case of double-side coating, and particularly in this work since the optical properties of the two sides are the same, the advantage is that the analysis can be speeded up scanning half of the angles range from  $0$  to  $\pi$ , but with the same accuracy. The abrupt discontinuity in the attitude in 4.2 b) are due to this simplification, but seeing as the acceleration does not change, in an actual scenario there are no sudden changes in the attitude of the solar sail.

In table 4.2, the difference in the attitude of the two coating is minimal, and in the worst case analysed (point D) it is less than one degree. For the attitude analysis of the six points, the range of angles has been split in 360. The result is in line with what expected; seeing as the Sun has been considered as a point, its photons can hit only one of the two sides of sail, so there is no difference between the cases. In the three other cases, a more relevant effect is expected.

Point	Single-side	Double-side	Ratio
A	1.8727	1.8779	99.72%
B	4.7255	4.7212	100.09%
C	4.2355	4.2473	99.72%
D	2.9228	2.9310	99.72%
E	—	—	—
F	3.9379	3.9314	100.17%

Table 4.2. Comparison of the cone angle  $\alpha_p$  for single-side and double-side coating in Earth area with only SRP [rad]

### Venus

The analysis has been repeated for Venus, showing similar results. For this reason, the comments are analogous. The different magnitude of the acceleration is clearly due to the closer distance from the Sun; as shown in table 4.1 the solar flux at Venus orbit is about double the one at Earth orbit.

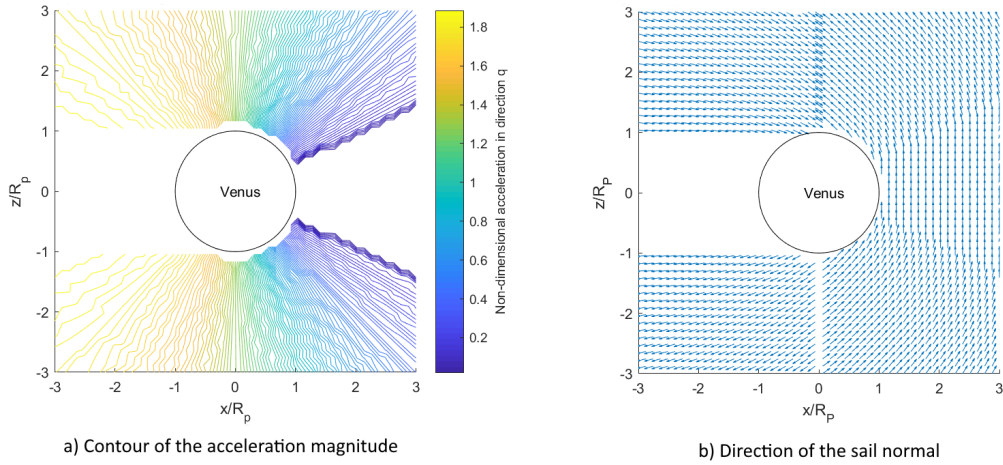


Figure 4.4. Maximisation of the radial acceleration for a double-side coating sail around Venus subject to SRP

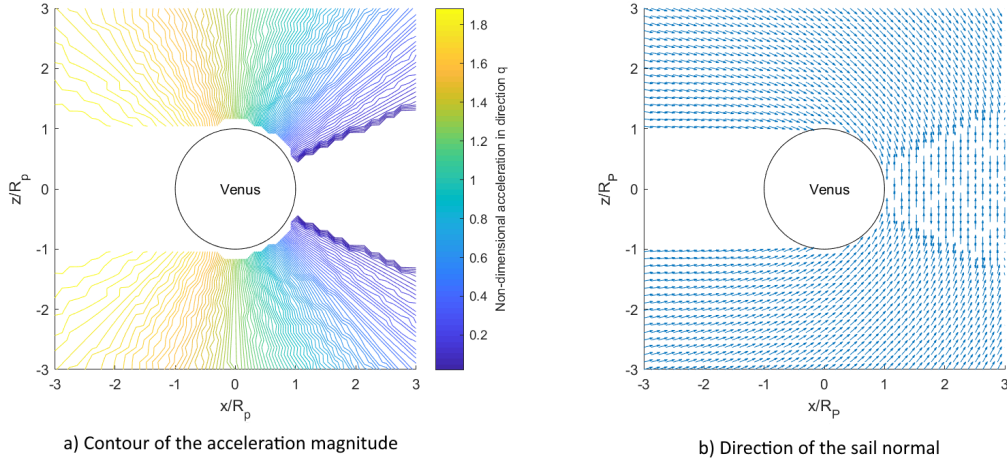


Figure 4.5. Maximisation of the radial acceleration for a single-side coating sail around Venus subject to SRP

Point	Single-side	Double-side	Ratio
A	1.8727	1.8779	99.72%
B	4.7255	4.7212	100.09%
C	4.2355	4.2473	99.72%
D	2.9228	2.9310	99.72%
E	—	—	—
F	3.9379	3.9314	100.17%

Table 4.3. Comparison of the cone angle  $\alpha_p$  for single-side and double-side coating in Venus area with only SRP [rad]

### 4.1.2 Albedo Radiation Pressure

This section focuses on the ARP contribution. As previously mentioned, its contribution exists only for positive  $x$ , where the planet can reflect the solar photons.

#### Earth

Again, the first results shown are about Earth.

The albedo contribution provides a radial acceleration in a region where SRP cannot due to its direction. However, for the Earth, the acceleration seems relevant only in the area very close to the planet. The dominating contribution will be visualised in the analysis with both SRP and PRP.

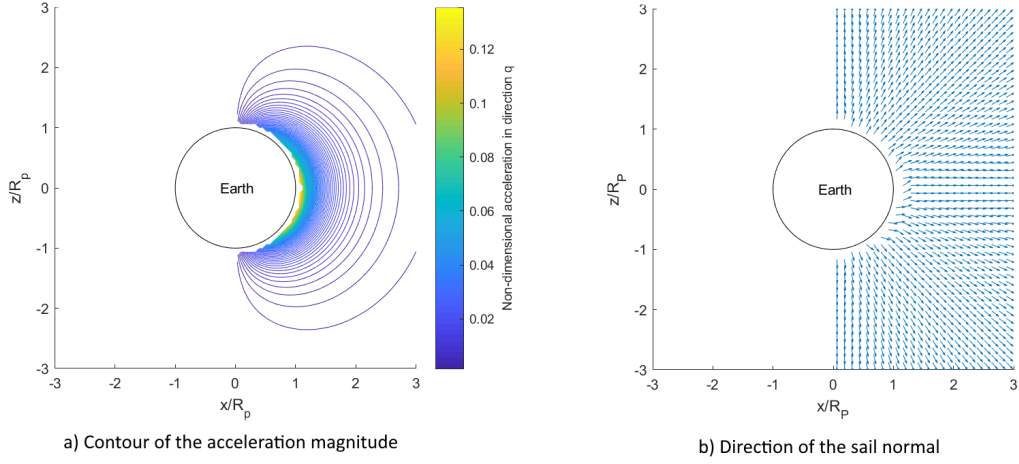


Figure 4.6. Maximisation of the radial acceleration for a double-side coating sail around Earth subject to ARP

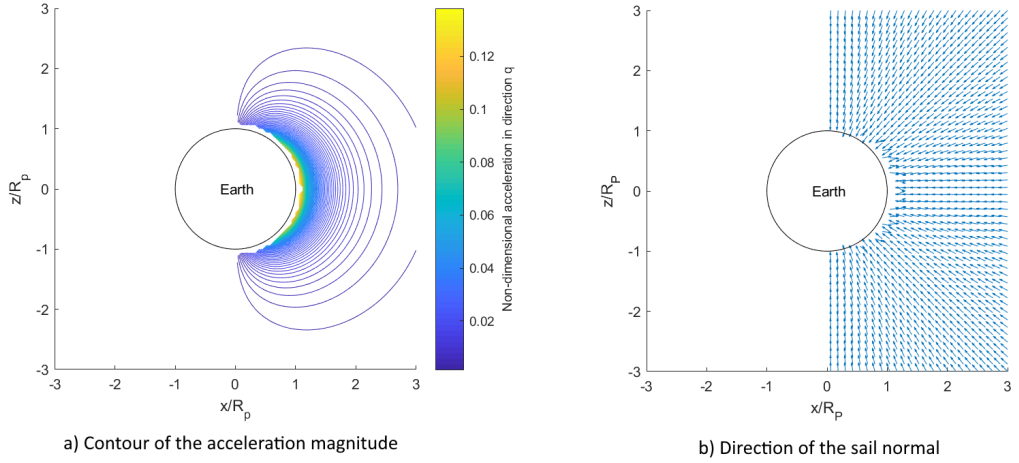


Figure 4.7. Maximisation of the radial acceleration for a single-side coating sail around Earth subject to ARP

Point	Single-side	Double-side	Ratio
A	3.1503	3.1416	100.28%
B	3.1503	3.1416	100.28%
C	3.1503	3.1416	100.28%

Table 4.4. Comparison of the cone angle  $\alpha_p$  for single-side and double-side coating in Earth area with only ARP [rad]

## Venus

The effect of the albedo becomes more relevant around Venus than around the Earth. In addition to the closer distance from the Sun, Venus has a higher albedo coefficient, and for this reason, the magnitude of the acceleration is more than double. The attitude of the sail does not change for the two coating case, as seen in table 4.5.

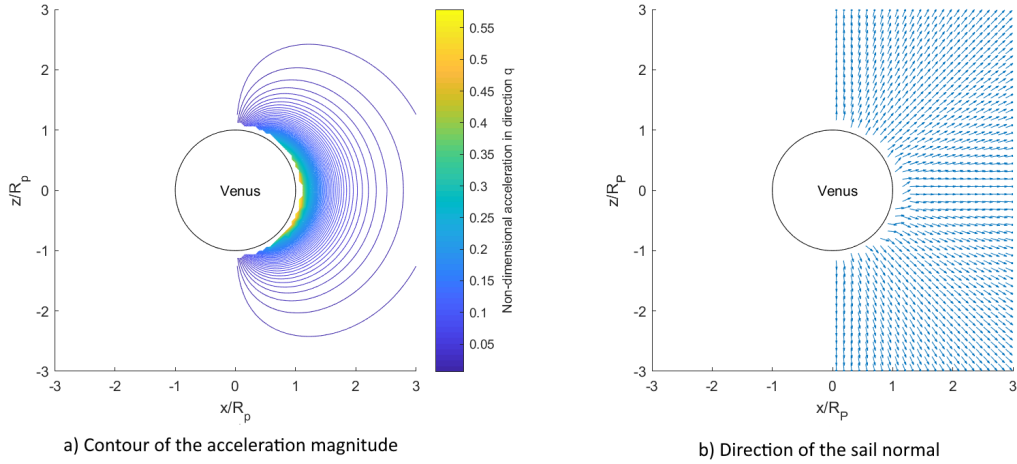


Figure 4.8. Maximisation of the radial acceleration for a double-side coating sail around Venus subject to ARP

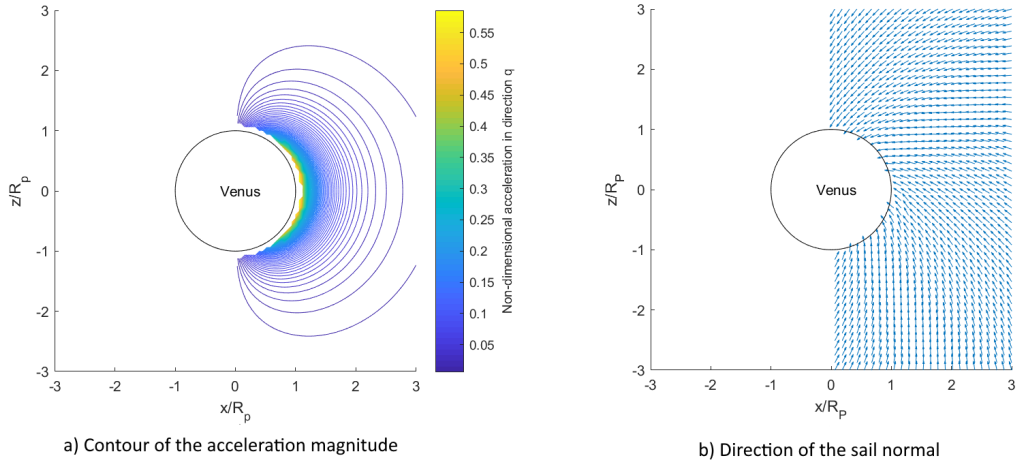


Figure 4.9. Maximisation of the radial acceleration for a single-side coating sail around Venus subject to ARP

Point	Single-side	Double-side	Ratio
A	3.1328	3.1416	99.72%
B	3.1503	3.1416	100.28%
C	3.1503	3.1416	100.28%

Table 4.5. Comparison of the cone angle  $\alpha_p$  for single-side and double-side coating in Venus area with only ARP [rad]

### 4.1.3 Black Body Radiation Pressure

The BBRP contribution is particularly relevant because it is the only radiation pressure that hits the sail in the eclipse region. Its magnitude can drastically change with the characteristics of the study planet; as it will see, for Venus BBRP is by far the dominating effect.

#### Earth

As anticipated, BBRP is uniform around the planet and mostly radial. The attitude analysis of the six points has been avoided, seeing that the two cases do not present differences; as previously mentioned, these are expected in the complete case.

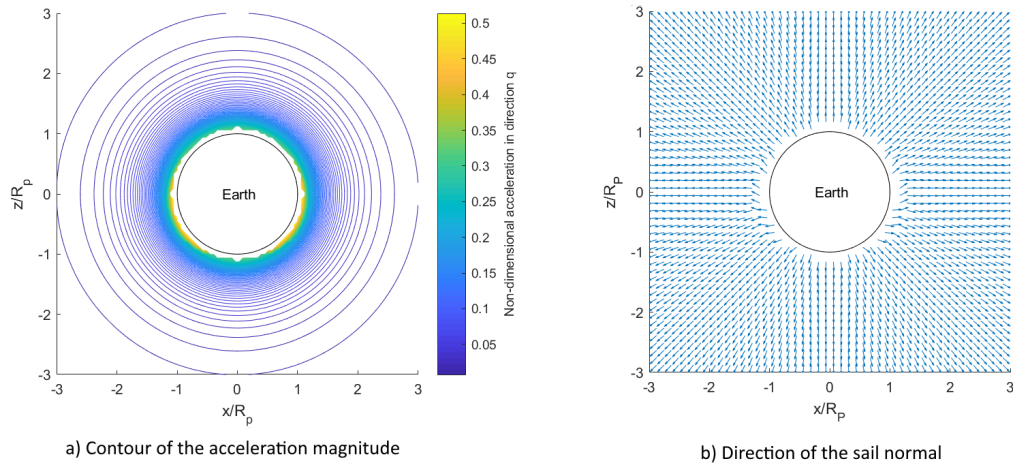


Figure 4.10. Maximisation of the radial acceleration for a double-side coating sail around Earth subject to BBRP

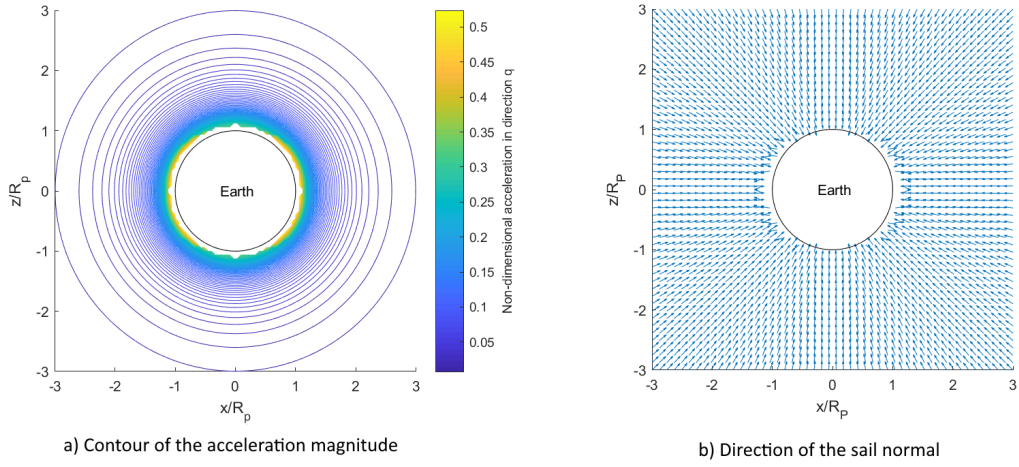


Figure 4.11. Maximisation of the radial acceleration for a single-side coating sail around Earth subject to BBRP

## Venus

Among the results of the planetary contribution, those for the black body radiation pressure of Venus are the most relevant. Due to its high mean temperature, Venus has by far a greater luminosity than Earth so that its BBRP provides a significant acceleration increase in a large area around the planet.

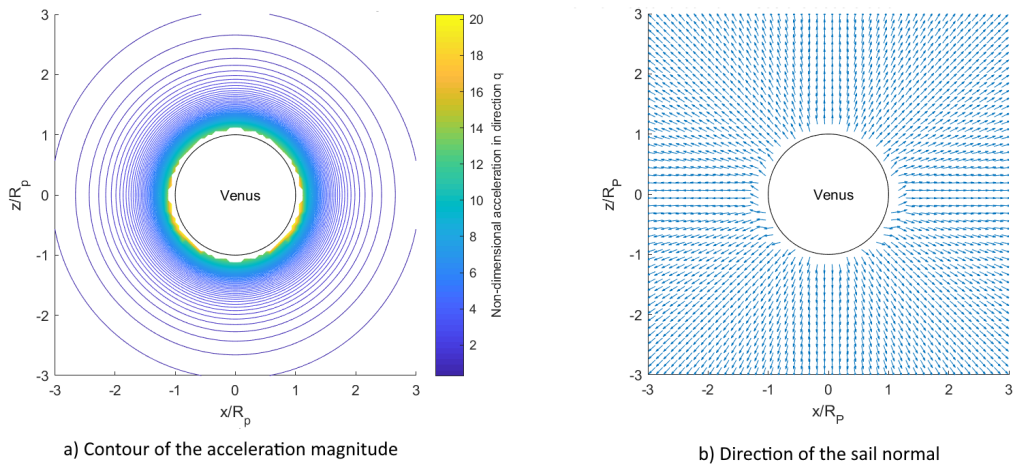


Figure 4.12. Maximisation of the radial acceleration for a double-side coating sail around Venus subject to BBRP

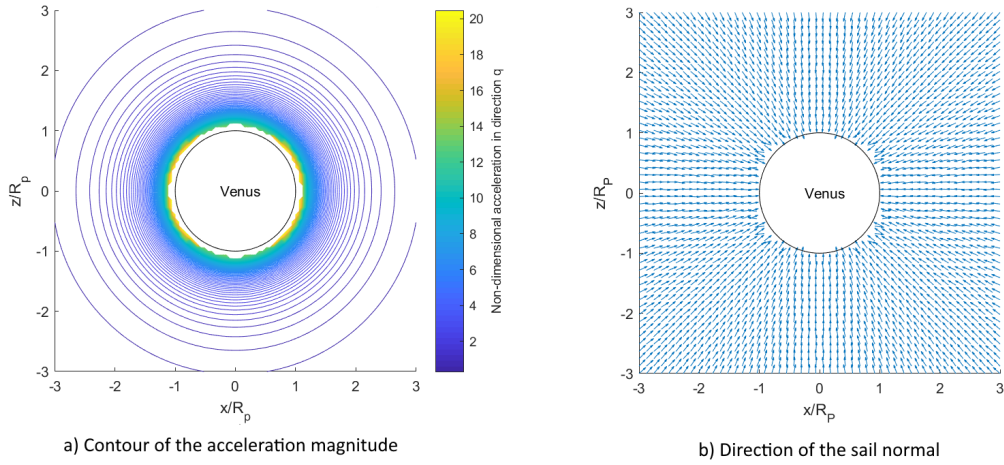


Figure 4.13. Maximisation of the radial acceleration for a single-side coating sail around Venus subject to BBRP

#### 4.1.4 Solar Radiation Pressure + Planetary Radiation Pressure

As said in the introduction, the planetary contribution has been almost always neglected and only in one work [21] SRP and PRP have been studied together, even if with a two-dimensional approach. Since one of the aims of this thesis is to extend the analysis to a three-dimensional case, this section constitutes the core of the first part of the project.

##### Earth

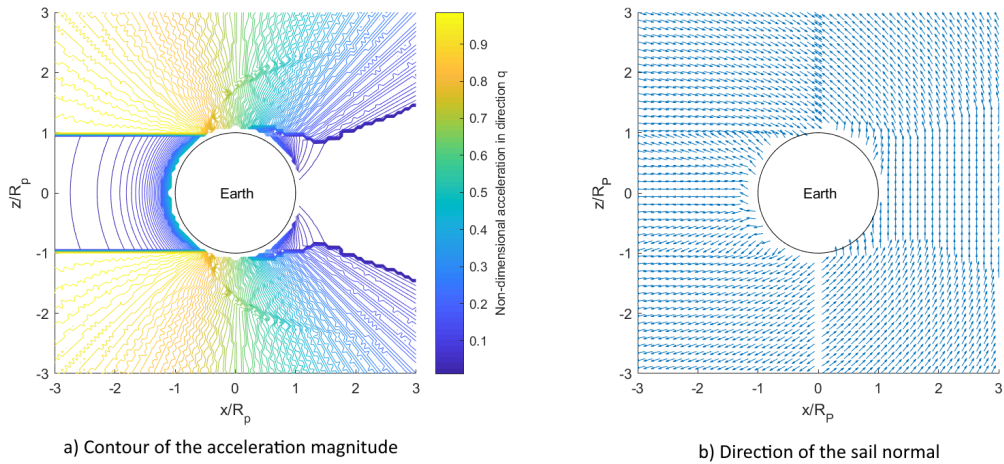


Figure 4.14. Maximisation of the radial acceleration for a double-side coating sail around Earth subject to SRP and PRP

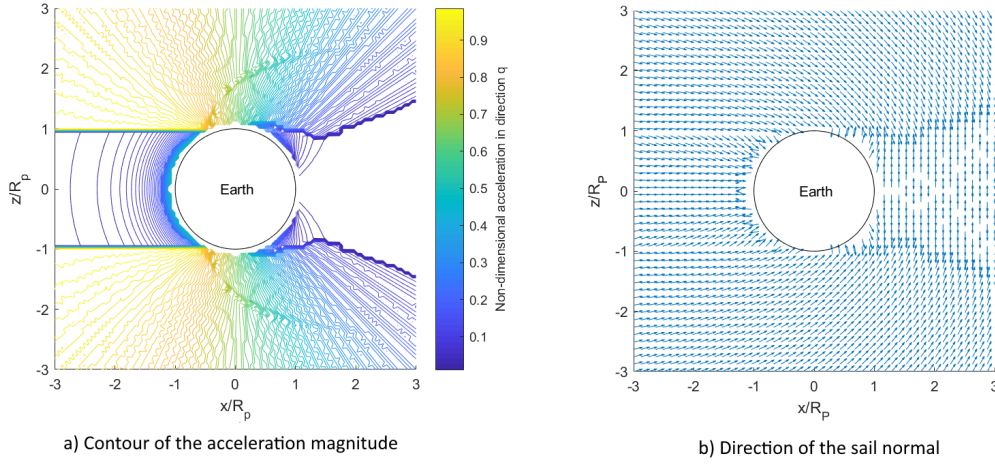


Figure 4.15. Maximisation of the radial acceleration for a single-side coating sail around Earth subject to SRP and PRP

As a consequence of the PRP presence and, in particular, due to BBRP, the sail provides acceleration in the eclipse region where the solar photons cannot hit its surface. Moreover, another beneficial effect is for positive  $x$ , in the area close to the surface of the planet, where solar contribution can be only negative or null. Where the PRP is the dominating radiation, the normal of the sail surface points to about the radial direction. However, the conclusion for Earth analysis is that, out of the umbra region and the strictly close region, the planetary radiation is negligible compared to the solar one. Regarding the two coating cases, the study of attitude in the chosen points does not show difference even for this case.

Point	Single-side	Double-side	Ratio
A	1.8727	1.8779	99.72%
B	4.7255	4.7036	100.47%
C	4.2355	4.2473	99.72%
D	2.9228	2.9310	99.72%
E	3.1503	3.1416	100.28%
F	3.9204	3.9314	99.72%

Table 4.6. Comparison of the cone angle  $\alpha_p$  for single-side and double-side coating in Earth area with only SRP+PRP [rad]

### Venus

The results for Venus represent the most promising effect of planetary radiation pressure. As anticipated in BBRP section, thanks to Venus characteristics, the sail has great benefits by the PRP and the acceleration raises up to ten times. When  $x \leq 2R_p$ , the PRP appears by far the dominating contribution, and this is clearly understandable looking at the direction of the sail normal in fig. 4.16 b) and fig. 4.17 b). The comparison between the two

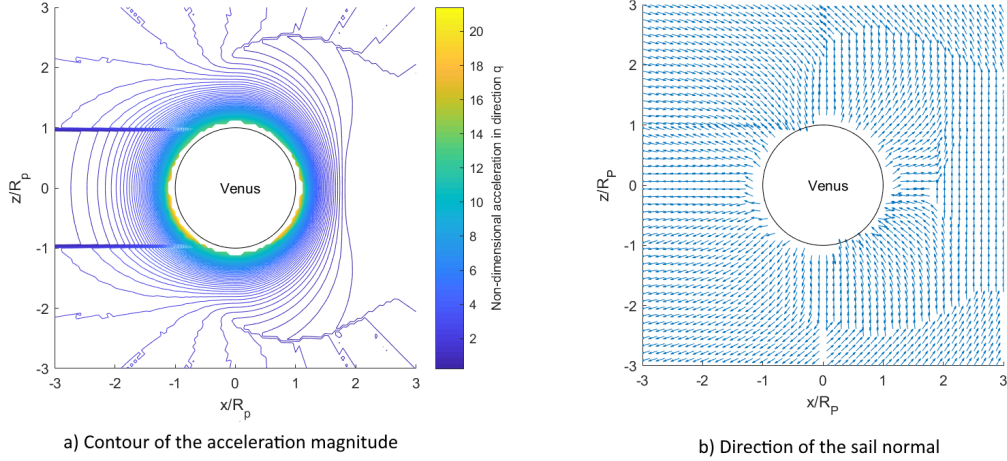


Figure 4.16. Maximisation of the radial acceleration for a double-side coating sail around Venus subject to SRP and PRP

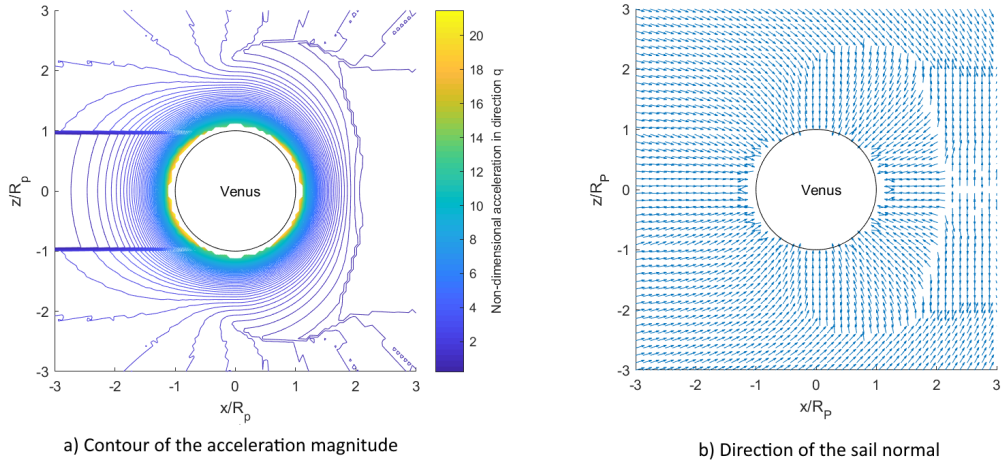


Figure 4.17. Maximisation of the radial acceleration for a single-side coating sail around Venus subject to SRP+PRP

coating cases has not produced the expected difference; for this reason, in the following

analyses, only the double-side coating study has been carried on, allowing to speed up the simulations.

Point	Single-side	Double-side	Ratio
A	5.5481	5.6338	98.48%
B	4.7255	4.7036	100.47%
C	4.2180	4.2122	100.14%
D	2.9578	2.9485	100.32%
E	3.1328	3.1416	99.72%
F	3.8679	3.8787	99.72%

Table 4.7. Comparison of the cone angle  $\alpha_p$  for single-side and double-side coating in Venus area with only SRP+PRP [rad]

An interesting comparison has been done for the double-side coating with and without PRP. In the area where PRP is the prevalent effect, the attitude of the sail change completely, as it can be seen in table 4.8 for point *A*; another point, *G* with coordinates  $(1.5R_p, 0, 0)$ , has been added to the analysis to have a better understanding of the area closer to the planet. Even for *G* the attitude of the sail changes due to PRP effect, moreover in this point the magnitude of the acceleration has a extremely high increase up to 2800%. For Venus the PRP is clearly not negligible, and affect drastically the results.

Point	Cone angle [rad]		Radial acceleration [ $m/s^2$ ]		
	SRP	SRP+PRP	SRP	SRP+PRP	SRP+PRP / SRP
A	1.8779	5.6338	$7.1830 \cdot 10^{-6}$	$1.0461 \cdot 10^{-5}$	145.64%
B	4.7212	4.7036	$-7.6266 \cdot 10^{-8}$	$-7.4383 \cdot 10^{-8}$	102.53%
C	4.2473	4.2122	$3.2999 \cdot 10^{-5}$	$3.4161 \cdot 10^{-5}$	103.52%
D	2.9310	2.9485	$1.5897 \cdot 10^{-4}$	$1.7807 \cdot 10^{-4}$	112.01%
E	—	3.1416	—	$1.7807 \cdot 10^{-4}$	—
F	3.9314	3.8787	$9.0803 \cdot 10^{-5}$	$9.6762 \cdot 10^{-5}$	106.56%
G	1.5796	5.8456	$-7.6253 \cdot 10^{-8}$	$2.1414 \cdot 10^{-4}$	2808.2%

Table 4.8. Comparison of the cone angle  $\alpha_p$  and of the radial acceleration for double-side coating in Venus area with and without PRP [rad]

## 4.2 Transverse Acceleration

Seeing as the planetary radiation pressure is radial to the planet, it is particularly interesting evaluating if its contribution is still relevant when the requested acceleration is

perpendicular to that direction. In order to maximise the transverse acceleration, the sail should modify its attitude and find the optimal angles to benefit the effect of PRP.

Moreover, for circular orbit the transverse direction corresponds to the velocity unit vector, and, as it will see, the acceleration along this direction is relevant for the orbital manoeuvres, and in particular for the change of the semimajor axis.

The study case are the same of the previous analysis, but the results will focus only in the double-side coating.

### 4.2.1 Solar Radiation Pressure

#### Earth

In the region with  $-R_p \leq x \leq R_p$  and negative  $z$  the transverse direction is against the solar rays. The sail is positioned perpendicularly to the SRP so that the acceleration is null and not negative. The opposite situation happens for positive  $z$ , where the two vectors have the same direction, and there is higher acceleration.

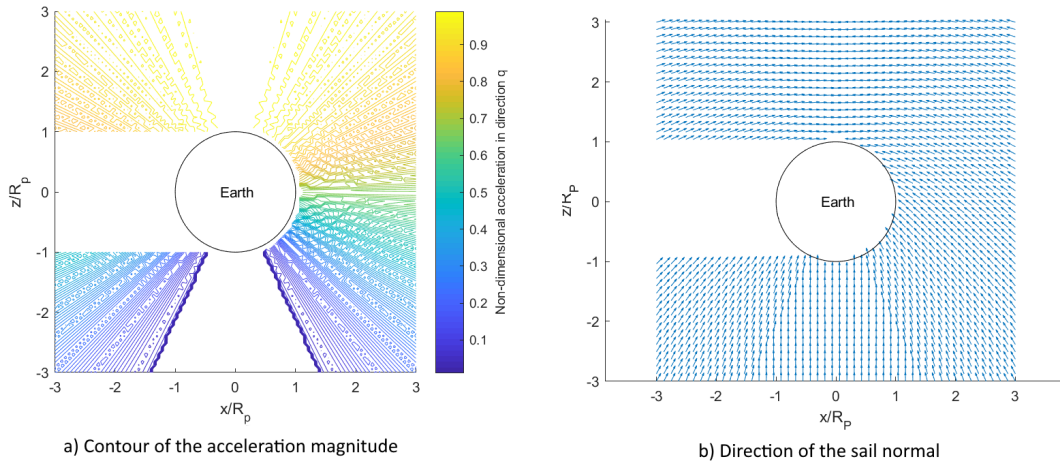


Figure 4.18. Maximisation of the transverse acceleration for a double-side coating sail around Earth subject to SRP

#### Venus

The considerations for Venus are analogous to those for the Earth.

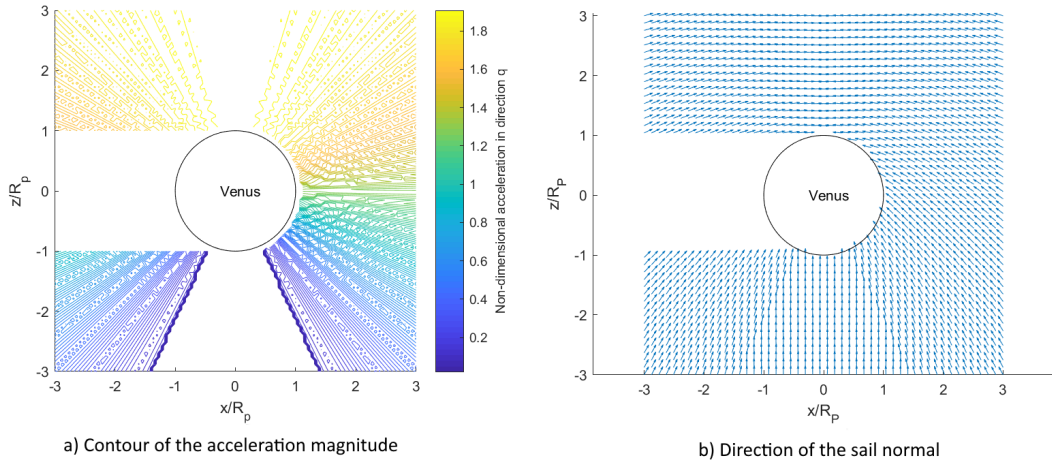


Figure 4.19. Maximisation of the transverse acceleration for a double-side coating sail around Venus subject to SRP

## 4.2.2 Albedo Radiation Pressure

### Earth

The albedo radiation pressure is mostly in radial direction, so the attitude of the sail has to balance the required acceleration with the direction of the photons that strike its surface. In fig. 4.20 it is possible to observe that the sail is not in the radial direction, but an angle exists between the two directions.

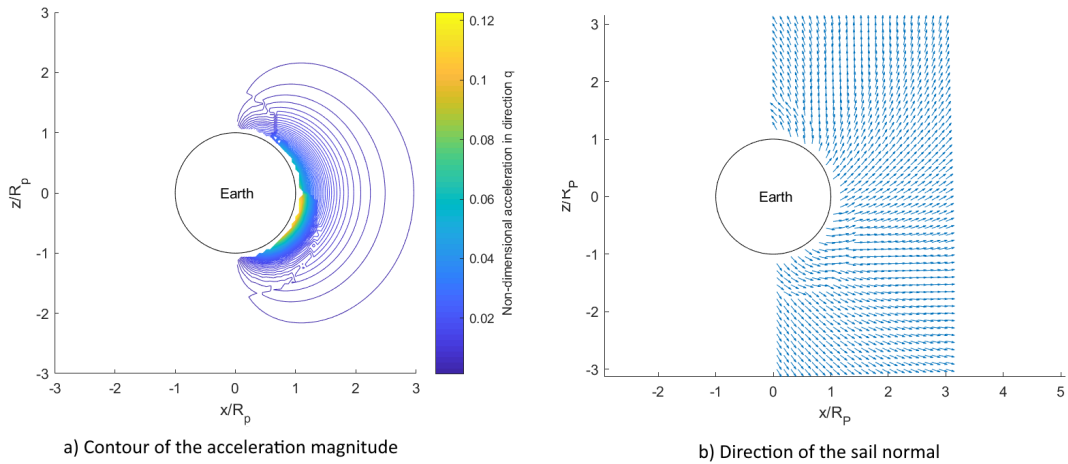


Figure 4.20. Maximisation of the transverse acceleration for a double-side coating sail around Earth subject to ARP

**Venus**

As explained in the radial study, the closer distance to the Sun and the higher albedo coefficient make Venus more reflecting than the Earth so that its albedo contribution is more than double.

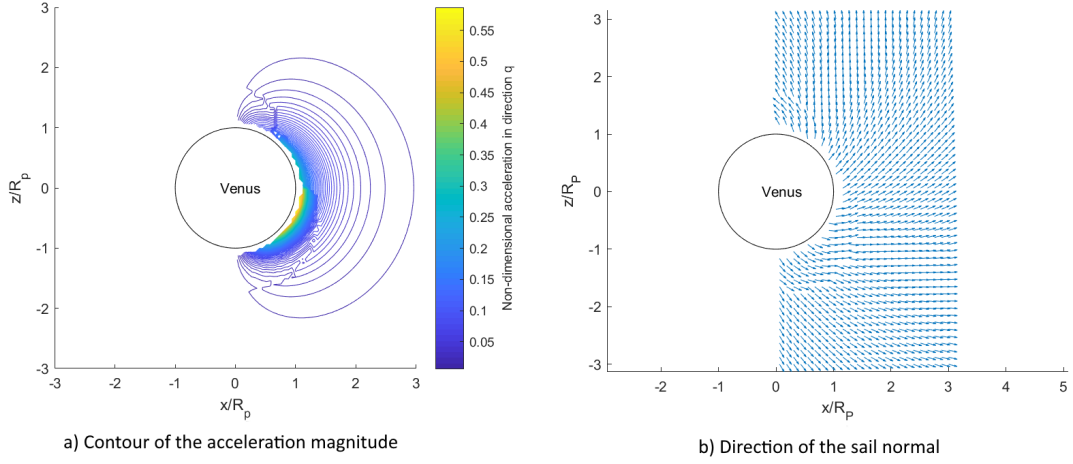


Figure 4.21. Maximisation of the transverse acceleration for a double-coating sail around Venus subject to ARP

**4.2.3 Black Body Radiation Pressure**

For both the planets, the contours apparently show anomalies in the magnitude of the acceleration. These have been justified with three motivations, and in particular they are due to the low density of the grid, the poor range of scanned angles that have a difference of 6 *deg* from each other and the view factor  $F$  that considers the two surfaces of the sail.

**Earth**

**Venus**

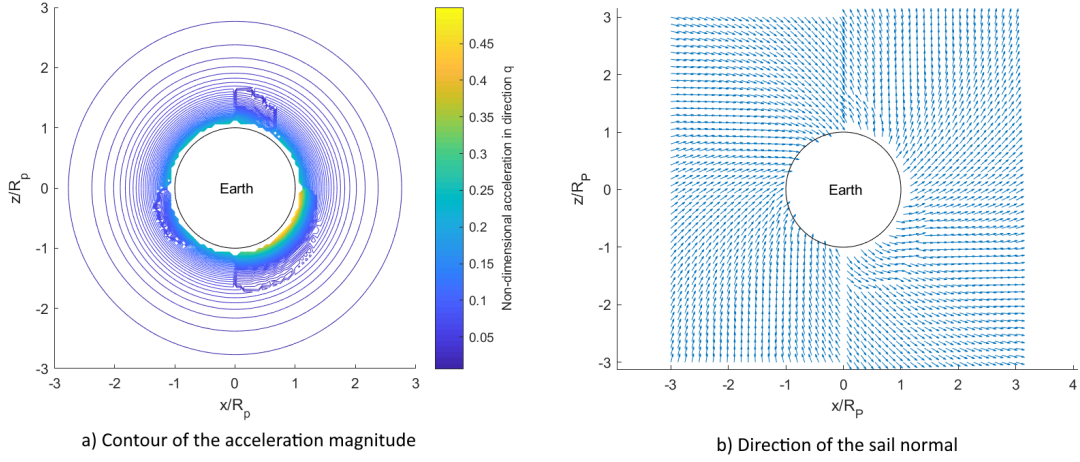


Figure 4.22. Maximisation of the transverse acceleration for a double-side coating sail around Earth subject to BBRP

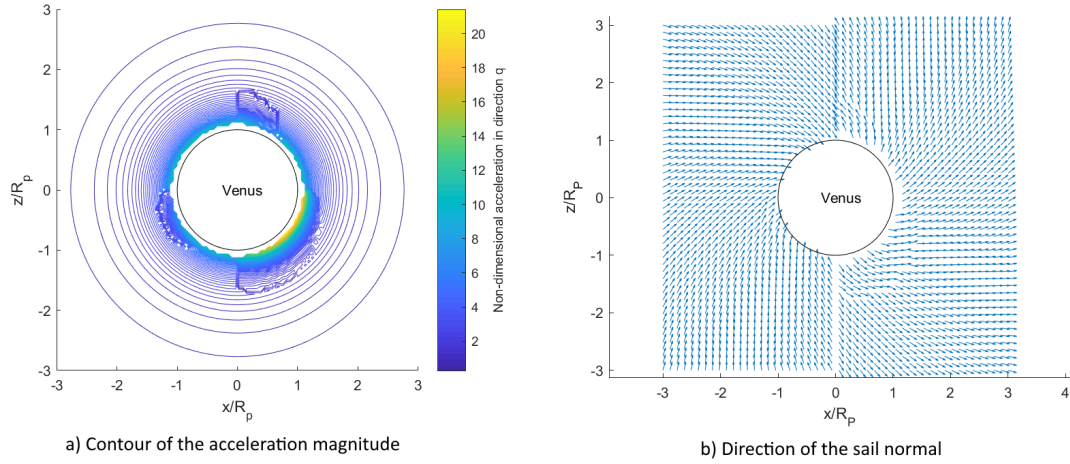


Figure 4.23. Maximisation of the transverse acceleration for a double-side coating sail around Venus subject to BBRP

#### 4.2.4 Solar Radiation Pressure + Planetary Radiation Pressure

##### Earth

In the complete study case, some areas in the vicinity of the planet have benefited the presence of PRP. Comparing the fig. 4.24 and fig. 4.18 it can be noticed that in some point where with only SRP the normal of the sail was perpendicular to the solar rays, the attitude changed.

The deepened analysis of chosen points has been conducted again, even for the point G.

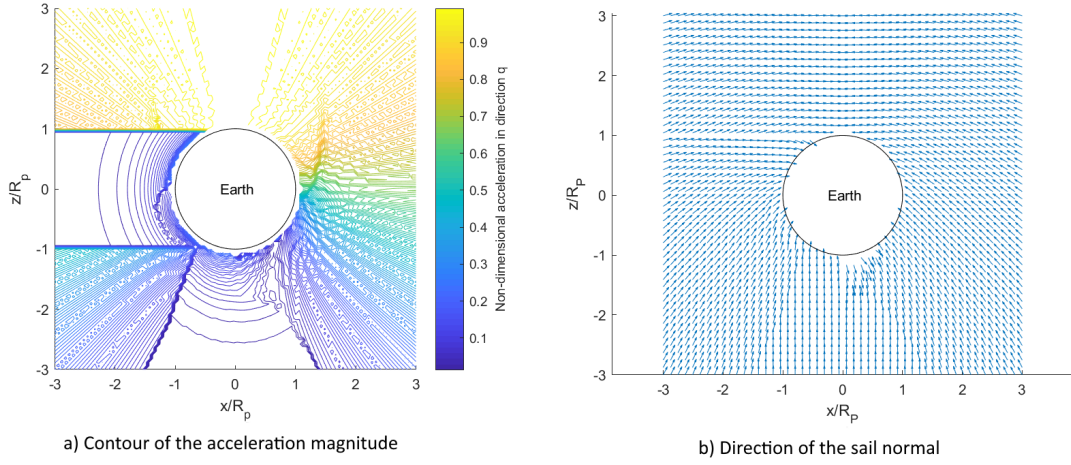


Figure 4.24. Maximisation of the transverse acceleration for a double-side coating sail around Earth subject to SRP and PRP

The results show that some points such as F benefit the presence of PRP, but in other parts of the grid, the SRP and PRP give opposite contributions that reduce the acceleration experienced by the sail. In point G this reduction is about 11

Point	Cone angle [rad]		Transverse acceleration [ $m/s^2$ ]		
	SRP	SRP+PRP	SRP	SRP+PRP	SRP+PRP / SRP
A	2.8432	2.8432	$3.7277 \cdot 10^{-6}$	$3.5118 \cdot 10^{-6}$	94.21%
B	2.5273	2.25736	$3.1206 \cdot 10^{-5}$	$3.0983 \cdot 10^{-5}$	99.28%
C	1.7902	1.7902	$8.2546 \cdot 10^{-5}$	$8.2546 \cdot 10^{-5}$	100%
D	2.3518	2.3518	$4.7197 \cdot 10^{-5}$	$4.7220 \cdot 10^{-5}$	100.24%
E	—	2.6151	—	$8.8863 \cdot 10^{-7}$	—
F	2.8257	2.8257	$-2.4580 \cdot 10^{-8}$	$9.7227 \cdot 10^{-8}$	495.56%
G	2.5273	2.5098	$3.1202 \cdot 10^{-5}$	$2.7986 \cdot 10^{-5}$	89.69%

Table 4.9. Comparison of the cone angle  $\alpha_p$  and of the transverse acceleration for double-side coating in Earth area with and without PRP [rad]

## Venus

As for the radial analysis, even the transversal acceleration has a great change when PRP is taken into account. Again, in the vicinity of the planet, the PRP is the dominating effect and modify the optimal attitude of the sail, while it returns similar to the SRP case after about 2 radii. The consideration previously done for the Earth are heightened for Venus.

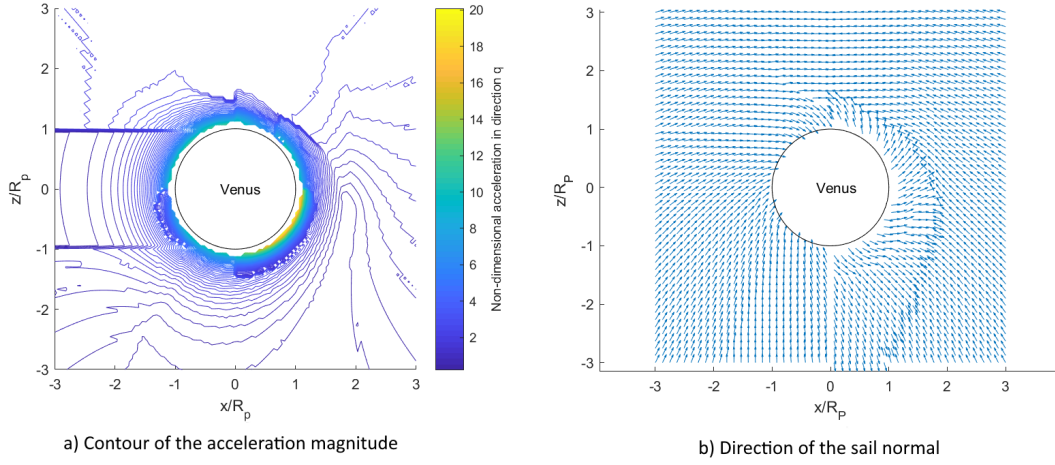


Figure 4.25. Maximisation of the transverse acceleration for a double-coating sail around Venus subject to SRP and PRP

In this case, the reduction of the acceleration is particularly significant in point A, a point close to the area where SRP becomes the dominating effect again, and so PRP is still strong. On the opposite, point F cannot provide an acceleration in the positive transverse direction with only SRP, but when PRP has been taken into account, the acceleration increases and become comparable to other areas of the grid.

Point	Cone angle [rad]		Transverse Acceleration [ $m/s^2$ ]		
	SRP	SRP+PRP	SRP	SRP+PRP	SRP+PRP / SRP
A	2.8432	2.9485	$7.1814 \cdot 10^{-6}$	$2.8644 \cdot 10^{-7}$	3.99%
B	2.5273	2.5098	$6.0129 \cdot 10^{-5}$	$5.2381 \cdot 10^{-5}$	87.11%
C	1.7902	1.7902	$1.5904 \cdot 10^{-4}$	$1.5905 \cdot 10^{-4}$	100%
D	2.3518	2.3869	$9.0751 \cdot 10^{-5}$	$9.5794 \cdot 10^{-5}$	105.56%
E	—	2.6151	—	$3.8109 \cdot 10^{-5}$	—
F	2.8257	2.8081	$-4.7664 \cdot 10^{-8}$	$5.3048 \cdot 10^{-6}$	11229.48%
G	2.5273	0.4739	$6.0119 \cdot 10^{-5}$	$5.9001 \cdot 10^{-5}$	98.14%

Table 4.10. Comparison of the cone angle  $\alpha_p$  and of the transverse acceleration for double-side coating in Venus area with and without PRP [rad]

Seeing as the reduction of the acceleration is due to the opposite contributions given by SRP and PRP, the use of a single-side coating can prevent this kind of situation, reducing the effect of the non-dominating radiation pressure. For this reason, the table 4.11 and the graphics of acceleration magnitude and direction of the normal (fig.4.26) have been

elaborated. In this case, the drastic reduction of the acceleration magnitude exerted by the sail in point A is significantly higher, and the same effect can be seen almost at all point. An interesting difference can be noted in point G, where the acceleration decreases with a double-side coating and increases with a single one. However, in both cases, G is the point where the attitude with or without PRP changes more.

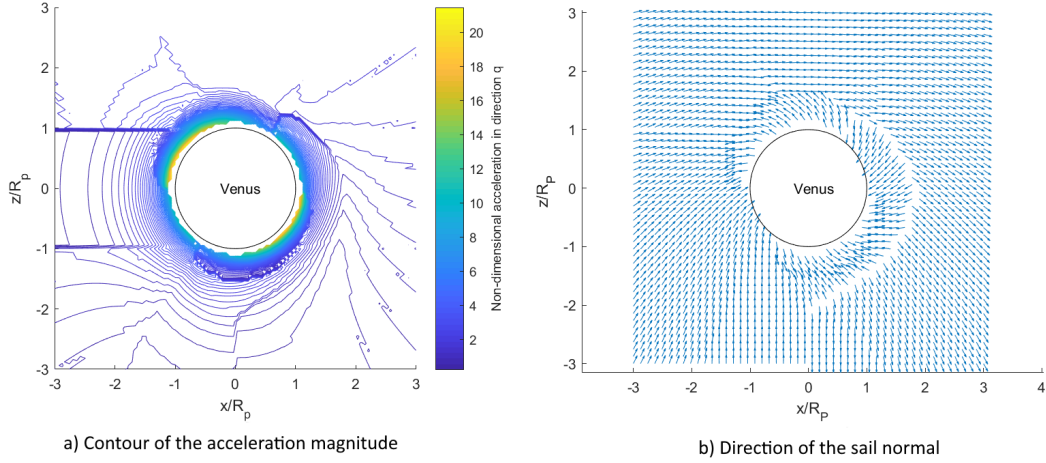


Figure 4.26. Maximisation of the transverse acceleration for a single-side coating sail around Venus subject to SRP and PRP

Point	Cone angle [ $rad$ ]		Transverse Acceleration [ $m/s^2$ ]		
	SRP	SRP+PRP	SRP	SRP+PRP	SRP+PRP / SRP
A	5.9857	6.0032	$7.1813 \cdot 10^{-6}$	$6.2986 \cdot 10^{-6}$	87.71%
B	5.6706	5.6706	$6.0128 \cdot 10^{-5}$	$5.9260 \cdot 10^{-5}$	98.56%
C	4.9355	4.9180	$1.5903 \cdot 10^{-4}$	$1.5868 \cdot 10^{-4}$	99.78%
D	2.3628	2.3803	$9.0759 \cdot 10^{-5}$	$9.5798 \cdot 10^{-5}$	105.55%
E	—	2.6253	—	$3.8102 \cdot 10^{-5}$	—
F	5.9506	5.9594	$-9.3119 \cdot 10^{-8}$	$5.1683 \cdot 10^{-6}$	5651.25%
G	5.6706	6.7995	$6.0118 \cdot 10^{-5}$	$1.1010 \cdot 10^{-4}$	183.15%

Table 4.11. Comparison of the cone angle  $\alpha_p$  and of the transverse acceleration for single-side coating in Venus area with and without PRP [rad]

### 4.3 3D example for Venus

An example of study for an inclined plane is show in this section. The analysis has been conducted on the plane  $z - y = 0$  that corresponds to the perifocal plane of an orbit with inclination  $i = 45 \text{ deg}$ , and has maximised the acceleration normal to the plane with and without PRP. A double-side coating has been chosen to speed-up the simulation and the reference planet is Venus. The grid is the same of the previous simulation and the points have been adapted for the inclined plane:

- $A=(2R_p, -2R_p, -2R_p)$ ;
- $B=(3R_p, 0, 0)$ ;
- $C=(R_p, 3R_p, 3R_p)$ ;
- $D=(-3R_p, R_p, R_p)$ ;
- $E=(-2R_p, 0, 0)$ ;
- $F=(-R_p, -3R_p, -3R_p)$ ;
- $G=(1.5R_p, 0, 0)$ ;

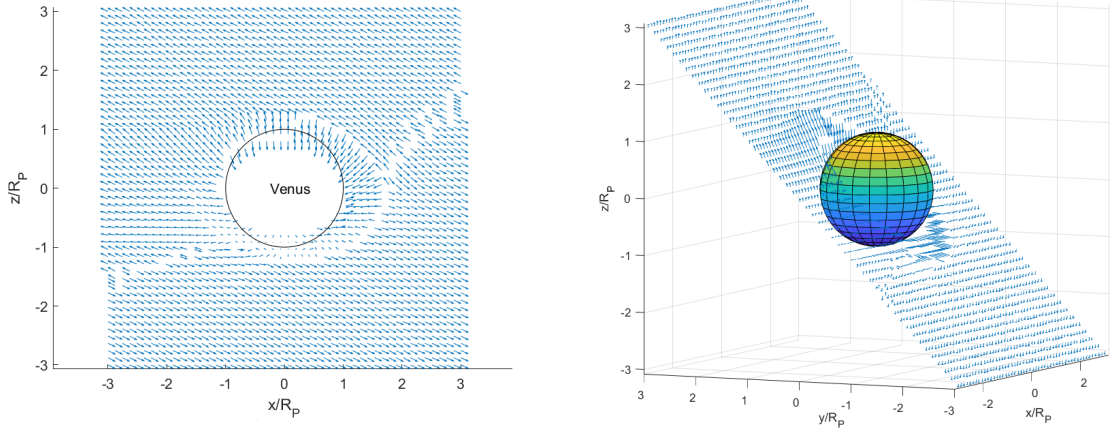


Figure 4.27. Maximisation of the out-of-plane acceleration for a double-side coating sail around Venus subject to SRP and PRP in an inclined plane

The results show that the sail can provide an out-of-plane acceleration, but, since the planetary radiation is radial to the planet, its contribution is not particularly significant. Moreover, in some area it opposes the solar contribution, reducing the resulting acceleration such as in point B in table 4.13. In the vicinity of the planet, the presence of PRP also changes the attitude of the sail as seen in table 4.12.

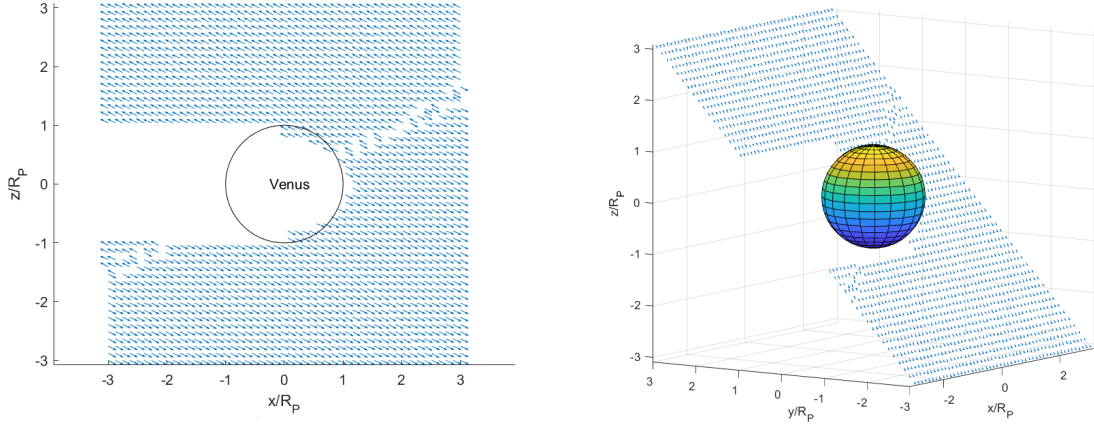


Figure 4.28. Maximisation of the out-of-plane acceleration for a double-side coating sail around Venus subject to SRP in an inclined plane

Point	Cone angle [rad]		Clock angle [rad]	
	SRP	SRP+PRP	SRP	SRP+PRP
A	1.4392	1.4392	1.4743	1.4743
B	0.6143	0.6318	1.5620	1.5620
C	2.1938	2.1763	0.8249	0.8073
D	0.9653	0.9477	1.7902	1.7726
E	—	0.5265	—	1.5620
F	2.1938	2.2114	2.3167	2.3167
G	0.6143	2.6677	1.5620	1.5620

Table 4.12. Comparison of cone angle  $\alpha_p$  and clock angle  $\delta_p$  for a double-side coating in Venus area with and without PRP [rad]

Point	Out-of-plane Acceleration [ $m/s^2$ ]		
	SRP	SRP+PRP	SRP+PRP / SRP
A	$6.0117 \cdot 10^{-5}$	$6.0094 \cdot 10^{-5}$	99.96%
B	$6.0127 \cdot 10^{-5}$	$5.2379 \cdot 10^{-5}$	87.11%
C	$6.0105 \cdot 10^{-5}$	$5.9416 \cdot 10^{-5}$	98.85%
D	$6.0081 \cdot 10^{-5}$	$6.1720 \cdot 10^{-5}$	102.73%
E	—	$3.8107 \cdot 10^{-5}$	—
F	$6.0102 \cdot 10^{-5}$	$6.0836 \cdot 10^{-5}$	101.22%
G	$6.0117 \cdot 10^{-5}$	$5.8999 \cdot 10^{-5}$	98.14%

Table 4.13. Comparison of the out-of-plane acceleration for double-side coating in Venus area with and without PRP [rad]

## Part II

# Dynamic of the sail



# Chapter 5

## Orbital Dynamic

In the study of the solar sail dynamic, the approximation of impulsive manoeuvres is unacceptable because the solar sails provide a continuous and small acceleration. Since it is smaller than the dominant gravitational effect, from the spacecraft point of view, the thrust given by the sail can be seen as a perturbation in its trajectory according to the two bodies problem.

$$\ddot{\vec{r}} = \frac{\mu}{r^3} \hat{r} + \vec{a}_p$$

The solution can be found numerically, thanks to Encke's method [26]. The guiding principle is to solve first the classic two-body problem, finding the mean trajectory in the form of a Keplerian orbit, and then to compute numerically another differential equation to find, after a chosen period of time, the deviation from the undisturbed case. The actual position and velocity are compared with the ideal results of the two-body problem and, if their difference is not within a certain tolerance, the osculating orbit (the Keplerian) is reset, and its parameters are updated. In other words, the actual orbit is built linking different Keplerian orbits, reset every time the deviation becomes too large. This process of rectification can be taken to its limit for time intervals  $dt$ , so every point is calculated at each instant of time. This method is called of variation of parameters and uses a set of six equations to calculate the instantaneous orbital parameters. It has been specified the term "instantaneous" because, due to the perturbative acceleration, these are no longer constants, but vary over time. In this chapter, after an introduction of Gauss' variational equations, some manoeuvres have been simulated with Gao's control laws to study the effect of PRP on the change of semimajor axis, eccentricity and inclination. Then, the capturing manoeuvre for Venus has been analysed.

### 5.1 Introduction to the Gauss' variational equations

Different sets of equations can be found in the literature [26], among all Gauss' variational equations have been chosen because they are particularly convenient in the rotating reference  $R = \{\hat{i}_r; \hat{i}_\theta; \hat{i}_h\}$ , where  $\hat{i}_r$  is along the orbit position vector,  $\hat{i}_h$  is along the orbit momentum vector, and  $\hat{i}_\theta$  is perpendicular to the previous two satisfying the right-hand rule. This frame is often referred to as a local-vertical-local-horizontal (LVLH) reference frame. Another possibility is to write the equations in the rotating reference frame  $R = \{\hat{i}_v; \hat{i}_n; \hat{i}_h\}$ ,

where  $\hat{i}_v$  is along the velocity vector,  $\hat{i}_h$  is again along the orbit momentum vector, and  $\hat{i}_n$  is perpendicular to the previous two according to the right-hand rule.

In fig. 5.1 the two different reference frames are shown. The rotating frame based on

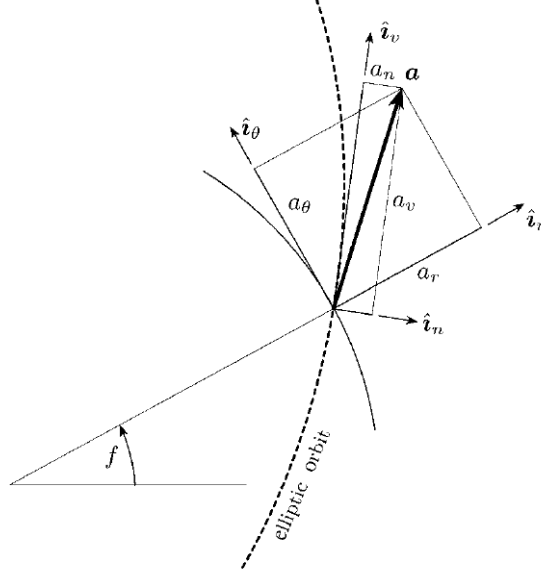


Figure 5.1. Illustration of orbit plane unit direction vectors [26]

position vector have been considered more convenient to move forward with the analysis. The six variational equations are taken from Schaub [26] and their parameters are the semimajor axis  $a$ , the eccentricity  $e$ , the orbit inclination  $i$ , the longitude of the ascending node  $\Omega$ , the argument of the perigee  $\omega$  and the true anomaly  $\nu$ .

$$\frac{da}{dt} = 2 \frac{a^2}{h} [e \sin(\nu) a_r + (1 + e \cos(\nu)) a_\theta] \quad (5.1)$$

$$\frac{de}{dt} = \frac{1}{h} \left\{ a(1 - e^2) \sin(\nu) a_r + \left[ \cos(\nu) \left( a(1 - e^2) + \frac{a(1 - e^2)}{1 + e \cos(\nu)} \right) + ea \frac{(1 - e^2)}{1 + e \cos(\nu)} \right] a_\theta \right\} \quad (5.2)$$

$$\frac{di}{dt} = \frac{a(1 - e^2)}{1 + e \cos(\nu)} \frac{1}{h} \cos(\theta) a_h \quad (5.3)$$

$$\frac{d\Omega}{dt} = \frac{a(1 - e^2)}{1 + e \cos(\nu)} \frac{1}{h} \frac{\sin(\theta)}{\sin(i)} a_h \quad (5.4)$$

$$\frac{d\omega}{dt} = \frac{1}{eh} \left[ -a(1 - e^2) \cos(\nu) a_r + a(1 - e^2) \left( 1 + \frac{1}{1 + e \cos(\nu)} \right) \sin(\nu) a_\theta \right] - \frac{\sin(\theta) \cos(i) a(1 - e^2)}{h \sin(i) (1 + e \cos(\nu))} a_h \quad (5.5)$$

$$\frac{d\nu}{dt} = \frac{h(1 + e \cos(\nu))^2}{a^2(1 - e^2)^2} + \frac{1}{eh} \left[ a(1 - e^2) \cos(\nu) a_r - a(1 - e^2) \left( 1 + \frac{1}{1 + e \cos(\nu)} \right) \sin(\nu) a_\theta \right] \quad (5.6)$$

where  $h$  is the angular momentum,  $a_r$ ,  $a_\theta$  and  $a_h$  are the acceleration components and  $\theta = \omega + \nu$

## 5.2 Gao’s control laws

A control law is an algorithm used by the controller to determine the output requested to do a certain change in the status of the spacecraft. In order to modify its orbit, the sail needs to know the optimal acceleration vector to perform the manoeuvres so that it can change its attitude and maximise its acceleration in that direction. Moreover, in order to modify one or orbital parameters and since they are dependent on each other, knowing the right area where to thrust is necessary to obtain the expected results and to have minimum side effects on the others orbital elements.

Various approaches are available in literature such as in Macdonald and McInnes [14] or in Dachwald [27], among them, the model presented by Gao [28] appears to be particularly interesting since it allows to increase or decrease three orbital elements at the same time. Gao proposed a direct approach for the solving of minimum-time orbital transfers by the using of three simple control laws, each of them used within the same revolution in different arcs of the orbit. In those arcs the three control laws are near-optimal strategies to change the semimajor axis  $a$ , the eccentricity  $e$  and the inclination  $i$ , so for after a complete revolution, all these three parameters could be changed. An example of the arcs division can be seen in fig.5.2. where  $s_1$ ,  $s_2$ ,  $y_1$ ,  $y_2$ ,  $e_1$ ,  $e_2$ ,  $y_3$ , and  $y_4$  are the beginning and

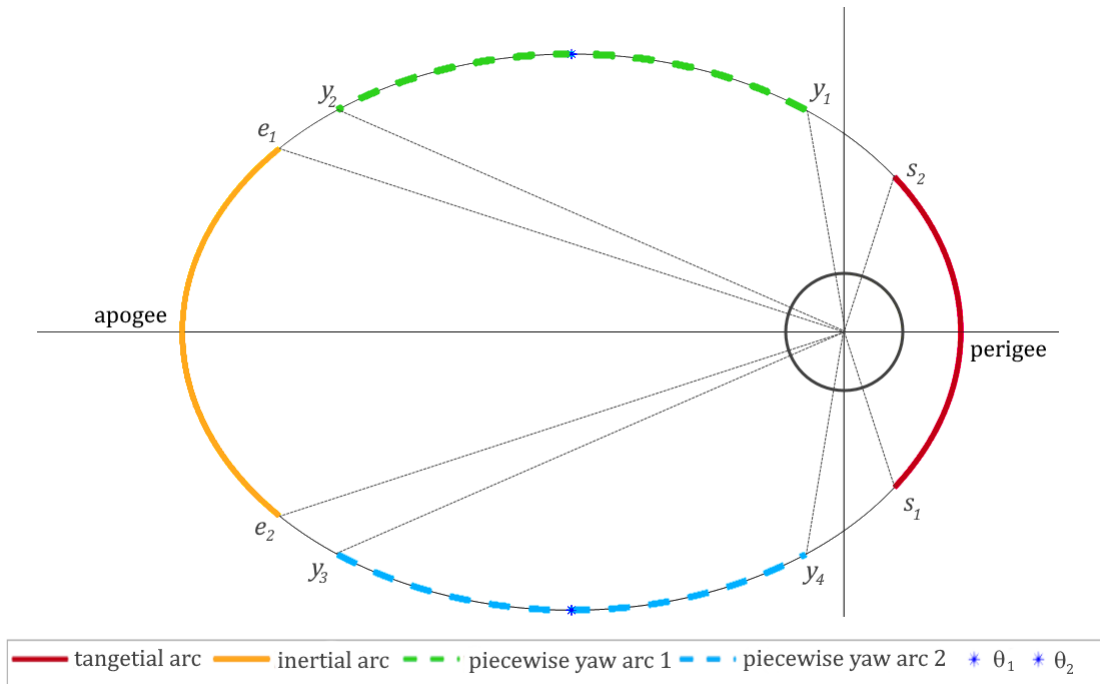


Figure 5.2. Example of the division of the orbit in arches proposed by Gao

ending point of each arc. Seeing as the position of these points, and so the arcs length, influences the performance of the manoeuvres, it is linked to few parameters that can be optimized over time. Nevertheless, as it will see in the following sections, in this phase of

the study, the parameters have been chosen arbitrarily and are constant; further analysis could optimise them over time.

The three control laws used in the different arcs are:

- the tangential steering, which is the most efficient strategy to change the semimajor axis and uses a thrust in the direction of the velocity;
- the inertial steering, which is a near-optimal strategy to change the eccentricity and uses a thrust perpendicular to the semimajor axis;
- the piecewise constant yaw steering, which is a strategy to change the inclination and uses a thrust in the out-plane direction of the orbit.

According to Gauss's equation the most efficient way to change the semimajor axis is when the velocity is higher, for this reason, as it can be seen in fig.5.2, the tangential steering is used in a perigee-centred arc.

$$s_1 = -|w_s|\pi \quad (5.7)$$

$$s_2 = |w_s|\pi \quad (5.8)$$

where, as mentioned before,  $s_1$  and  $s_2$  are the beginning and ending point of the arc and  $-1 \leq w_s \leq 1$  is the parameter of its length.

According to Gao [28] and reference therein, the inertial steering perpendicular to the semimajor axis is a near optimal strategy to change eccentricity; since the variation of eccentricity is inversely proportional to the velocity, the best location to use the inertial steering is in a apogee-centred arc, where the velocity is smaller.

$$e_1 = \pi - |w_e|\pi \quad (5.9)$$

$$e_2 = \pi + |w_e|\pi \quad (5.10)$$

where again  $e_1$  and  $e_2$  are the beginning and ending point of the arc and  $-1 \leq w_e \leq 1$  is the parameter of its length.

The piecewise constant yaw steering is used in two different arches close to the nodal line. The points are indicated as  $y_1$ ,  $y_2$ ,  $y_3$  and  $y_4$  and their location is calculated solving a non linear equation.

$$\theta_1^m = \arcsin(-e \sin \omega) - \omega \quad (5.11)$$

$$\theta_2^m = \pi - \arcsin(-e \sin \omega) - \omega \quad (5.12)$$

$$\left[ \frac{di}{dt} \right]_{max} = \max \left( \left| \frac{\cos(\omega + \theta_1^m)}{1 + e \cos \theta_1^m} \right|, \left| \frac{\cos(\omega + \theta_2^m)}{1 + e \cos \theta_2^m} \right| \right) \quad (5.13)$$

$$\frac{\cos(\omega + \nu)}{1 + e \cos \nu} = w_y \left[ \frac{di}{dt} \right]_{max} \quad (5.14)$$

$$y_1 = \arccos \left( w_y \left[ \frac{di}{dt} \right]_{max} / A_1 \right) - \varphi_1 \quad (5.15)$$

$$y_2 = -\arccos \left( w_y \left[ \frac{di}{dt} \right]_{max} / A_1 \right) - \varphi_1 \quad (5.16)$$

$$y_3 = \arccos \left( w_y \left[ \frac{di}{dt} \right]_{max} / A_2 \right) - \varphi_2 \quad (5.17)$$

$$y_4 = -\arccos \left( w_y \left[ \frac{di}{dt} \right]_{max} / A_2 \right) - \varphi_2 \quad (5.18)$$

where  $0 \leq w_y \leq 1$  and  $A_1$ ,  $A_2$ ,  $\varphi_1$  and  $\varphi_2$  are respectively

$$A_1 = \sqrt{1 - 2e \cos \omega w_y \left[ \frac{di}{dt} \right]_{max} + \left( e w_y \left[ \frac{di}{dt} \right]_{max} \right)^2} \quad (5.19)$$

$$A_2 = \sqrt{1 + 2e \cos \omega w_y \left[ \frac{di}{dt} \right]_{max} + \left( e w_y \left[ \frac{di}{dt} \right]_{max} \right)^2} \quad (5.20)$$

$$\sin \varphi_1 = \frac{\sin \omega}{A_1}, \quad \cos \varphi_1 = \left( \cos \omega - e w_y \left[ \frac{di}{dt} \right]_{max} \right) / A_1 \quad (5.21)$$

$$\sin \varphi_2 = \frac{\sin \omega}{A_2}, \quad \cos \varphi_2 = \left( \cos \omega + e w_y \left[ \frac{di}{dt} \right]_{max} \right) / A_2 \quad (5.22)$$

The parameter  $w_y$  represents the percentage threshold value, dividing the region where it is worth to thrust from the one where the change of inclination is considered too small. Using the parameters of fig. 5.2 is possible to elaborate a plot to better understand the meaning of  $w_y$ . In fig. 5.3 the green line is  $\frac{\cos(\omega+\nu)}{1+e \cos \nu}$ , while the red lines are the solution of eq. 5.14. The trend depends on the orbital parameters of the orbit, it is also possible that only one of the two arcs exists.

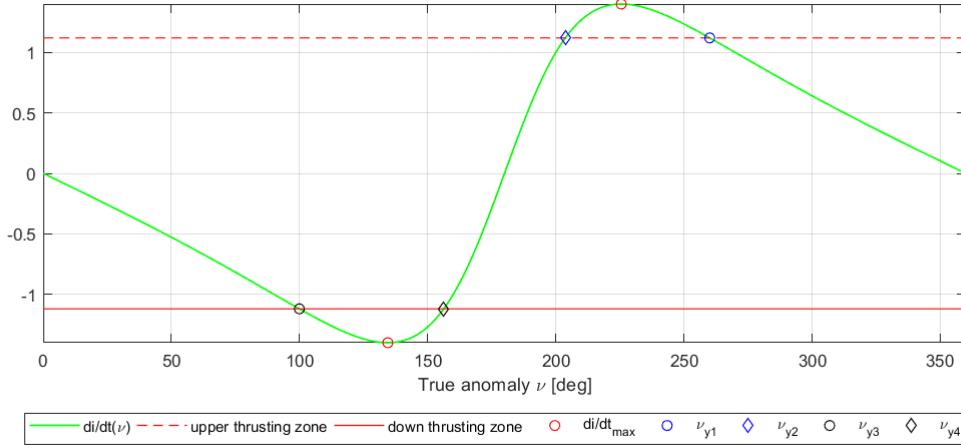


Figure 5.3. Example of  $\frac{di}{dt}(\nu)$  trend and threshold value

All the considerations written above give information about where to manoeuvre in orbit; regarding the acceleration vector, Gao proposed a minimum-time guidance scheme,

where

$$a_{out} = \begin{cases} a_{max} w_a \text{sign}[\cos \omega + \nu] & \text{if } \left| \frac{\cos \omega + \nu}{1 + e \cos \nu} \right| \geq w_y \left[ \frac{di}{dt} \right]_{max} \\ 0 & \text{otherwise} \end{cases} \quad (5.23)$$

where  $-1 \leq w_a \leq 1$  is the last of the four optimization parameters and represents the percentage of acceleration destined for the out-of-plane acceleration when the inclination change manoeuvre is performed.

$$a_{in} = \sqrt{a_{max}^2 - a_{out}^2} \quad (5.24)$$

$$a_r = a_{in} \sin \alpha \quad a_\theta = a_{in} \cos \alpha \quad (5.25)$$

with  $\alpha$

$$\alpha = \begin{cases} \begin{cases} \nu & \text{if } w_e > 0 \\ \pi + \nu & \text{if } w_e < 0 \end{cases} & \text{if } \cos \nu(t) \leq \cos(\pi - |w_e| \pi) \\ \begin{cases} \gamma & \text{if } w_s > 0 \\ \pi + \gamma & \text{if } w_s < 0 \end{cases} & \text{otherwise} \end{cases} \quad (5.26)$$

Gao used this algorithm for an electric thruster that has a maximum acceleration and can provide it constantly; for this reason  $a_{max}$  appears in the equations. An example is shown in fig. 5.4. However, since the sail acceleration depends on the surrounding environment and on the orientation of the sail surface, it is not constant and has not a maximum. Hence, the MATLAB script elaborated searches for the most similar acceleration vector that the sail can provide.

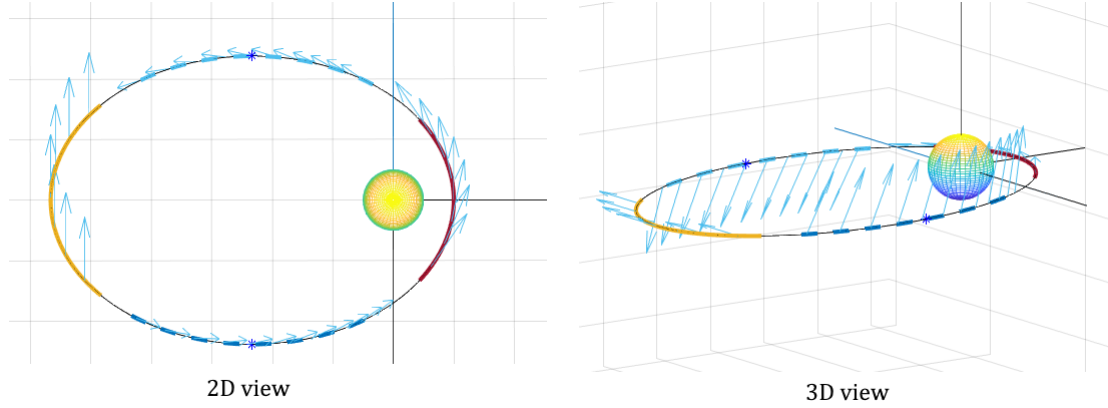


Figure 5.4. Example of the direction of acceleration vector requested to increase orbital elements with Gao's guidance scheme

### 5.3 Capturing manoeuvre

The interplanetary trajectories can be modelled with the patched conic approximation that divides them into different areas of influence, where the gravitational effect of one

celestial body is dominating respect to that one of the others. In each sphere of influence, it is possible to use the assumption of the two-body problem, maintaining good accuracy. Imagining a trajectory from Earth to Venus, three spheres of influence can be found:

- the geocentric region, near to the Earth;
- the heliocentric region, where the Sun is the main body;
- the aphrodiocentric region, near to Venus.

Typically, the purpose of a spacecraft that approaches a celestial body is to increase or decrease the velocity with a fly-by or to be captured and orbit around the body. This work has been focused on a capturing manoeuvre for Venus, in order to analyse the effect of PRP on the manoeuvre.

Seeing as the capture is achieved when the orbit becomes closed and so from hyperbolic turns into elliptical, the Gauss' variational equations are not suitable any more due to the discontinuity in the equations when the eccentricity becomes equal to 1. A new strategy has to be used to overpass the problem, and a possible way is to solve numerically the equations of motion adding the contribution of the sail as a perturbative acceleration; the system has six equations, respectively three for the position vector and three for the velocity vector.

$$\begin{pmatrix} \dot{r}_x \\ \dot{r}_y \\ \dot{r}_z \\ \dot{v}_x \\ \dot{v}_y \\ \dot{v}_z \end{pmatrix} = \begin{pmatrix} v_x \\ v_y \\ v_z \\ -\frac{\mu}{r^3}r_x + a_{sx} \\ -\frac{\mu}{r^3}r_y + a_{sy} \\ -\frac{\mu}{r^3}r_z + a_{sz} \end{pmatrix} \quad (5.27)$$

The integration has been done with `ode113`, but the initial conditions are not known. A parametric study has been conducted to find the combination of initial conditions and characteristic acceleration that allow the capture. In particular, three parameters have been used:

- the characteristic acceleration  $a_o$
- the periapsis of the hyperbolic orbit  $r_p$
- the eccentricity of the hyperbolic orbit  $i_h$

The capture has been considered achieved when the eccentricity at the end of the manoeuvre is less than 1. In order to reduce it, in all the braking phase the sail has to give acceleration in the opposite direction of the velocity. The thrust is applied when

$$-\frac{1}{2} \theta_\infty \leq \nu \leq \frac{1}{2} \theta_\infty \quad (5.28)$$

where  $\theta_\infty$  is the angle of hyperbola asymptote of the initial orbit.

$$\theta_\infty = \arccos\left(-\frac{1}{e}\right) \quad (5.29)$$

An example of the hyperbolic orbit for Venus and of the capturing control law is shown in fig. 5.5.

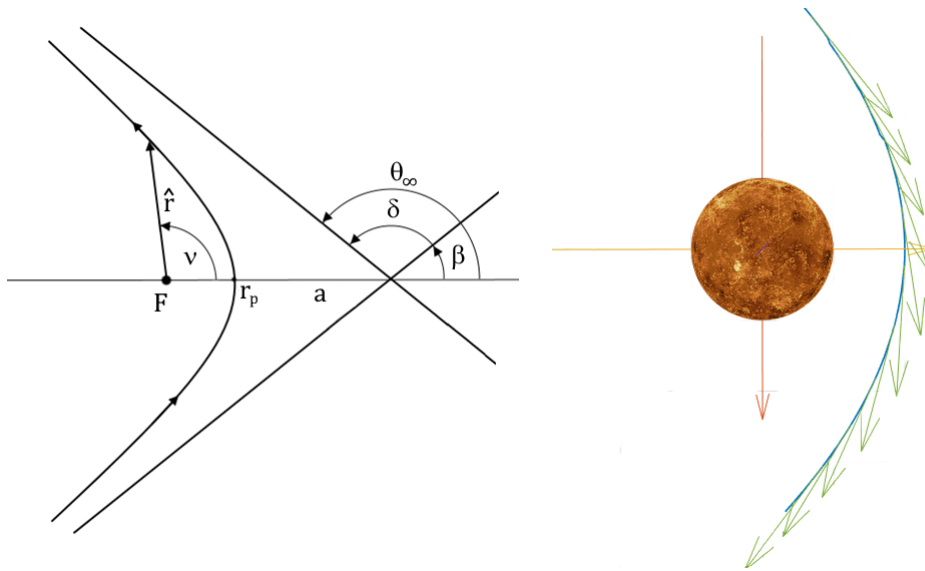


Figure 5.5. Example of hyperbolic orbit and capturing control law

# Chapter 6

## Results

Once the control laws have been established, some manoeuvres have been simulated to analyse the effect of PRP on their performance. The first section of this chapter is dedicated to the results with Gao's control law to change inclination, semimajor axis and eccentricity; the second section instead has been dedicated to the capturing manoeuvre.

### 6.1 Results of orbital manoeuvre with Gao's control law

As previously mentioned, the advantage of Gao's guidance scheme is that three different parameters can be changed within the same revolution. The analysis has been conducted for Venus with different initial orbits, and in this phase of the study, the four Gao's parameters have been chosen arbitrarily after some attempts and have been maintained constant over the time.

$$w_s = 0.3$$

$$w_e = 0.2$$

$$w_y = 0.6$$

$$w_a = 0.8$$

Only the sign of  $w_s$ ,  $w_e$ ,  $w_a$  change, and in particular they are positive when the manoeuvre is to increase the relative orbital element and negative to decrease it.

The analyses have been conducted with and without PRP and monitor the trend of the six orbital elements and the acceleration components during three revolutions around the planet. The time-step is 20s, and the sail has a characteristic acceleration of  $0.001m/s^2$  and a double-side coating.

#### 6.1.1 Quasi-circular orbit - decrease of $a$ , $e$ , $i$

In this study case a quasi-circular orbit with low inclination has been analysed in order to simulate the decrease of all the three orbital elements. The characteristic of the orbit has been summarised in table 6.1. In fig. 6.2 the results shows relevant improvement due

Periapsis $r_p$	Eccentricity $e$	Inclination $i$	RAAN $\Omega$	Argument of periapsis $\omega$
1.5 $R_V$	0.2	5 <i>deg</i>	5 <i>deg</i>	5 <i>deg</i>

Table 6.1. Orbital elements quasi-circular orbit

to the presence of PRP. The decreasing trend of all the three parameters is quicker than the case with only the solar contribution, and moreover, since the manoeuvring arc for the change of eccentricity is in the eclipse region, this element could not be modified with Gao's control laws without PRP.

In fig. 6.3 the magnitude of the acceleration and its three components are shown. The increase of the acceleration thanks to PRP is evident, in particular when the sail is in eclipse and SRP is zero. The SRP gives a null contribution even when the direction of the solar photons is against the required acceleration vector; in this situation, the sail is perpendicular to the photons not to provide a negative contribution. In fig. 6.4 the trend of the orbital elements have been simulated for a longer time, ten orbits. The target parameters have been set in 95% of the initial ones for the decreasing manoeuvres and 105% for the increasing ones, and some tolerances have been defined to establish when the final orbit can be considered reached. These tolerances are:

- $toll_a = 50 \text{ m}$
- $toll_e = 0.00001$
- $toll_i = 0.005 \text{ deg}$

Since the acceleration is higher with PRP, the results appear more oscillating, but they can be accepted with good approximation; moreover, integrating the optimization of Gao's parameters, the thrusting arc can be reduced. In table 6.2 the orbital elements after three revolutions have been listed with the percentage respect to the target values.

	Semimajor axis $a$	Eccentricity $e$	Inclination $i$
Target	10811 <i>km</i>	0.19	4.75 <i>deg</i>
SRP	11290 <i>km</i> 104.4 %	0.1998 105.2 %	4.95 <i>deg</i> 104.2 %
SRP+PRP	11120 <i>km</i> 102.9 %	0.1899 99.9 %	4.73 <i>deg</i> 99.5 %

Table 6.2. Semimajor axis, eccentricity and inclination after three revolutions

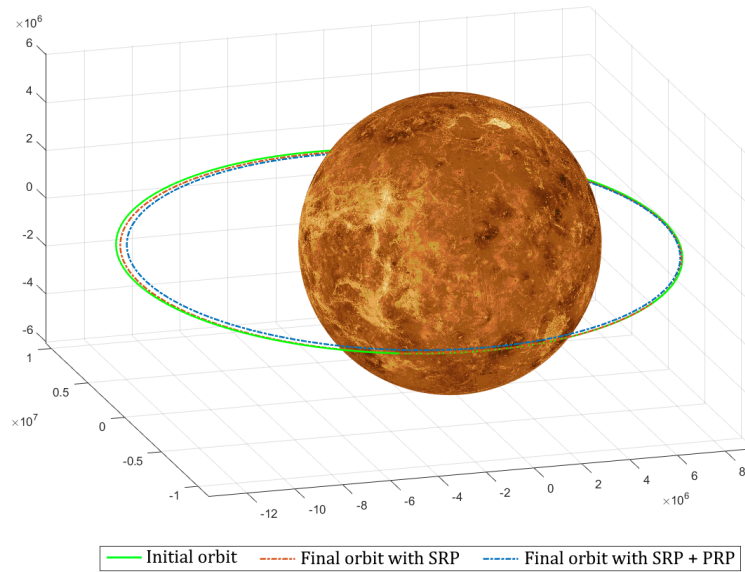


Figure 6.1. Initial and final orbit with and without PRP, quasi-circular orbit with low inclination around Venus

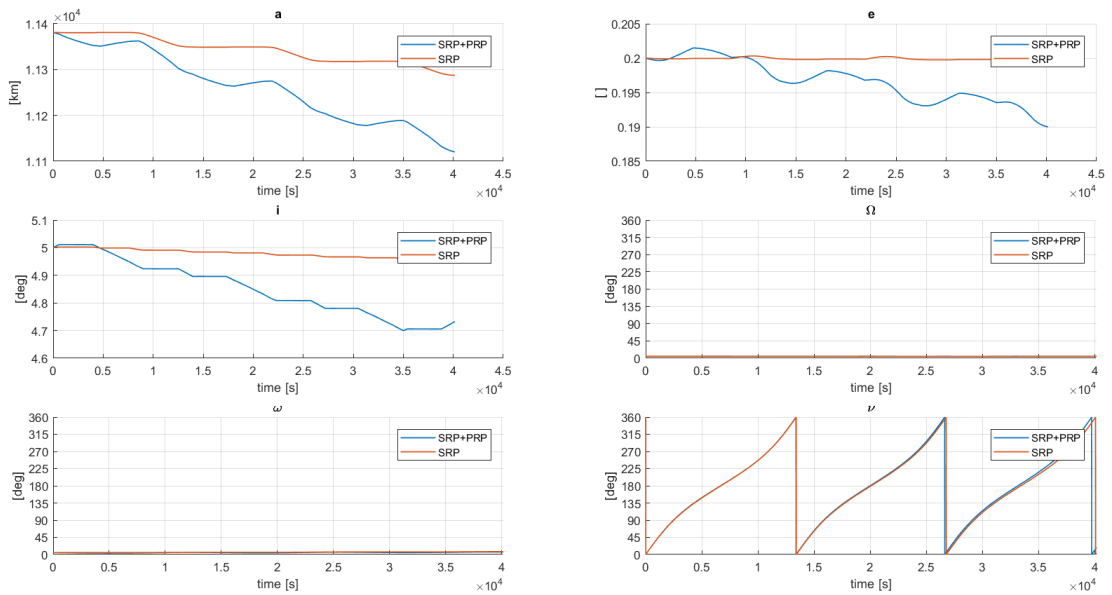


Figure 6.2. Trend of the orbital elements with and without PRP during three revolutions, quasi-circular orbit with low inclination around Venus

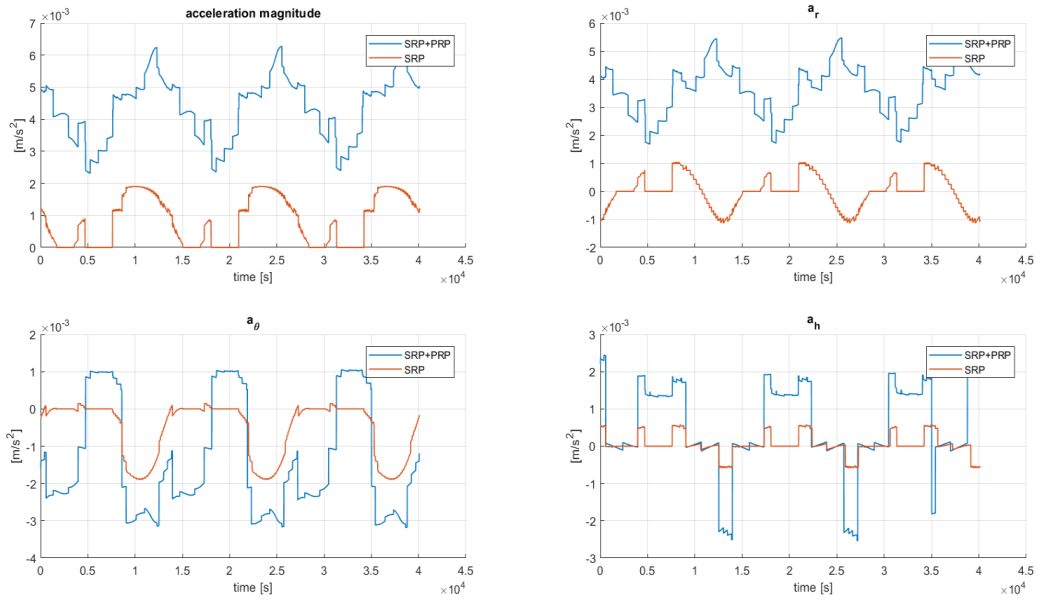


Figure 6.3. Trend of the acceleration with and without PRP during three revolutions, quasi-circular orbit with low inclination around Venus

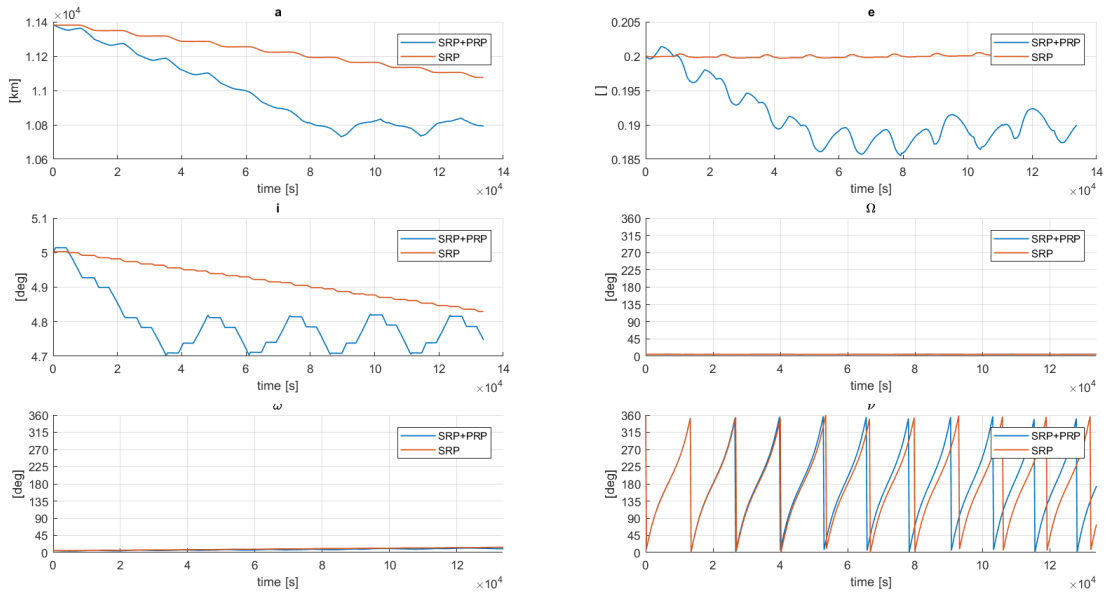


Figure 6.4. Trend of the orbital elements with and without PRP during ten revolutions, quasi-circular orbit with low inclination around Venus

### 6.1.2 Quasi-circular orbit - increase of $a$ , $e$ and decrease of $i$

The analysis has been repeated with the same parameters, but increasing semimajor axis and eccentricity, and decreasing the inclination to test the possibility of changing independently the orbital elements.

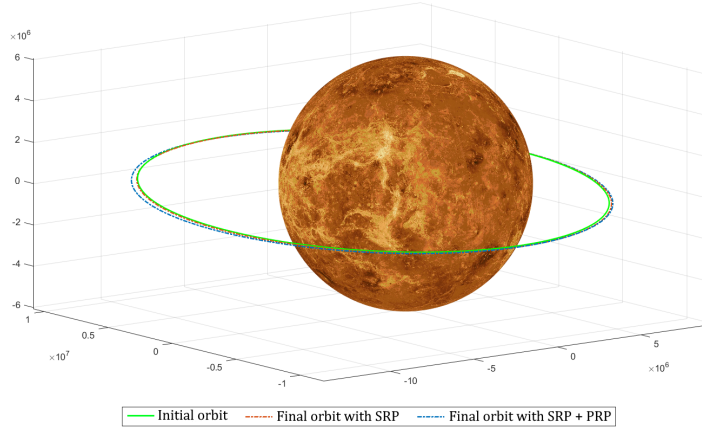


Figure 6.5. Initial and final orbit with and without PRP, quasi-circular orbit with low inclination around Venus

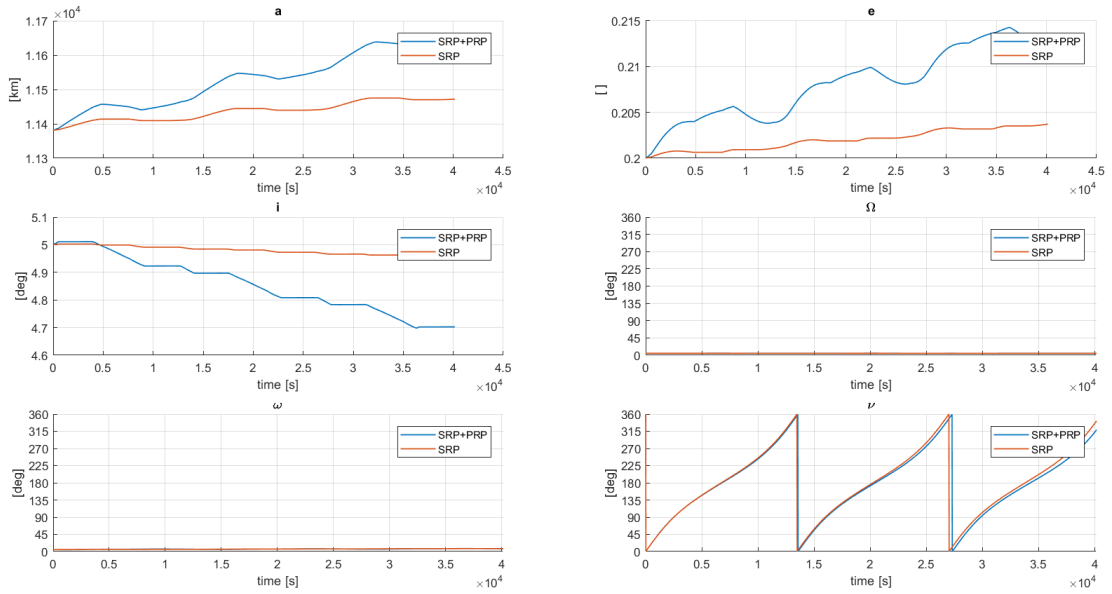


Figure 6.6. Trend of the orbital elements with and without PRP during three revolutions, quasi-circular orbit with low inclination around Venus

Same considerations can be done for this study-case, where again the PRP is relevant in the manoeuvre.

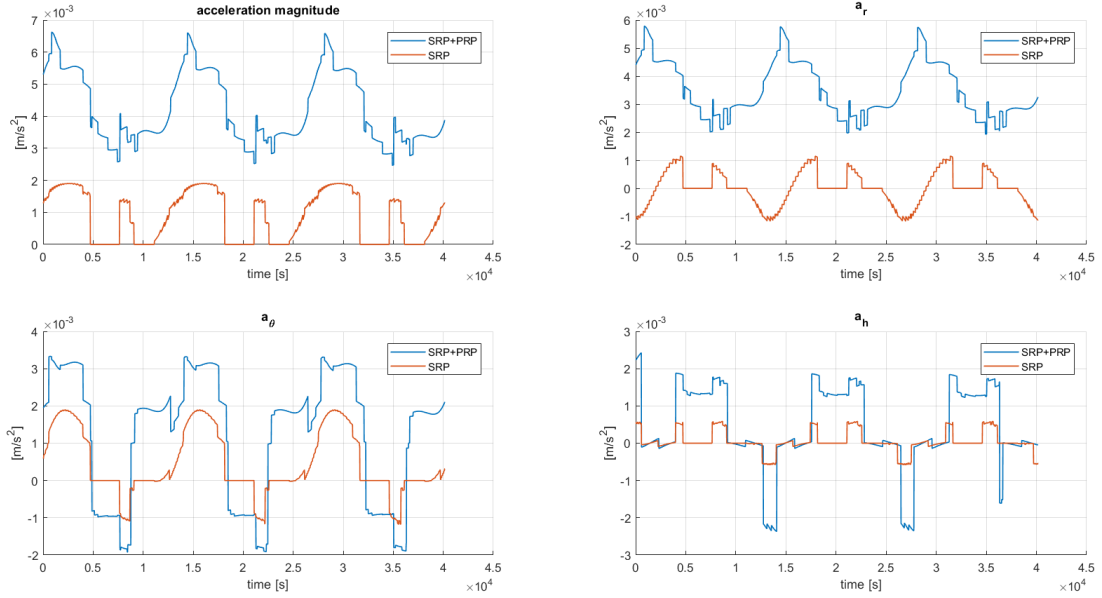


Figure 6.7. Trend of the acceleration with and without PRP during three revolutions, quasi-circular orbit with low inclination around Venus

	Semimajor axis $a$	Eccentricity $e$	Inclination $i$
Target	11949 km	0.21	4.75 deg
SRP	11470 km 96.0 %	0.2037 97.0 %	4.95 deg 104.2 %
SRP+PRP	11670 km 97.7 %	0.2092 99.6 %	4.70 deg 98.9 %

Table 6.3. Semimajor axis, eccentricity and inclination after three revolutions

### 6.1.3 Highly-elliptical orbit - decrease of $a$ , $e$ , $i$

In this study case, a highly-elliptical orbit with low inclination has been analysed in order to simulate the decrease of all the three orbital elements. The characteristic of the orbit have been summarised in table 6.4.

After three revolutions, the result with and without PRP are similar and the planet contribution seems not to have a beneficial effect such as in the quasi-circular orbit case.

Periapsis $r_p$	Eccentricity $e$	Inclination $i$	RAAN $\Omega$	Argument of periapsis $\omega$
$1.5 R_V$	0.7	5 deg	5 deg	5 deg

Table 6.4. Orbital elements highly-elliptical orbit

On average, the sail is farther from the planet than in the previous analysis, so the acceleration is mostly the same with or without PRP. As can be seen in fig. 6.10, the only difference is that the acceleration with PRP has a peak in the radial component in the arc of orbit closer to the planet. In fig. 6.11, it can be noticed the planet contribution slightly benefits the change of eccentricity in a longer time. Better results probably could be obtained optimising the four parameters of the control laws.

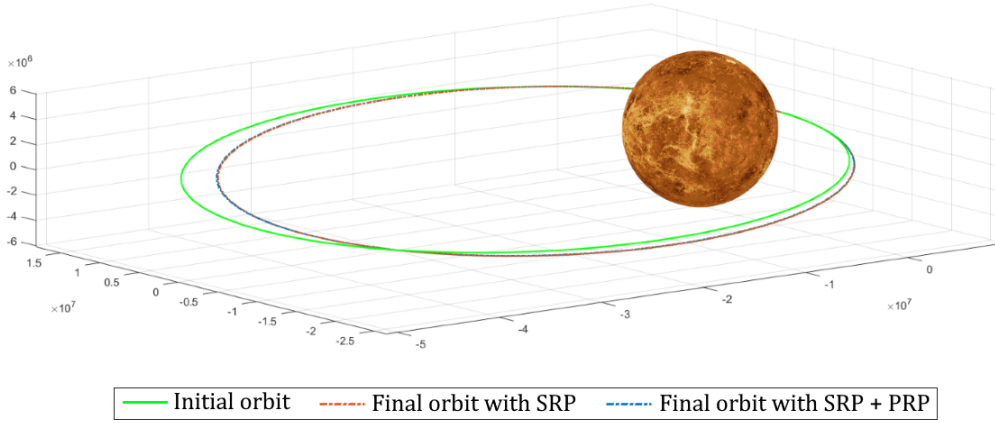


Figure 6.8. Initial and final orbit with and without PRP, highly-elliptical orbit with low inclination around Venus

	Semimajor axis $a$	Eccentricity $e$	Inclination $i$
Target	28832 km	0.665	4.75 deg
SRP	29390 km 101.9 %	0.6905 103.8 %	4.54 deg 95.6 %
SRP+PRP	28770 km 94.8 %	0.681 102.4 %	4.47 deg 94.1 %

Table 6.5. Semimajor axis, eccentricity and inclination after three revolutions

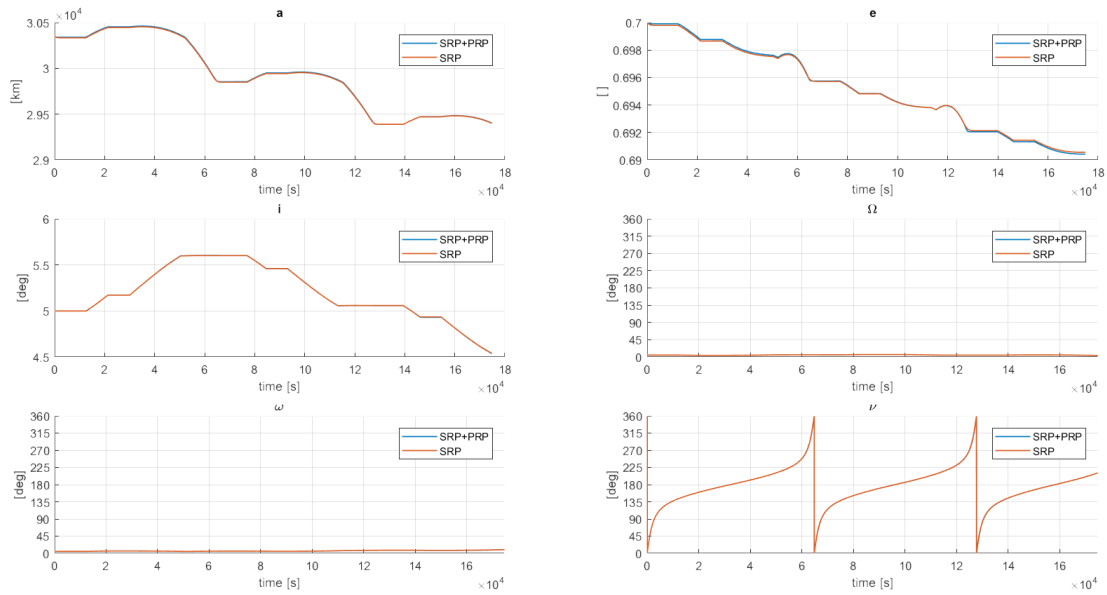


Figure 6.9. Trend of the orbital elements with and without PRP during three revolutions, highly-elliptical orbit with low inclination around Venus

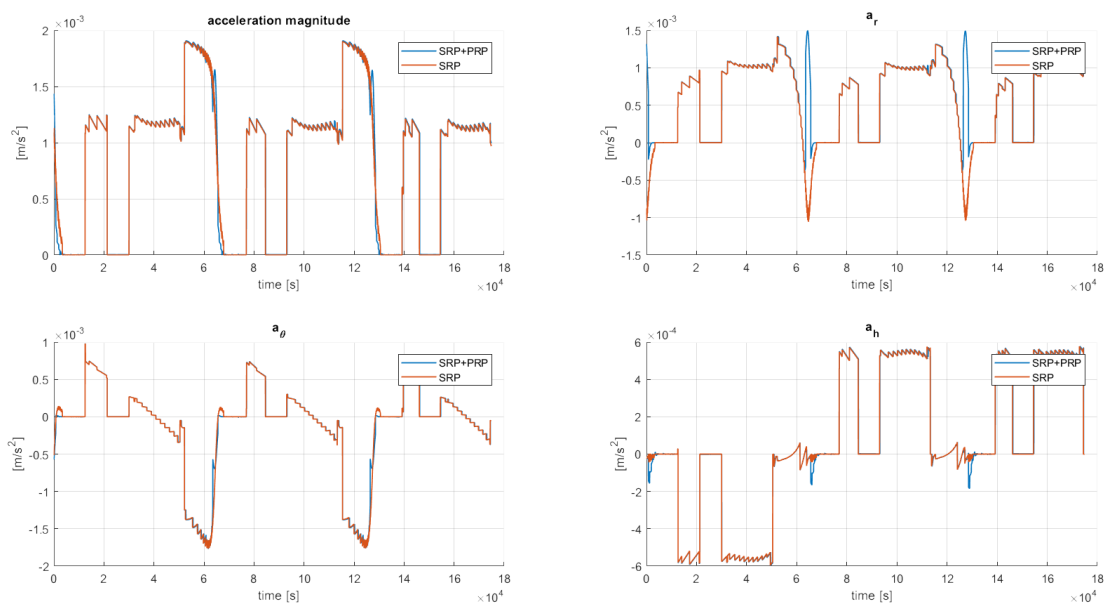


Figure 6.10. Trend of the acceleration with and without PRP during three revolutions, highly-elliptical orbit with low inclination around Venus

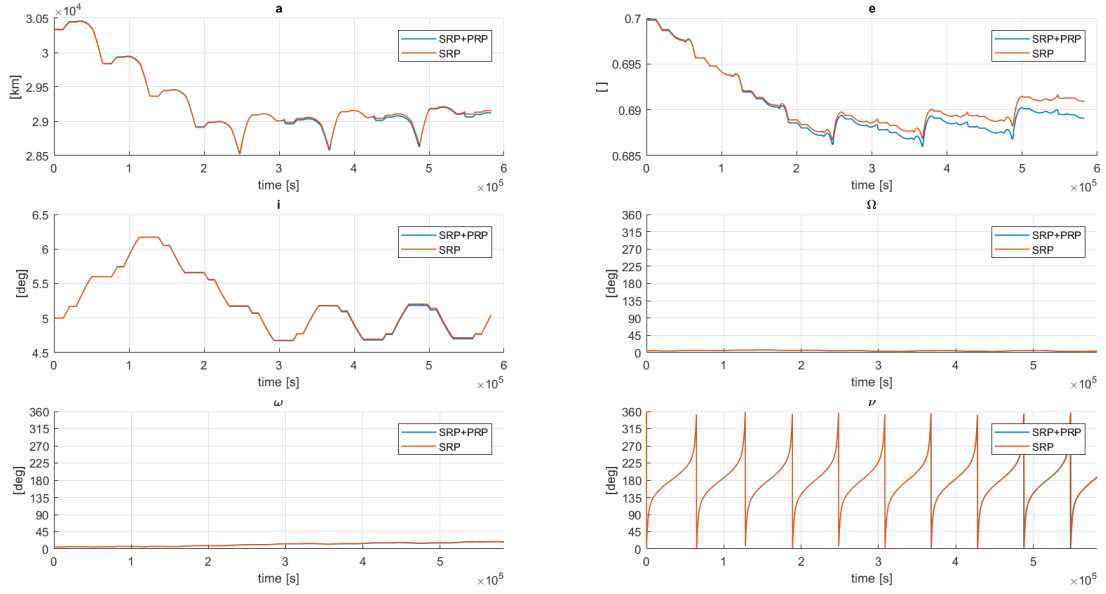


Figure 6.11. Trend of the orbital elements with and without PRP during ten revolutions, highly-elliptical orbit with low inclination around Venus

#### 6.1.4 Inclined orbit - increase of $a$ , $e$ , $i$

The analyses previously done have been repeated for a quasi-circular orbit with a high inclination; in this case, the purpose is to increase all the three orbital elements.

Periapsis $r_p$	Eccentricity $e$	Inclination $i$	RAAN $\Omega$	Argument of periapsis $\omega$
$1.5 R_V$	0.2	75 deg	5 deg	5 deg

Table 6.6. Orbital elements highly-elliptical orbit

Even for this example, the results with PRP are promising and show a quicker trend when all the contributions are considered. This is particularly evident in fig. 6.14 where the acceleration components with PRP and SRP are significantly higher than the ones with only SRP.

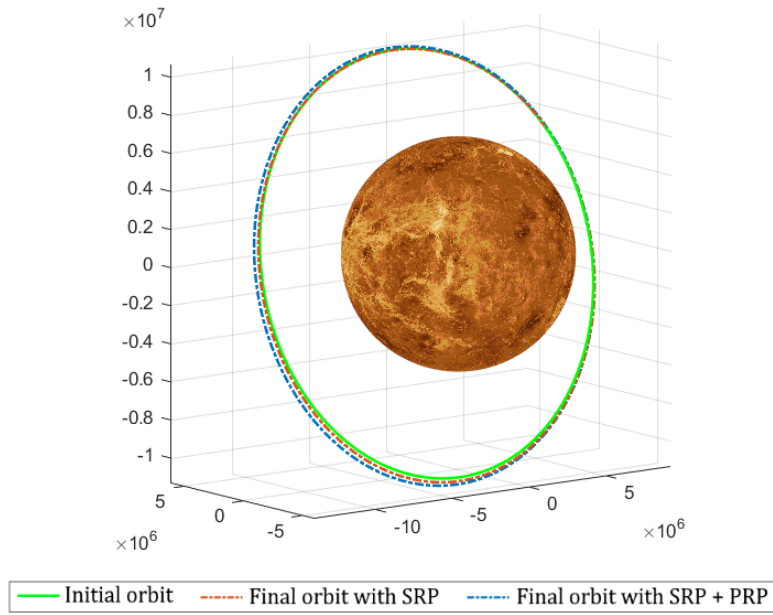


Figure 6.12. Initial and final orbit with and without PRP, quasi-circular orbit with high inclination around Venus

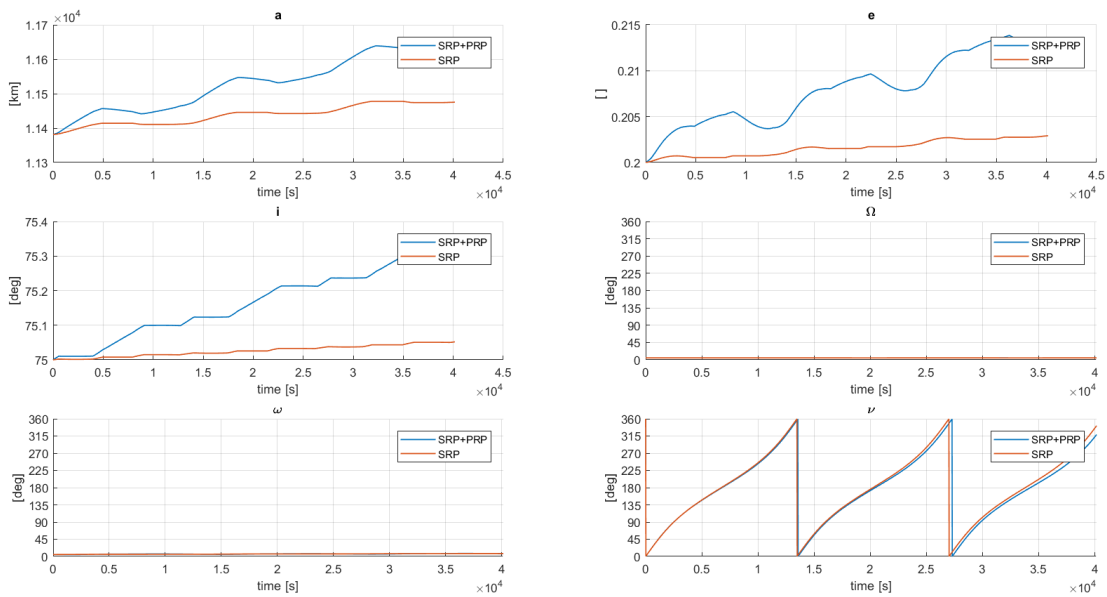


Figure 6.13. Trend of the orbital elements with and without PRP during three revolutions, quasi-circular orbit with high inclination around Venus

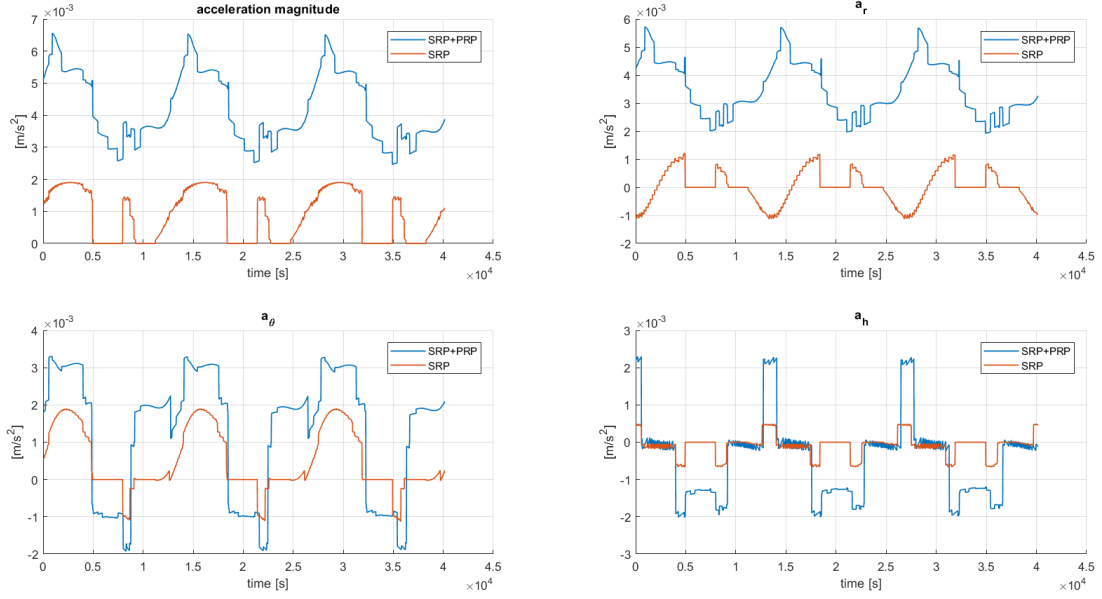


Figure 6.14. Trend of the acceleration with and without PRP during three revolutions, quasi-circular orbit with high inclination around Venus

	Semimajor axis $a$	Eccentricity $e$	Inclination $i$
Target	11949 km	0.21	78.75 deg
SRP	11470 km 96.0 %	0.2029 96.6 %	75.05 deg 95.3 %
SRP+PRP	11670 km 97.7 %	0.2088 99.4 %	75.33 deg 95.7 %

Table 6.7. Semimajor axis, eccentricity and inclination after three revolutions

### 6.1.5 Inclined orbit with RAAN - increase of $a$ , $e$ and decrease of $i$

A more generic orbit has been analysed in this section. In particular, the right ascension of the ascending node has been rotated of  $90 \text{ deg}$  respect to the sun rays and the orbit is inclined of  $45 \text{ deg}$ . The aim is to increase the semimajor axis  $a$  and the eccentricity  $e$  and to decrease the inclination  $i$ .

The results are particularly interesting since the trend of inclination is the opposite in the two cases. In particular, it cannot be decreased with only the solar radiation pressure due to the direction of its photons, so the planetary contribution is fundamental to perform the manoeuvre. This consideration is even clearer when the analysis is done for ten revolutions such as in fig. 6.18. In fig. 6.17 it is possible to see that the out-of-plane acceleration of the

Periapsis $r_p$	Eccentricity $e$	Inclination $i$	RAAN $\Omega$	Argument of periapsis $\omega$
$1.5 R_V$	0.4	45 deg	90 deg	5 deg

Table 6.8. Orbital elements elliptical orbit with medium inclination

sail without PRP is only negative, instead of the positive contribution that the planetary photons give. The two other orbital elements benefits the planetary radiation pressure too, improving the performance of the manoeuvre.

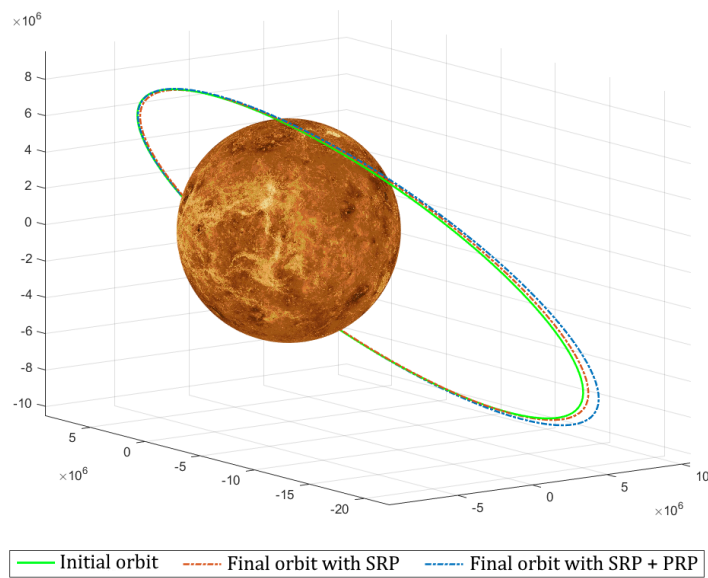


Figure 6.15. Initial and final orbit with and without PRP, elliptical orbit with medium inclination and rotated RAAN around Venus

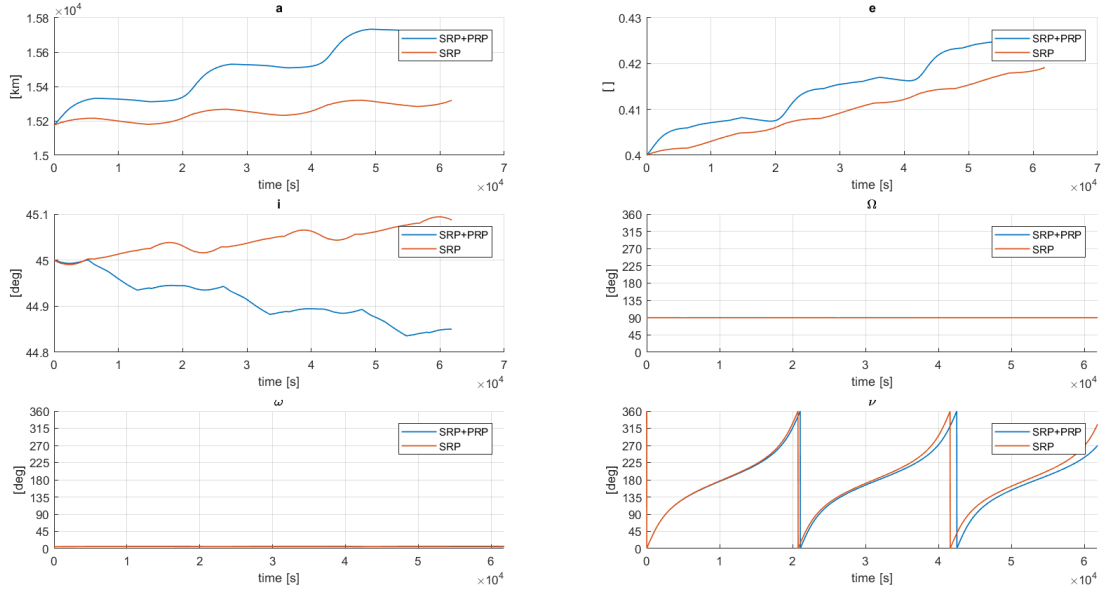


Figure 6.16. Trend of the orbital elements with and without PRP during three revolutions, elliptical orbit with medium inclination and rotated RAAN around Venus

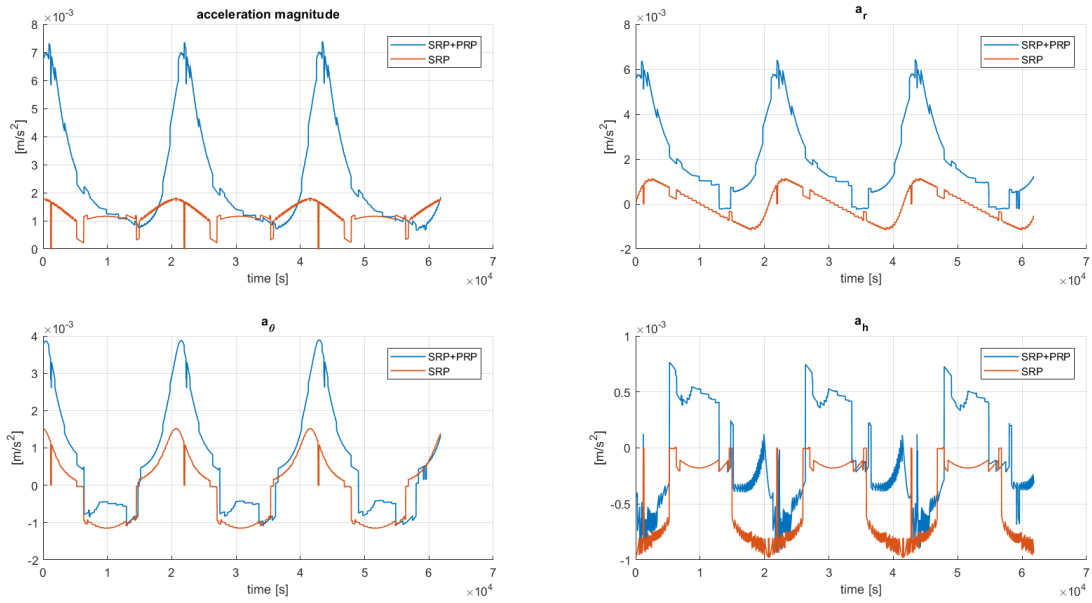


Figure 6.17. Trend of the acceleration with and without PRP during three revolutions, elliptical orbit with medium inclination and rotated RAAN around Venus

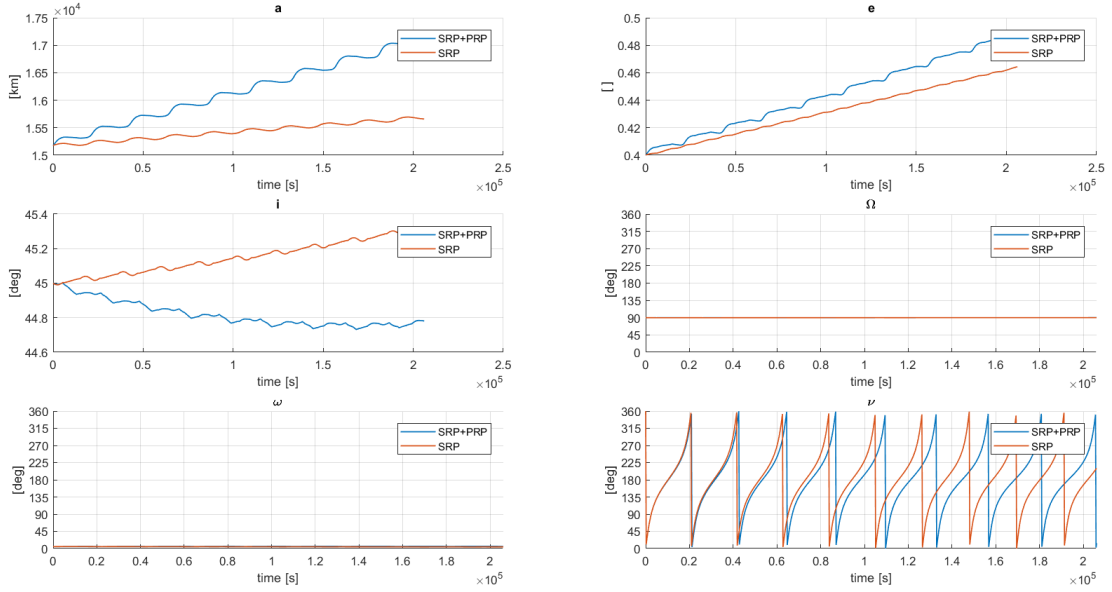


Figure 6.18. Trend of the orbital elements with and without PRP during ten revolutions, elliptical orbit with medium inclination and rotated RAAN around Venus

	Semimajor axis $a$	Eccentricity $e$	Inclination $i$
Target	15939 $km$	0.42	42.75 $deg$
SRP	15320 $km$	0.4191	45.09 $deg$
	96.1 %	99.8 %	105.5 %
SRP+PRP	15740 $km$	0.4221	44.83 $deg$
	98.8 %	100.5 %	104.9 %

Table 6.9. Semimajor axis, eccentricity and inclination after three revolutions

### 6.1.6 Inclined orbit with RAAN - increase of $a$ , $e$ and $i$

Since the previous analysis shows that solar radiation pressure cannot provide acceleration to decrease the inclination, the analysis has been repeated increasing all the three orbital elements.

The PRP contribution for semimajor axis and eccentricity is still relevant; however, the curves for inclination, that in the previous analysis were in the opposite direction, are now the same so that the PRP has no relevance in the increasing of inclination in this orbit.

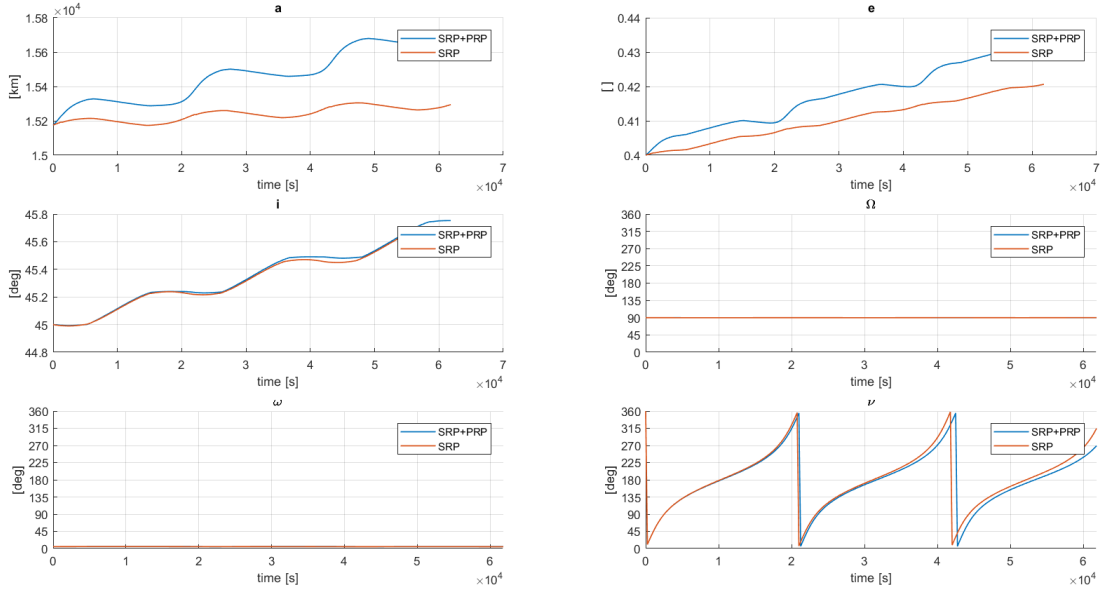


Figure 6.19. Trend of the orbital elements with and without PRP during three revolutions, elliptical orbit with a medium inclination and rotated RAAN around Venus

	Semimajor axis $a$	Eccentricity $e$	Inclination $i$
Target	15939 $km$	0.42	47.25 $deg$
SRP	15300 $km$ 96.1 %	0.421 100.2 %	45.7 $deg$ 101.6 %
SRP+PRP	15690 $km$ 98.4 %	0.4264 101.5 %	45.71 $deg$ 101.6 %

Table 6.10. Semimajor axis, eccentricity and inclination after three revolutions

### 6.1.7 Quasi-circular orbit out of PRP dominating region - increase of $a$ , $e$ and decrease of $i$

The last simulation with Gao's control laws has been done for a quasi-circular orbit further from Venus. In chapter 4 has been seen that after some radii from the planet, the PRP becomes less relevant in the results. For this study-case, the aim is to decrease the inclination and increase semimajor-axis and eccentricity. The orbit data has been summarised in table 6.11.

As expected, the further distance from Venus decreases the planetary contribution, and the acceleration with and without PRP tends to be more similar than in the other study-case. The inclination decreases faster in the case with PRP and starts oscillating as it can be noticed in fig. 6.22 and in fig. 6.23. In fig. 6.22, for the last revolution the SRP+PRP

Periapsis $r_p$	Eccentricity $e$	Inclination $i$	RAAN $\Omega$	Argument of periapsis $\omega$
$3 R_V$	0.2	5 deg	5 deg	5 deg

Table 6.11. Orbital elements elliptical orbit with medium inclination

out-of-plane acceleration changes sign since target inclination have been exceeded. In the longer time simulation, the oscillating of the inclination around the target inclination is evident; in addition, the manoeuvres for semimajor-axis and eccentricity have slightly better performance in the case with only SRP.

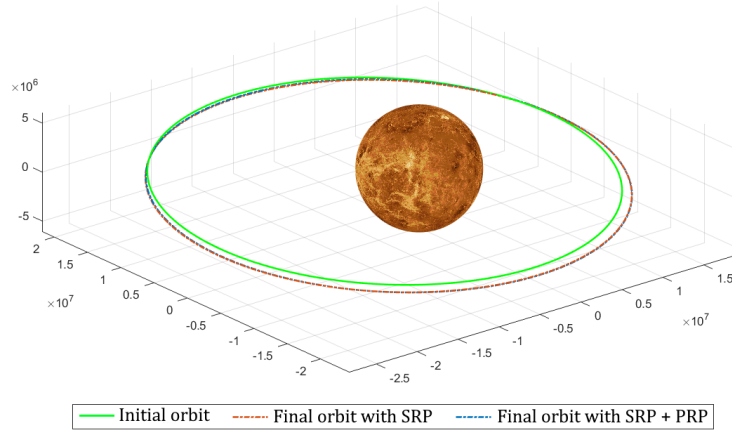


Figure 6.20. Initial and final orbit with and without PRP, quasi-circular orbit with low inclination around Venus

	Semimajor axis $a$	Eccentricity $e$	Inclination $i$
Target	23898 km	0.21	4.75 deg
SRP	23570 km 98.6 %	0.2154 102.6 %	4.69 deg 98.7 %
SRP+PRP	23620 km 98.8 %	0.2095 99.8 %	102.5 deg 104.9 %

Table 6.12. Semimajor axis, eccentricity and inclination after three revolutions

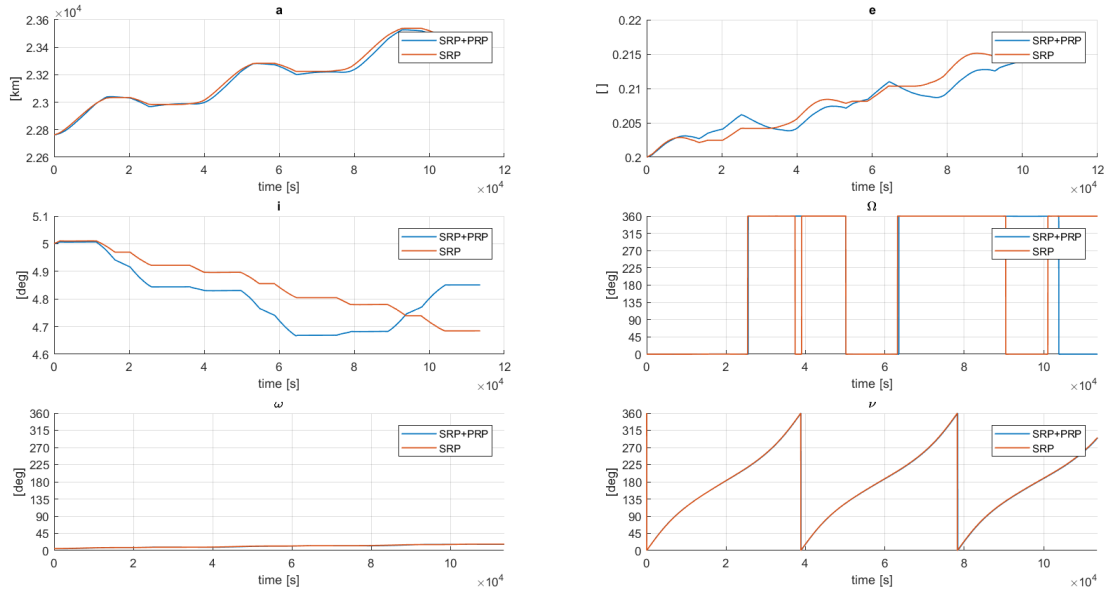


Figure 6.21. Trend of the orbital elements with and without PRP during three revolutions, quasi-circular orbit with low inclination around Venus

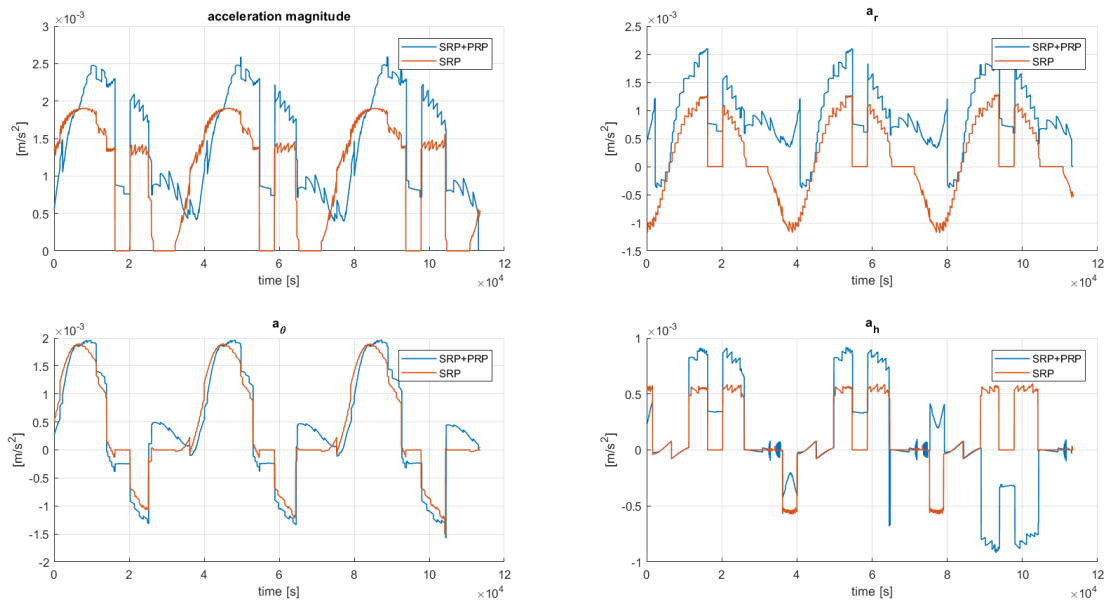


Figure 6.22. Trend of the acceleration with and without PRP during three revolutions, quasi-circular orbit with low inclination around Venus

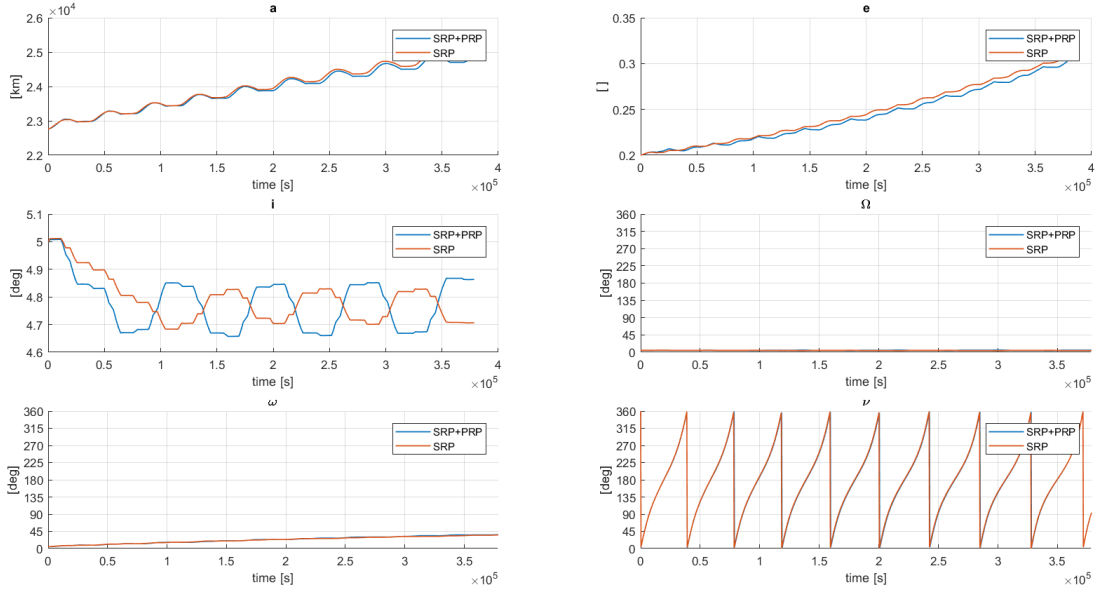


Figure 6.23. Trend of the orbital elements with and without PRP during ten revolutions, quasi-circular orbit with low inclination around Venus

## 6.2 Results of capturing manoeuvre

As previously mentioned, the study of the capturing manoeuvre has been conducted with a parametric approach. In the first phase, three parameters have been used:

- the characteristic acceleration  $a_o$
- the periapsis of the hyperbolic orbit  $r_p$
- the eccentricity of the hyperbolic orbit  $i_h$

This preliminary step is needed to find a plausible characteristic acceleration that allows the capturing manoeuvre. After choosing the characteristic acceleration, the analysis has been deepened comparing the possible combinations of periapsides and eccentricity with and without PRP.

### 6.2.1 Parametric study - $a_o$ , $r_p$ and $i_h$

A grid of  $50 \times 50 \times 50$  has been used with a range of the periapsides that goes from  $1.5 R_V$  to  $15 R_V$ , that one of eccentricity from 1.0005 to 1.05 and that one of characteristic acceleration from  $0.1 \text{ mm/s}^2$  to  $3 \text{ mm/s}^2$ . The other parameters of the analysis are:

- $i = 5 \text{ deg}$ ,  $\omega = 0 \text{ deg}$ ,  $\Omega = 5 \text{ deg}$

An example of a possible orbit and the resulting velocity vector is shown in fig. 6.24. The analysis has been conducted only with SRP+PRP and the capturing has been considered

achieved when the eccentricity at the end of the manoeuvre is less than one. All the combination of parameters above the curve in the results allow the capturing manoeuvre.

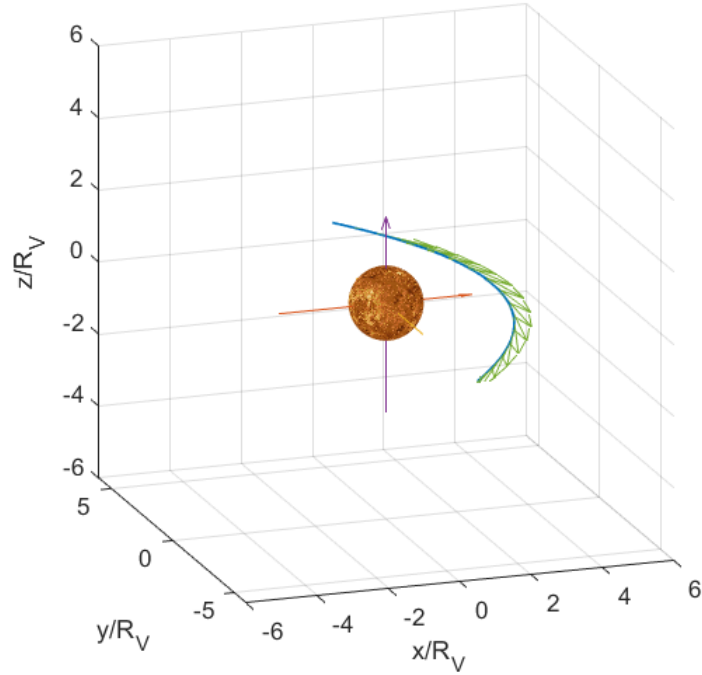


Figure 6.24. Example of the four study-case orbits

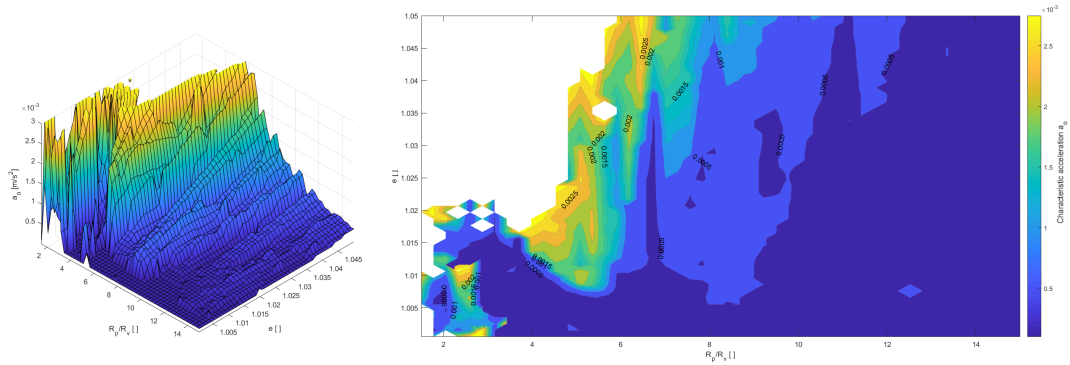


Figure 6.25. Curve of the parameters that allow the capturing manoeuvre -  $i$  5 deg,  $\omega$  0 deg

All the combinations of parameters above the surface in fig. 6.25 allows the capturing manoeuvre, so in the chosen range of characteristic accelerations there are acceptable

values. In the contour it is possible to evaluate the minimum required characteristic acceleration. As expected, this increases for high initial eccentricity and when the manoeuvre is performed close to the planet, since the velocity to brake is higher. Moreover, the surface is extensively influenced even by the other orbital elements, that indicate the region where the manoeuvre is done.

According to McInnes [1],  $1 \text{ mm/s}^2$  is a reasonable characteristic acceleration, technologically possible. Hence, this has been used in the following analyses.

## 6.2.2 Parametric study - Comparison with and without PRP

In this section of results, the plausible characteristic acceleration of  $1 \text{ mm/s}^2$  has been chosen to compare the different initial conditions that allow the capturing manoeuvre. The grid used is  $50 \times 50$ , and the ranges of periapsides and eccentricity are the same as the previous simulations. More study-cases than in the previous analysis have been investigated, and in particular the combinations between the two inclinations,  $5 \text{ deg}$  and  $85 \text{ deg}$ , and four different arguments of periapsis:

- $\omega = 0 \text{ deg}$  (a)
- $\omega = 90 \text{ deg}$  (b)
- $\omega = 180 \text{ deg}$  (c)
- $\omega = 270 \text{ deg}$  (d)

In the fig. 6.26, results of an orbit with inclination equal to  $5 \text{ deg}$  are shown. The sets of values that allow the manoeuvre are those under the curve and are particularly different in every case. In fig. 6.26 (a), the periapsis is between the planet and the Sun; for lower periapsis, the sail is closer to the planet but, since planetary radiation pressure is mostly radial to the planet, the allowed initial eccentricity is very similar to when PRP is not taken into account. After 2 radii, PRP becomes even less significant, and the two curves are the same. However, results do appear quite rough, so a denser grid should be used in future more accurate simulations. As regard fig. 6.26 (b) and (d), same consideration can be done. It is interesting to notice that when the argument of periapsis is  $90 \text{ deg}$ , the allowed initial eccentricity is strictly lower than any other case, and in particular of the opposite one. The reason is linked to the direction of the incident photons and the requested acceleration; in fact, when  $\omega = 90 \text{ deg}$  the velocity and the solar incident photons point mostly in the same direction, so the sail can hardly provide an acceleration against the velocity vector. The opposite situation happens when  $\omega = 270 \text{ deg}$ . In this case, again, the solar incident photons are almost parallel to the velocity vector, but point in the opposite direction. For the study of planetary contribution, the analysis with the argument of periapsis equal to  $180 \text{ deg}$  is the most relevant; since part of the manoeuvre is in the eclipse area, the PRP is more significant than in the other cases, and, as can be seen in the figure, it allows a wider range of possible initial values. However, its contribution is limited to closest area to Venus, within 2 radii of distance.

The same considerations can be repeated for the results of the orbit with an inclination of  $85 \text{ deg}$ . The case with a part of the manoeuvre in the eclipse area benefits the planetary effect again, but the effect is smaller than the low inclined orbit. Deepened analysis has

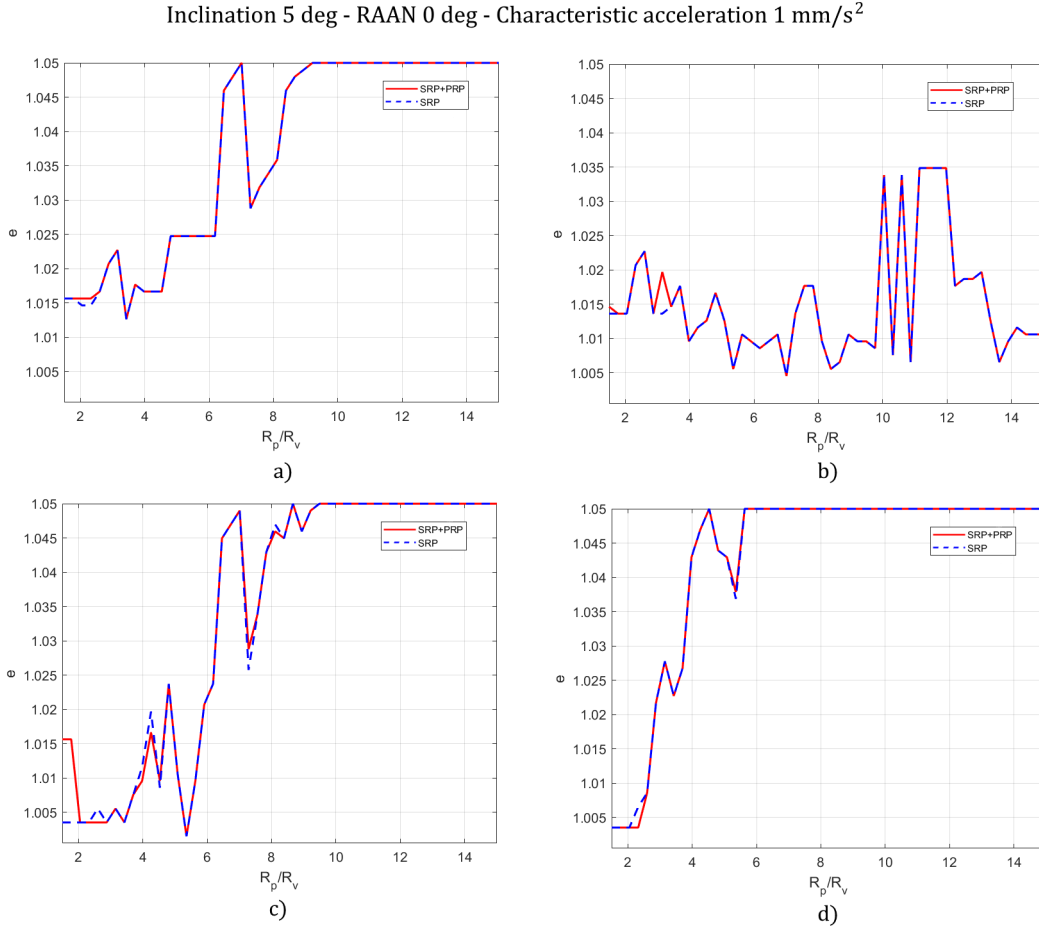


Figure 6.26. Initial conditions that allow the capturing manoeuvre for an orbit with inclination-  $i$  5 deg

been conducted choosing a point and simulating the manoeuvre so that the trend of the acceleration can be studied and a validation test can be done on the parametric study. Due to its position in the plots, the set of initial conditions that has been chosen to perform the test is:

- $r_p = 1.5R_V$ ,  $e = 1.0075$

The analysis has been conducted for the two different inclinations and the arguments of periaapsis equal to 0 deg and 180 deg. Results in fig. 6.29 shows the trends of the acceleration components and its magnitude. The acceleration along the velocity vector is similar in both the cases, with a slightly worse performance for the SRP+PRP analysis. As expected, the trend of eccentricity in fig. 6.28 (a) shows that the capture is achieved in both the cases, but in fig. 6.28 (b) it should be noticed that the presence of PRP changes the attitude of the sail, so not considering its contribution could influence the success of the manoeuvre.



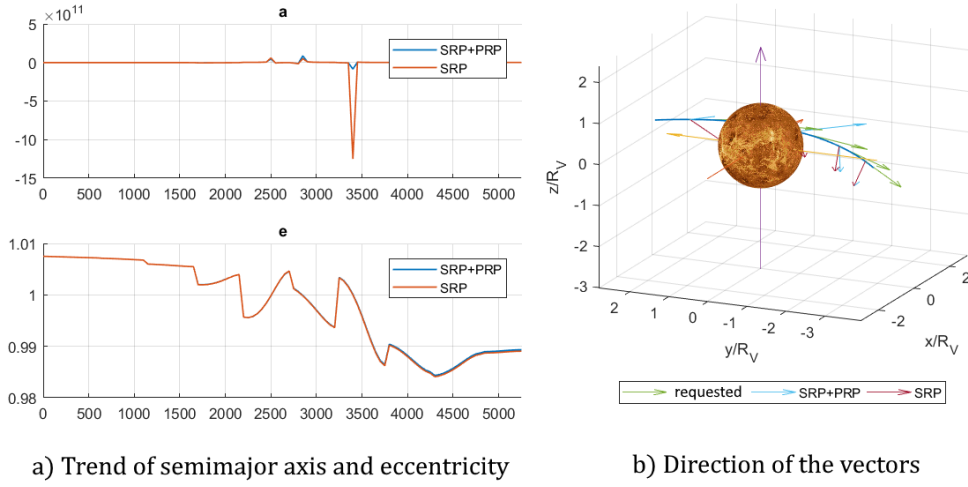


Figure 6.28. Trend of semimajor axis and eccentricity (a), and direction of the acceleration vectors -  $i 5 \text{ deg}$ ,  $\omega 0 \text{ deg}$

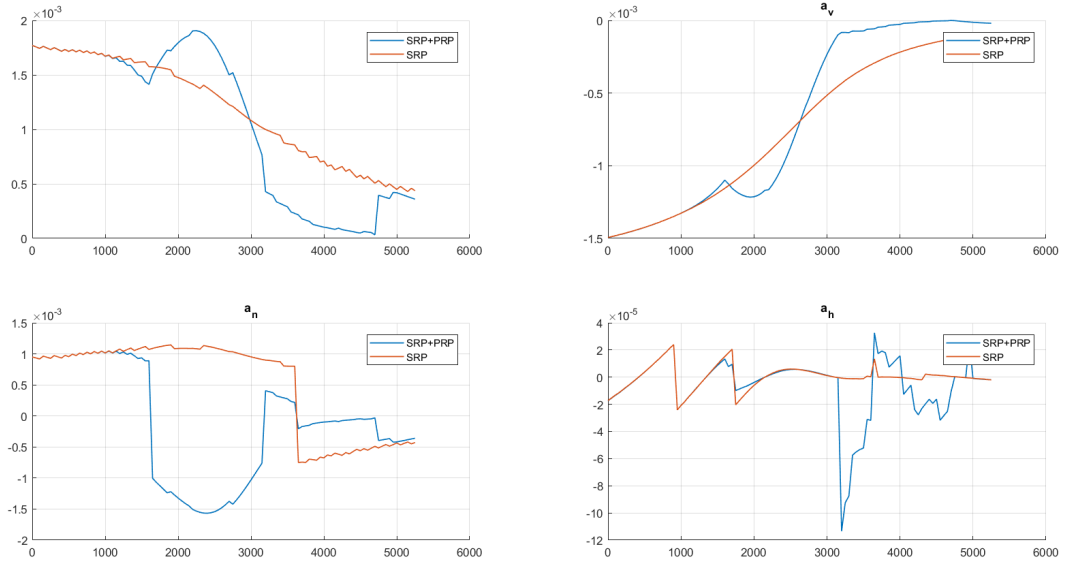


Figure 6.29. Magnitude and components of the acceleration vector -  $i 5 \text{ deg}$ ,  $\omega 0 \text{ deg}$

confirm this thesis and with or without planetary contribution the capture is achieved. However, comparing the results in fig. 6.34 with the ones of the other study-case, it can be noticed that the presence of PRP in the analysis allows to close the orbit about 500s before the case with only SRP and leads to a smaller eccentricity at the end of the braking phase.

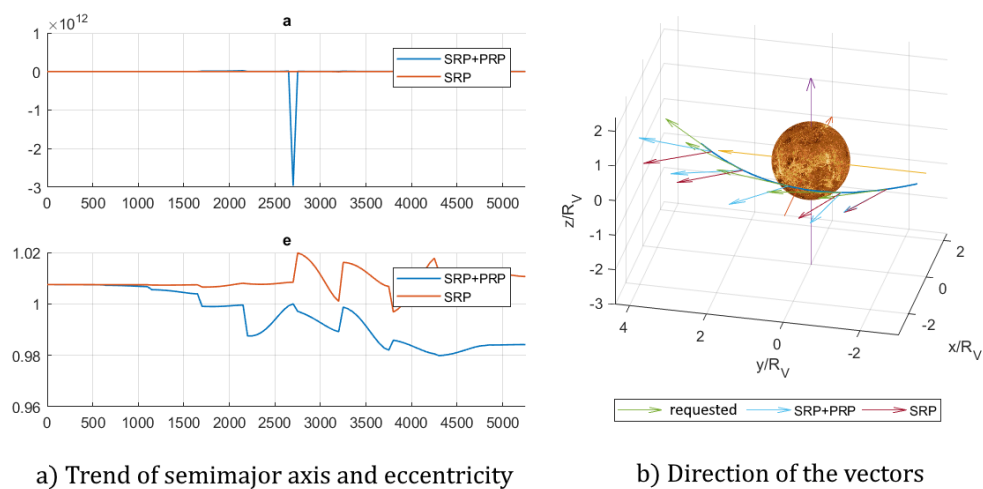


Figure 6.30. Trend of semimajor axis and eccentricity (a), and direction of the acceleration vectors -  $i$  5 deg,  $\omega$  180 deg

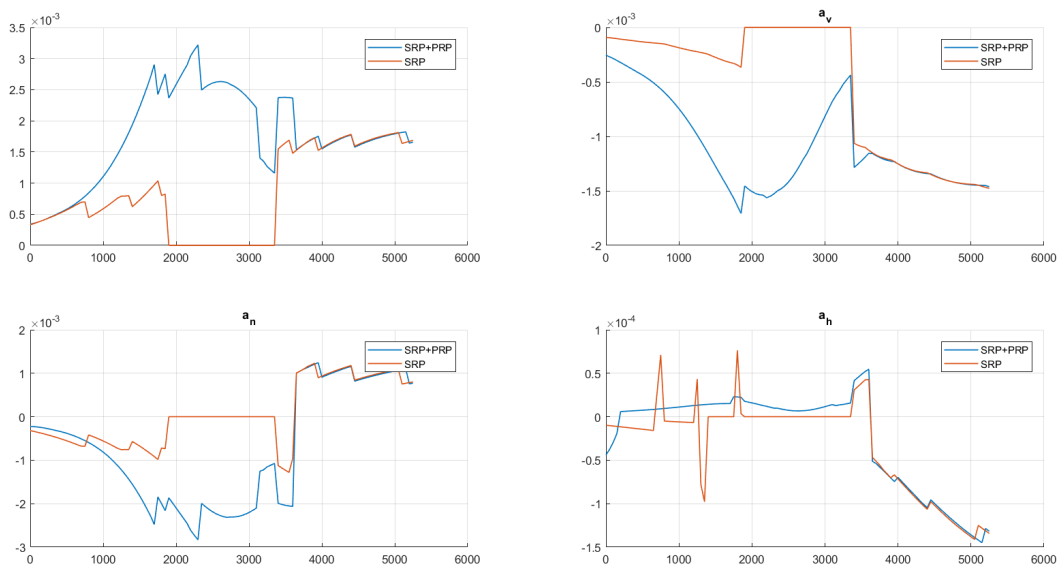


Figure 6.31. Magnitude and components of the acceleration vector -  $i$  5 deg,  $\omega$  180 deg

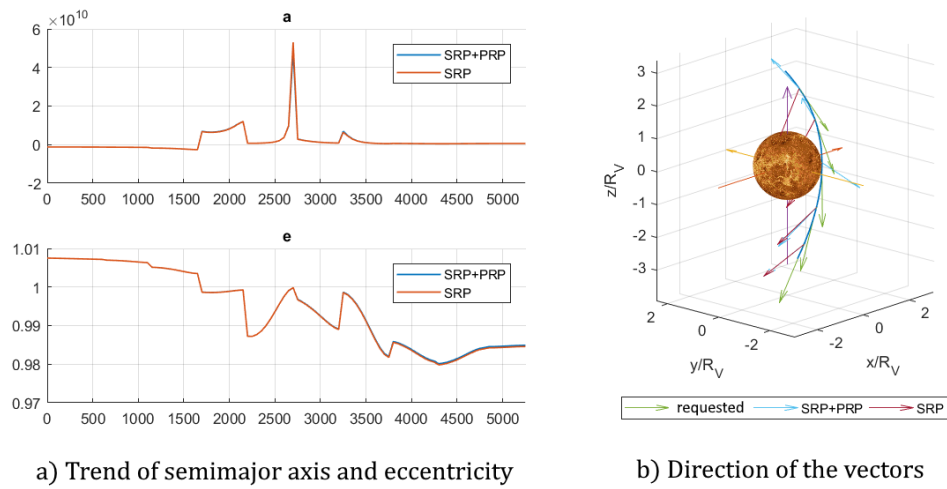


Figure 6.32. Trend of semimajor axis and eccentricity (a), and direction of the acceleration vectors -  $i$  85 deg,  $\omega$  0 deg

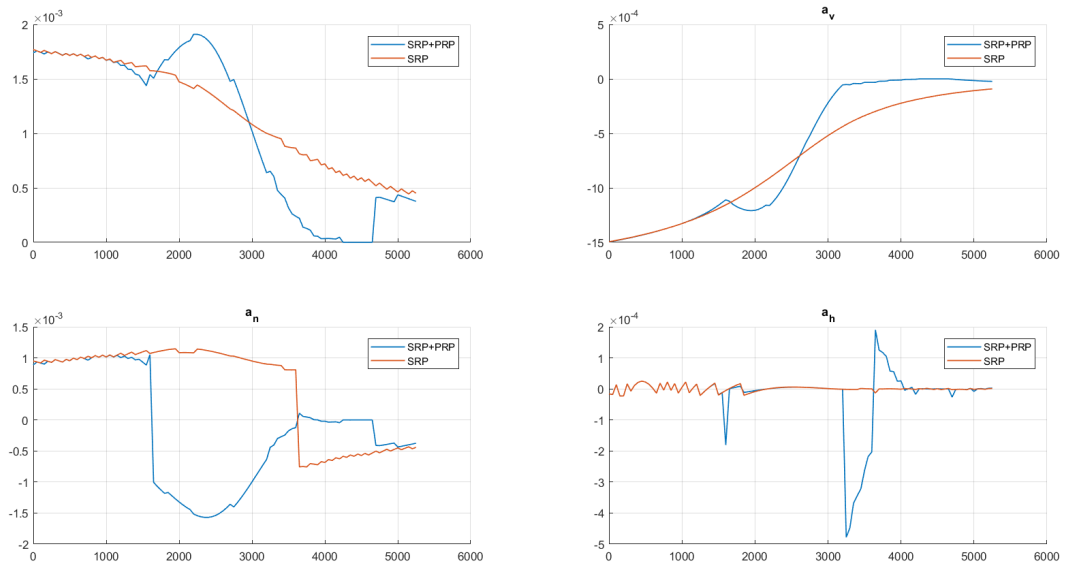


Figure 6.33. Magnitude and components of the acceleration vector -  $i$  85 deg,  $\omega$  0 deg

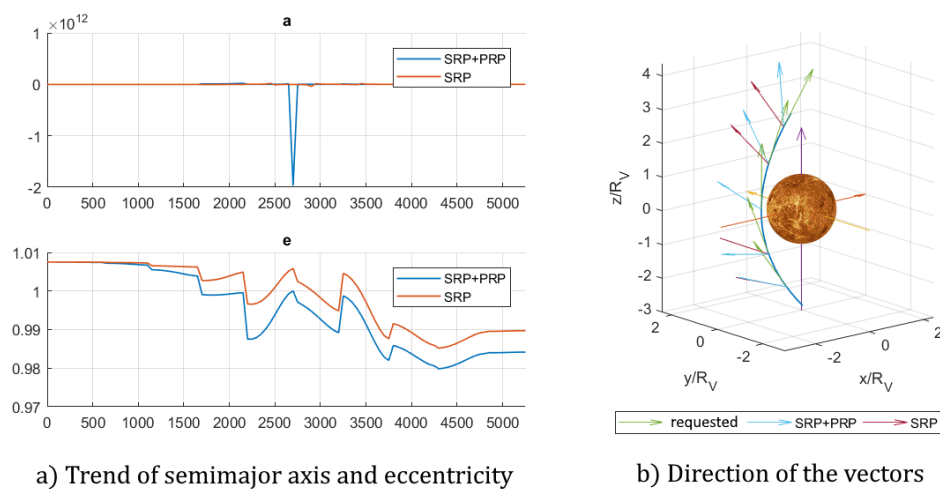


Figure 6.34. Trend of semimajor axis and eccentricity (a), and direction of the acceleration vectors -  $i$  85 deg,  $\omega$  180 deg

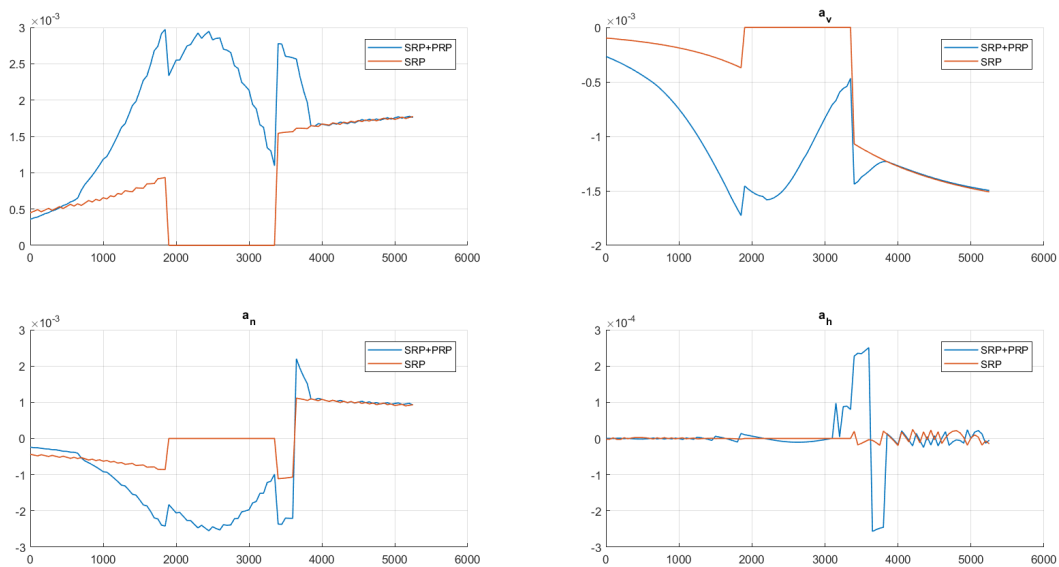


Figure 6.35. Magnitude and components of the acceleration vector -  $i$  85 deg,  $\omega$  0 deg

# Chapter 7

## Conclusion

Following and extending a previous work where the analysis was only two-dimensional, this thesis has investigated, with a three-dimensional approach, the effect of planetary radiation pressure on the acceleration of a solar sail orbiting around a planet. In the planetary radiation, two contributions have been taken into account, the black body emission and the albedo.

The acceleration due to both solar and planetary radiation has been calculated with opportune relations that also considered the optical properties of the materials and the direction of incident photons. For this last reason, two angles have been used to describe the attitude of the sail in three-dimensional space and to know its orientation respect to the photons. All the possible orientations could be scanned, and the one that maximises the acceleration along a chosen direction could be found. A grid of points around the Earth and Venus has been analysed, maximising the radial and the transverse acceleration. Results show that the effect of the planetary contribution is minimal if the sail is orbiting around Earth, but becomes dominating in a considerable region when the planet is Venus. In this case, both the attitude of the sail and the acceleration magnitude changed, especially due to the contribution of black body radiation.

Thanks to the developed model, some manoeuvres have been simulated with Gauss' variational equations and Gao's control laws, in order to change the inclination, the semimajor axis and the eccentricity of an orbit around Venus. The influence of planetary radiation pressure on the performance of the manoeuvres depends on the initial orbital elements and on the requested orbital changes; in particular, the planetary contribution has provided relevant benefits in the vicinity of the planet, where its radiation is dominating, and in the eclipse region, where only the black body radiation is present. Out of these areas, PRP has been less relevant in the manoeuvres, even if it should not be neglected especially in the region between the planet and the Sun since it can provide a contribution against the solar one and decrease the net acceleration.

The effect of PRP on a capturing manoeuvre for Venus has been studied too. In this case, the equations of motion have been integrated, while an acceleration in the opposite direction of the velocity vector has been requested from the sail. Unlike the sail acceleration, this manoeuvre is cheaper when it is done far from the planet. However, results show that the planetary contribution allowed a wider range of initial conditions, in terms of periapsis and eccentricity of the initial hyperbola, when the orbit had an argument of periapsis equal

to 180 *deg*, and so the manoeuvre has been performed in the umbra area, and within a certain distance from the planet. With different arguments of periapsis, the advantage has been less significant, and in some cases has become even negative.

In this study, the investigation of solar sailing that considered both solar and planetary radiation pressure has been only in a preliminary phase. Future analyses could obtain more accurate results, improving the models used for black body emission, albedo and eclipse area. The planet could be modelled as a uniformly bright sphere rather than a disc so that the results could be more realistic. Moreover, the divergence of the Sunlight rays could be taken into account, creating an eclipse region model more consistent with reality, unlike the cylindrical one. The assumption of fixed Sun could be relaxed, and a more elaborated model could be used of the albedo. As regards the study of the manoeuvres with Gao's control law, future works could implement the optimisation of the parameters proposed by Gao, studying how they change whether the PRP is considered or not; in addition, the analysis conducted for manoeuvres around Venus could be repeated for the Earth, even if its results are not so promising, for the wide range of possible applications. Interesting further analyses could consider the effect of the aerodynamic forces in the calculation of the net acceleration, focusing the study in the area close to the planet, where the planetary contribution is higher. In the end, after the capturing manoeuvre, the whole interplanetary trajectory could be studied either with the patched conic approximation or solving a three-body problem.

# Bibliography

- [1] Colin Robert McInnes. *Solar sailing: technology, dynamics and mission applications*. Astronomy and Planetary Sciences. London: Springer, 1999. DOI: [10.1007/978-1-4471-3992-8](https://doi.org/10.1007/978-1-4471-3992-8). URL: <http://cds.cern.ch/record/1663677>.
- [2] Malcolm Macdonald and Colin R McInnes. «Solar sail mission applications and future advancement». In: *2nd International Symposium on Solar Sailing, ISSS 2010* (2010).
- [3] Satoshi Eguchi, Nobuaki Ishii, and Hiroki Matsuo. «Guidance strategies for solar sails to the moon». In: *Astrodynamics 1993* (1994), pp. 1419–1433.
- [4] Thomas André Fekete. «Trajectory design for solar sailing from low-earth orbit to the moon». PhD thesis. Massachusetts Institute of Technology, 1992.
- [5] C Garner et al. «Activities In Solar Sail Propulsion». In: AIAA-2001-3234, 37th AIAA/ASME/SAE/ASEE Joint Propulsion Conference, Salt ... 2001.
- [6] M. Leipold et al. «Mercury sun-synchronous polar orbiter with a solar sail». In: *Acta Astronautica* 39.1 (1996). Second IAA International Conference on Low-Cost Planetary Missions, pp. 143 –151. ISSN: 0094-5765. DOI: [https://doi.org/10.1016/S0094-5765\(96\)00131-2](https://doi.org/10.1016/S0094-5765(96)00131-2). URL: <http://www.sciencedirect.com/science/article/pii/S0094576596001312>.
- [7] M Leipold. «Solar sail mission design». PhD thesis. 2000.
- [8] Giovanni Mengali and Alessandro A Quarta. «Optimal three-dimensional interplanetary rendezvous using non-ideal solar sail». In: *Journal of Guidance, Control, and Dynamics* 28.1 (2005), pp. 173–177.
- [9] Alessandro Peloni, Matteo Ceriotti, and Bernd Dachwald. «Solar-sail trajectory design for a multiple near-earth-asteroid rendezvous mission». In: *Journal of Guidance, Control, and Dynamics* (2016), pp. 2712–2724.
- [10] M. Leipold et al. «Heliopause Explorer—a sailcraft mission to the outer boundaries of the solar system». In: *Acta Astronautica* 59.8 (2006). Selected Proceedings of the Fifth IAA International Conference on Low Cost Planetary Missions, pp. 785 –796. ISSN: 0094-5765. DOI: <https://doi.org/10.1016/j.actaastro.2005.07.024>. URL: <http://www.sciencedirect.com/science/article/pii/S0094576505002377>.
- [11] Guido Colasurdo and Lorenzo Casalino. «Optimal control law for interplanetary trajectories with nonideal solar sail». In: *Journal of Spacecraft and Rockets* 40.2 (2003), pp. 260–265.

- [12] John Bookless and Colin McInnes. «Control of Lagrange point orbits using solar sail propulsion». In: *Acta Astronautica* 62.2 (2008), pp. 159–176. ISSN: 0094-5765. DOI: <https://doi.org/10.1016/j.actaastro.2006.12.051>. URL: <http://www.sciencedirect.com/science/article/pii/S0094576507001774>.
- [13] Malcolm Macdonald et al. «GeoSail: an elegant solar sail demonstration mission». English. In: *Journal of Spacecraft and Rockets* 44.4 (July 2007), pp. 784–796. ISSN: 0022-4650. DOI: [10.2514/1.22867](https://doi.org/10.2514/1.22867).
- [14] Malcolm Macdonald and Colin R McInnes. «Realistic earth escape strategies for solar sailing». In: *Journal of Guidance, Control, and Dynamics* 28.2 (2005), pp. 315–323.
- [15] Victoria Coverstone and John E. Prussing. «A technique for earth escape using a solar sail». English (US). In: *Advances in the Astronautical Sciences* 103.PART 1 (Dec. 2000), pp. 507–519. ISSN: 1081-6003.
- [16] Matteo Ceriotti and Colin R McInnes. «Generation of optimal trajectories for Earth hybrid pole sitters». In: *Journal of Guidance, Control, and Dynamics* 34.3 (2011), pp. 847–859.
- [17] Jeannette Heiligers et al. «Design of optimal earth pole-sitter transfers using low-thrust propulsion». In: *Acta Astronautica* 79 (2012), pp. 253–268. ISSN: 0094-5765. DOI: <https://doi.org/10.1016/j.actaastro.2012.04.025>. URL: <http://www.sciencedirect.com/science/article/pii/S0094576512001403>.
- [18] Alan K Betts and John H Ball. «Albedo over the boreal forest». In: *Journal of Geophysical Research: Atmospheres* 102.D24 (1997), pp. 28901–28909.
- [19] A. Thornton. *Thermal Structures for Aerospace Applications*. AIAA education series. American Institute of Aeronautics & Astronautics, 1996. ISBN: 9781600861260. URL: <https://books.google.co.uk/books?id=VQ0Ad6WdxkEC>.
- [20] Mariusz E. Grötte and Marcus J. Holzinger. «Solar sail equilibria with albedo radiation pressure in the circular restricted three-body problem». In: *Advances in Space Research* 59.4 (2017), pp. 1112–1127. ISSN: 0273-1177. DOI: <https://doi.org/10.1016/j.asr.2016.11.020>. URL: <http://www.sciencedirect.com/science/article/pii/S0273117716306469>.
- [21] Alessia Iuliis et al. «Sailing with Solar and Planetary Radiation Pressure». In: *Advances in Space Research* (Dec. 2019). DOI: [10.1016/j.asr.2019.11.036](https://doi.org/10.1016/j.asr.2019.11.036).
- [22] David R Williams. NASA.
- [23] Shahid Baig and Colin McInnes. «Artificial Three-Body Equilibria for Hybrid Low-Thrust Propulsion». In: *Journal of Guidance, Control, and Dynamics* 31.6 (2008), pp. 1644–1655. DOI: [10.2514/1.36125](https://doi.org/10.2514/1.36125). eprint: <https://doi.org/10.2514/1.36125>. URL: <https://doi.org/10.2514/1.36125>.
- [24] Ian R. Cole. «Modelling CPV». In: (June 2015). URL: [https://repository.lboro.ac.uk/articles/Modelling\\_CPV/9523520](https://repository.lboro.ac.uk/articles/Modelling_CPV/9523520).
- [25] F.G. Cunningham, United States. National Aeronautics, and Space Administration. *Power Input to a Small Flat Plate from a Diffusely Radiating Sphere with Application to Earth Satellites*. NASA technical note D-710.

## BIBLIOGRAPHY

---

- [26] Hanspeter Schaub and John L. Junkins. *Analytical Mechanics of Space Systems*. 2nd. Reston, VA: AIAA Education Series, 2009. DOI: [10.2514/4.867231](https://doi.org/10.2514/4.867231).
- [27] Bernd Dachwald. «Minimum transfer times for nonperfectly reflecting solar sailcraft». In: *Journal of Spacecraft and Rockets* 41.4 (2004), pp. 693–695.
- [28] Yang Gao. «Near-Optimal Very Low-Thrust Earth-Orbit Transfers and Guidance Schemes». In: *Journal of Guidance, Control, and Dynamics* 30.2 (2007), pp. 529–539. DOI: [10.2514/1.24836](https://doi.org/10.2514/1.24836). eprint: <https://doi.org/10.2514/1.24836>. URL: <https://doi.org/10.2514/1.24836>.



# Acknowledges

Trascorsi i cinque anni e mezzo di questo incredibile percorso di laurea, prima triennale e poi magistrale, dei ringraziamenti sono doverosi e, oserei dire, persino essenziali. Penso infatti che, anche con il rischio di risultare banale, e pur con la certezza che ognuno di voi sappia già quanto sia stato fondamentale per me, ogni tanto sia necessario che certe cose vengano dette anche esplicitamente.

Per prima cosa voglio ringraziare il Dr. Matteo Ceriotti per aver creduto nelle mie potenzialità e avermi dato l'opportunità di sviluppare questo progetto all'università di Glasgow. Grazie per tutti i preziosi consigli e per la grande disponibilità nel fugare tutti i miei dubbi e le mie insicurezze. Lavorare sotto la sua supervisione è stata una grande opportunità di crescita professionale e di questo le sono infinitamente grato.

Grazie a tutti i miei amici. Grazie per essere stati sempre al mio fianco in tutti gli alti e bassi che l'università regala, dalle notti scatenate in giro per Torino a quelle disperate chiusi in casa sui libri. Grazie anche per le aule studio private che si trasformavano in pasticcerie, per la caccia ossessiva a posti freschi in cui studiare d'estate, per le interminabili digressioni politiche e filosofiche, per le serate sul divano davanti a un film, per aver sopportato le mie dolci melodie notturne, per aver creduto che potessi davvero andare a correre, per non esservi lamentati troppo in sfiancanti gite ai quattro angoli della Scozia, o in Northumbria, magari scalzi e con i piedi nel fango mentre scappavamo dall'alta marea. Forse dovrei ringraziarvi anche per avermi assecondato quando mi distraevo a lezione e per quelle brevi pause che non finivano mai. O forse no. Insomma, di motivi ce ne sarebbero tanti e non è neanche il caso di citarli tutti, quello che però volevo si capisse è che ricorderò ogni attimo del tempo trascorso insieme ed il merito è vostro per aver reso ogni momento speciale.

Una menzione particolare merita anche chi era un po' più lontano fisicamente, ma non ha mai smesso di essermi vicino. Grazie per aver sopportato tutti i miei eterni monologhi e le mie continue lamentele. Da qualche parte so che c'è una statua che ti aspetta.

Ed infine alla mia famiglia, che più di tutti merita questi ringraziamenti ma a cui probabilmente grazie lo ho detto troppe poche volte. In futuro spero in qualche modo di poter ripagare tutti i sacrifici che avete fatto per me. Grazie per avermi sostenuto e incoraggiato in tutti questi anni; ogni pacco "da giù" che arrivava trasudava tutto il vostro amore e l'impegno che ci mettevate e dava a me la carica per continuare. Il vostro aiuto è stato essenziale.



*See you,  
space cowboy*